2019

Detrital Zircon Provenance and Correlation of Two Newly Discovered Ripley Formation Bentonites: Pontotoc County, Mississippi

Elizabeth Jayne Vitale
University of Mississippi

DETRITAL ZIRCON PROVENANCE AND CORRELATION OF TWO NEWLY DISCOVERED RIPLEY FORMATION BENTONITES: PONTOTOC COUNTY, MISSISSIPPI

A Thesis
Presented in partial fulfillment of requirements
for the degree of Master of Science
in the Department of Geology and Geological Engineering
The University of Mississippi

by

ELIZABETH J. VITALE

May 2019

ABSTRACT

Two newly discovered bentonite deposits in northern and southern Pontotoc County, Mississippi occur in the Upper Cretaceous outcrop in a banded pattern on the northeastern margin of the Mississippi Embayment (MSE). The entire Ripley Formation (Fm) consists of ~73 m of fossiliferous clay, sand, and calcareous sand beds. The bentonites are located stratigraphically within the Chiwapa Sandstone Member (CSM) at the top of the Ripley Fm and stratigraphically lie above previously mined bentonites in central Pontotoc County. Since the northern and southern bentonites differ stratigraphically from the previously mined bentonites, it is possible that there are other unknown bentonite deposits throughout Pontotoc County. This study utilizes heavy mineral separation, scanning electron microscopy (SEM), detrital zircon U-Pb geochronologic dating, stratigraphic analysis, and X-ray diffraction to determine and refine the possible sources and depositional environments of the upper Ripley bentonites.

Detrital zircon ages (n = 649) were collected from the northern and southern bentonite locations and yielded ages ranging from Mesoarchean (~2,870 Ma) to Pennsylvanian (~305 Ma) and contained approximately 91% Appalachian source derived grains, including Appalachian-Ouachita (~490–265 Ma), Gondwanan Terranes (~900–500 Ma), and Grenville (~1,350–900 Ma) source terranes. Other igneous province source regions include the Mid-Continent Granite Rhyolite Province (MCGRP) (~1,600–1,350 Ma), Yavapai-Mazatzal (~1,800–1,600 Ma), Trans-Hudson/Penokean (~1,900–1,800 Ma), and Superior (>2,500 Ma).

A high input of Appalachian derived sediment, heavy mineral abundances, and clay mineral composition all indicate that the bentonites were deposited in a deltaic/delta-platform environment and that sediment feeding the northeastern MSE likely originated from the Appalachian foreland basin and Appalachian-Ouachita fold thrust belt. The southern samples are rich in montmorillonite and suggest that they were deposited in a pro-delta marine setting during a marine transgression at the end of the Cretaceous. The kaolinite rich northern samples suggest input into a low energy deltaic environment. However, montmorillonite rich Ripley Fm clays have not been previously noted and possibly indicate that bentonites could have been deposited by a younger source of Late Cretaceous volcanism. By evaluating the depositional environments and sources of the Pontotoc bentonites, the Upper Cretaceous strata of the MSE and Gulf Coastal plain, may show an occurrence of previously unidentified bentonites and may indicate that volcanism occurred in the MSE during Maastrichtian time

DEDICATION

This work is dedicated to my Mom and Dad, David and Linda Vitale. I would not have accomplished what I have and became who I am without them. Also, my late grandfather Albert John Rustige Jr., who would have loved to explore the world of geology with me.

LIST OF ABBREVIATIONS

AB	Arkoma Basin
AFB	Appalachian Foreland Basin
ARBM	Arbuckle Mountains
CDF	Cumulative Density Function
CDP	Cumulative Density Plot
CL	Cathodoluminesence
CSM	Chiwapa Sandstone Member
FCB	Forest City Basin
Fm	Formation
Ga	Billion years
GCP	Gulf Coastal Plain
GoM	Gulf of Mexico
GSMRB	Great Smokey Mountain Rift Basin
IB	Illinois Basin
ICP-MS	Inductively-Coupled Plasma Mass Spectrometer
K-Pg	Creteacous-Paleogene
K-S	Kolmogorov-Smirnov
LA-ICP-MS	Laser Ablation Inductively-Coupled Plasma Mass Spectrometer
LST	Lithium Polytungstates

Ma	Million years
MB	Michigan Basin
MCGRP	Mid-Continent Granite Rhyolite Province
MCR	Mid-Continent Rift
MSE	Mississippi Embayment
Nu-ICP-MS	Nu Plasma HR Multicollector Inductively-Coupled Plasma Mass Spectrometer
PDP	Probability Density Plot
RCG	Rough Creek Graben
RR	Reelfoot Rift
SE	Secondary Electron
SEM	Scanning Electron Microscopy
SG	Specific Gravity
XRD	X-Ray Diffraction

ACKNOWLEDGMENTS

Firstly, I would like to thank my advisor, Dr. Jennifer Gifford, for providing me with the idea and support for my thesis project and for elevating my passion and knowledge of geology. I would have been lost without her support and encouragement. I also would like to thank my committee members Drs. Brian Platt and Inoka Widanagamage for their support and expertise. Thank you to the Department of Geology and Geological Engineering for all of the knowledge and the ability to grow academically and professionally over the past six years. Thank you to all of the faculty of the Department of Geology and Geological Engineering for allowing me to work as a teaching assistant for four years in the department and also to my students, because if it weren't for them, I would not be able to earn this graduate degree.

Thank you to all of those in the scientific community that helped make this project possible including: Rooban and Orion at Mississippi State University for their help with SEM and XRD analysis, Berry Shaulis at the University of Arkansas for the quick U-Pb analyses, Paul O'Sullivan from Geoseps also with U-Pb analyses, Charles Swann for his expertise and help in the field, Dr. George Kamenov at the University of Florida for his help running ICP-MS analyses, and Dr. Paul Mueller for the use of his data reduction protocol.

Also, I would like to thank those who were by my side through graduate school and during the harder times of this project. You are all the reason I kept my sanity and stayed optimistic. Alex Warren, Anna McWhirter, Adam Schildhammer, Steve Terracina, Bram Allen,

Bradley Lewis, Jarett Bell, and Zack Lepchitz, I will miss you and will miss working alongside you. Meaghan Dice and Cat Henry, thank you for answering your phones whenever I needed graduate school advice and also for the endless encouragement.

Lastly, I would like to thank my family for their support and love through the entire thesis process. I owe everything I am to my parents, David and Linda Vitale, thank you for the unwavering love and support. I would also like to thank my brother and sister, Anthony and Olivia, for never failing to make me laugh when I needed it.

TABLE OF CONTENTS

LIST OF TABLES

LIST OF FIGURES

1. INTRODUCTION

The Maastrichtian (72.1 Ma to 66.0 Ma) upper Ripley Formation (Fm) represents the maximum extent of the Mississippi Embayment (MSE) (Fig. 1) during the Mesozoic Era and outcrops in Alabama (AL), Mississippi (MS), and Tennessee (TN) (Cushing et al., 1964). The northeastern Late Cretaceous sediments of the MSE are increasingly marine upsection and represent onlap onto the upper Gulf Coastal Plain margin (Dockery and Thompson, 2016). The Late Cretaceous marked a period of volcanic activity within the MSE, which was responsible for the deposition of extensive volcaniclastics material within Upper Cretaceous rocks, such as the bentonitic clays of the upper Ripley Fm. that outcrop in Pontotoc County, MS (e.g., Cushing et al., 1964; Dockery and Thompson, 2016). These bentonites were mined in the 1940s by the Mississippi Minerals Company and Eastern Clay Products Inc. (Priddy, 1943; Mellen, 1958; Dockery and Thompson, 2016), and it was suggested that a continuation of the study of the sedimentology of the upper Ripley Fm Chiwapa Sandstone Member might reveal undiscovered mineable bentonite deposits Mellen (1958). In 2016, a bentonite deposit was discovered at the top of the Chiwapa Sandstones in a Poe Brothers Trucking Inc. quarry in central Pontotoc County, MS (Fig. 1). The location of the newly discovered bentonite is ~10 km south of the 1940s mined bentonite location. In 2018, another expansive clay deposit, exhibiting the field

characteristics of bentonite, was also found above the Chiwapa Sandstone Member (CSM) in northeastern Pontotoc County ~7 km northeast of the 1940s mined bentonites in 2018 (Fig. 1).

This study utilizes the interpretation of detrital zircon U-Pb geochronologic age data of the newly discovered bentonite beds that are located above the limestone unit of the CSM to better constrain the sediment provenance and the possibility of additional bentonite accumulation in the upper Ripley Fm during the Late Cretaceous. U-Pb zircon age dating of Cretaceous sediment sources in the MSE have previously been done in the Cenomanian Tuscaloosa and Woodbine Fms and Paleocene Wilcox strata by Blum and Pecha (2014). Potter-McIntyre et al. (2018) expanded on the work of Blum and Pecha (2014) by determining the U-Pb provenance of the correlative McNairy Formation in southern Illinois. The Ripley Fm bentonites in this study lie stratigraphically and geographically between the sample locations for Blum and Pecha (2014) and Potter-McIntyre et al. (2018) along with the Cretaceous sediments within the MSE. Depositional environments of the observed CSM at the two new bentonite localities were also interpreted based on lithostratigraphy, biostratigraphy, and mineralogic composition. Correlating possible bentonite deposits in northern and southern Pontotoc County may reveal where other economic bentonite deposits may occur.

2. GEOLOGIC SETTING

2.1. Mississippi Embayment

The Mississippi Embayment (MSE) is a 259,000 km^2 trough that extends from southern Illinois (IL) into parts of Alabama (AL), Arkansas (AR), Kentucky (KY), Louisiana (LA), Mississippi (MS), Missouri (MI), Tennessee (TN), and Texas (TX) (Fig. 1). Jurassic to Quaternary rocks and sediments fill the south-plunging syncline and are as thick as 5,500 m in the southern portion of the MSE (Cushing et al., 1964). Cretaceous strata rest unconformably on Jurassic rocks in the MSE and are of marine and terrigenous origin and include calcareous sands, clays, chalks, marls, and some limestones (Cushing et al., 1964).

Maastrichtian rocks within the MSE outcrop in a band that extends southward to the Gulf of Mexico (GoM) (Fig. 1). Clastic rocks primarily constitute Maastrichtian strata in the MSE and GoM and are overlain by Paleogene units (Salvador, 1991). Maastrichtian deposits on the northeastern rim of the GoM are indicative of a shallow inner shelf environment (Dockery and Thompson, 2017). Within the MSE, the Ripley Fm is comprised of fine-grained bioturbated sands that are fossil- and mica-rich along with clay-rich sections that are present in some portions (Dockery and Thompson, 2017). The characteristic sands and clays of the Ripley Fm range from 30 m thick in the east (KY) to 180 m thick in the north and west (TN and AR) (Salvador, 1991).

2.2. Tectonics of the Mississippi Embayment

The Reelfoot Rift zone is a Cambrian aulacogen formed during the breakup of Rodinia in the Proterozoic. This zone underlies the MSE and hosts a thick succession of Phanerozoic strata overlying basement rock, and is the most seismically active structural province in the eastern United States (Ervin and McGinnis, 1975; Cox, 1988; Csontos et al., 2008). The New Madrid Fault Zone is situated in the northwestern and central MSE and is characterized by Late Proterozoic to Early Paleozoic seismogenic faulting (Ervin and McGinnis, 1975; Cox et al., 2001; Csontos et al., 2008). Also, known epicenters are linearly located along the southeastern margin of the Reelfoot Rift showing that faulting in the area is still active (Chiu et al., 1997).

Previous authors suggested that the Reelfoot Rift originated at the intersections of Precambrian terranes in the North American craton and uplift within the rift was the result of mantle upwelling between these terranes (Csontos et al., 2008; Dart and Swolfs, 1998). However, the mechanism for rifting is debated. The first possible scenario for rifting is that the Reelfoot Rift formed within the boundaries of the Eastern Granite Rhyolite Province as a result of right-lateral strike-slip faulting within Laurentia (Kane et al., 1981; Hildenbrand, 1985; Nelson and Zhang, 1991; Dart and Swolfs, 1998; Thomas, 1985, 1991). The second suggested mechanism is that rifting in the Reelfoot region began when mantle upwelling occurred along the terrane boundaries (Dart and Swolfs, 1988).

During Cambrian time, the Reelfoot region rifted by listric normal faulting (Howe and Thompson, 1984; Hildenbrand, 1985; Howe, 1985; Nelson and Zhang, 1991). As sediment began to accumulate within the Reelfoot Rift basin, faulting continued into the Middle Cambrian and through the Middle Ordivician. Sediment deposition in the Reelfoot Rift basin occurred at

the same rate as subsidence from the Late Cambrian to Middle Ordovician (Howe and Thompson, 1984; Howe, 1985; Dart and Swolfs, 1998). The Taconic (490–440 Ma), Acadian (450–320 Ma), and Alleghanian (330–265 Ma) orogenic events resulted in the repeated uplift and then subsidence of the Reelfoot Rift from the Ordovician to Pennsylvanian (Howe, 1985). When Pangea began to assemble in the late Paleozoic, the Reelfoot Rift again became structurally unstable and faulting continued (Thomas, 1985; Howe, 1985).

From the Middle Ordovician through the Early Cretaceous, deposition in the MSE and the Reelfoot Rift basin halted due to paleodrainage routes that show mid-continent sediment input extending further west (Blum and Pecha, 2014; Finzel, 2014). Then uplift followed by erosion resulted in an unconformity above the Late Paleozoic strata (Csontos et al., 2008). As a result, an Early Cretaceous drainage system extended from the Appalachians to the eastern shoreline of the western interior basin from Iowa and Wyoming (Blum and Pecha, 2014; Finzel, 2014).

Faults bounding the Reelfoot Rift show normal displacement and the northwestern extent of the rift is marked by a steep normal fault dipping to the southeast, lowering the boundary between the Precambrian basement rock and overlying Proterozoic strata by as much as 3 km (Howe, 1985; Nelson and Zhang, 1991). The southeastern rift boundary is denoted by two northwest dipping normal faults with displacement ranging from 0.5 km to 3 km (Howe, 1985). Stark (1997) suggested that deformation due to thrusting and transpression occurred during the Grenville orogenic event, which produced the southeast and northeast trending basement.

Subsidence rerouted sediment input into the MSE and sediment accumulation continued throughout the Cenozoic. Quaternary southwestern tilting of the MSE in northeastern AR is seen

in geomorphological features such as Crowley's Ridge, which was formed due to erosion by the ancestral Mississippi and Ohio Rivers along with the reactivation of the bounding faults. Sediment accumulation at the perimeter of the MSE is attributed to increased accommodation due to the subsidence as a result of tectonic activity within the Reelfoot Rift, along with the transgressive and regressive cycles that deposited the Cretaceous sediments exposed today at the surface.

2.3. Study Area

The Ripley Fm (lower to middle Maastrichtian) outcrops in Pontotoc County, MS, and comprises clay, sandy clay, sand, and thin beds of sandstone. The subdivisions of the Ripley Fm, in ascending stratigraphic order, are the transitional clay, lower Ripley, middle Ripley, and the upper Ripley which contains the CSM (Priddy, 1943) (Fig. 2). The previously mined Pontotoc Bentonite (Priddy, 1943; Mellen, 1958) was occurs within the CSM, however the newly recognized southern and northern bentonites are located above the CSM sand interval at the contact between the Ripley Fm and Owl Creek Fm.

2.4. Ripley Formation Stratigraphy

In Pontotoc County, the Ripley Fm is conformably underlain by the Demopolis Chalk and unconformably overlain by the Owl Creek/Prairie Bluff Fm. (Fig. 2). The thickness of the Ripley Fm in Pontotoc County ranges from ~8 m to ~82 m. Priddy (1943) described the composition of the Ripley Fm. as dominantly bedded micaceous sand that contains lenses of silty chalk, chalky limestone, sandy limestones at some locations, and bentonite beds that underlie sandy limestones.

The oldest subdivision of the Ripley Fm is the transitional clay member and is described by Priddy (1943) as a well-bedded calcareous sandy clay that marks the transitional zone between the Ripley Fm and upper silt of the Demopolis Chalk (Fig. 2). It is between 12 m and 15 m thick in Pontotoc County. More specifically, the transitional clay is green/grey, and shows no lamination. Depending on the degree of weathering, the transitional clay turns from greenish to reddish-tan which helps distinguish the clay from the underlying Demopolis Chalk.

The second oldest subdivision of the Ripley Fm is the lower Ripley member, which is 9 m to 15 m thick in Pontotoc County. The lower Ripley includes lenses of micaceous chalky sands and fossiliferous silty chalk or chalky limestones. The chalky sands weather to a red color and grade into the overlying middle Ripley. The sandy limestones weather grey/white making them distinguishable from the chalky sands (Priddy, 1943).

The middle Ripley member (Priddy, 1943) conformably overlies the lower Ripley and ranges from 15 m to 46 m in thickness. The middle Ripley member consists of well-bedded micaceous sands that contain lenses of chalky silts, marls, or glauconitic sands in the lower portion. The mid portion of the middle Ripley contains unfossiliferous sands and lignitic beds. The upper portion of the middle Ripley member is well-bedded fine-to-medium sands that are comparable to the McNairy Sand to the north. The entire middle Ripley outcrops in few places in Pontotoc County and the basal chalky silt/marl lenses or glauconitic sands are the only resistant units preserved in the middle Ripley. The chalky fossiliferous limestone beds overlie the fossiliferous sands in northeast Pontotoc, but they are overlain by bentonitic clays or very fossiliferous limestones in eastern Pontotoc where the bentonites were eroded.

The bentonitic clays that are the focus of this study occur either within or above the sandy limestones of the upper Ripley Fm. The bentonites were extensive and pure enough to be considered an economic resource in the 1940s (Priddy, 1943; Mellen, 1958). The bentonite outcrops described by Priddy in 1943 start with a basal coarse sand that occur either within or above the CSM, which grades into a less silty, less calcareous clay that then grades into a dark blue/grey, silty, and calcareous clay (Priddy, 1943). The maximum thickness of ~2.7 m occurs in northern Pontotoc County and thins to ~0.6 m to the southeast (Mellen, 1958). The bentonite is not exposed entirely throughout the upper Ripley due to erosion before the deposition of the overlying upper Ripley member (Priddy, 1943).

3. METHODS

3.1. Sample Collection and Preparation

Sampling occurred at the northern and southern locations within Pontotoc County (Fig. 1). Southern samples were collected from two trenches that were excavated ~15 m apart, one to the northeast (NE) and one to the southeast (SE) in a weathered high wall from previous sand mining within the upper Ripley (34°12'15"N, 88°58'40"W) (Fig. 1 and 3). Detailed stratigraphic sections were measured and described at each location (Fig. 3). Sampling at the southern location started in the lower sand and bulk samples of sand and bentonite were collected in ~1-meter intervals moving up section. Additional samples were collected from the gradational contact between the bentonite and bounding sand and from 2 locations within the bentonite. The southeast trench bulk samples were taken at 60 cm, 140 cm, and 200 cm from the trench base and the northeast bulk samples were collected twice in the lower bounding sand (NE-S) and at 0 cm, 100 cm, and 180 cm from the trench base because of the high amount of bioturbation that could have possibly moved zircons into the sands (Fig. 3). Northern samples were collected from exposed sections from previous mining activities (34°20'57"N, 88°54'26"W) (Fig. 1). Detailed descriptions of the units comprising the upper and middle Ripley were noted and the stratigraphic section was measured using a precision Jacob staff and Abney level. The four northern samples were given the prefix TR for the location on Tuscumbia Road. Sampling at the northern location consisted of collecting 4 samples at the top and base of

the bentonite ~15 m apart. Samples TR-01 and TR-03 were collected ~1 m down from the top of the bentonite with the purpose of collecting possible finer grained material. About two gallons for samples TR-02 and TR-04 were collected ~1 m above the base of the bentonite and lower sand contact due to an observed higher amount of purer bentonitic clays that occurred as grey pieces of clay material mixed in with the brown clays.

Samples were then dried and pulverized using a disk mill. The southern sample zircons were initially separated using a centrifugal bowl that separated sediment based on grain density and slightly on grain size as finer particles were washed out of the sample in addition to lighter density particles. The northern samples were separated using a JCR zircon concentrating table. After washing, the heavy fractions were gathered and dried before undergoing heavy liquid separation. Lithium Polytungstates (LST; specific gravity (SG) = ~2.85) were used to separate lighter minerals from the heavy fraction based on density and were then run through a magnetic separator (Franz LB-1). The non-magnetic fraction was separated with methylene iodide (MI) (SG = ~3.30) to yield zircon grains.

Zircon grains were handpicked under a microscope based on size, color, iridescence, and grain morphology. After the selection of >120 grains per sample, grains were mounted on a glass plate using adhesive tape. The selected zircon grains were embedded in a 1" epoxy plug and polished for imaging approximately halfway through the zircon grains.

3.2. SEM Imaging

Zircons were imaged at the Mississippi State University Institute for Imaging and Analytical Techniques using a Zeiss EVO 5.0 high-vacuum Scanning Electron Microscope (SEM) and a Gatan miniCL cathodoluminescence attachment. Secondary Electron (SE) and

cathodoluminescence (CL) images were collected and used to characterize grain zoning and classification (igneous, metamorphic, or detrital) (Fig. 4). Targets for U-Pb laser ablation (~20 μm) were selected on the CL images for each grain based on zonation. Some grains had multiple U-Pb sites based on the presence of a core and rim in the same grain that could possibly yield different ages.

3.3. U-Pb Zircon Isotopic Analysis

U-Pb analyses for samples SE140 and NE100 were performed on a Nu Plasma HR Multi-collector inductively coupled plasma mass spectrometer (Nu-ICP-MS) at the University of Florida Department of Geosciences, Geochronology Laboratory. Zircon ablation occurs in a stream of He and is then mixed into an Ar gas flow that carries minute particles of zircon into the plasma stream, which ionizes them, allowing U and Pb isotopes to be measured simultaneously using the multi-collector. Ion collectors on the end of the Nu-ICP-MS simultaneously collect ^{204}Pb (^{204}Hg), ^{206}Pb, and ^{207}Pb ions and Faraday detectors collect ^{235}U and ^{238}U signals. A 20-second integration that clears the gas blank and the ^{204}Hg input precedes a 30-second period that clears the previous analysis. After the completion of Nu-ICP-MS analysis, isotopic ratios of ^{206}Pb/^{238}U, ^{207}Pb/^{235}U, and ^{207}Pb/^{206}Pb were provided from the Nu-Instruments Time Resolved Analysis software. In order to correct the fractionation and drift errors that occurred, corrections were calibrated against a known standard (FC-1 natural zircon standard; Duluth Gabbro; 1098 Ma; Paces and Miller, 1993; Black et al., 2003). Analyses were arranged with 2 ablations of FC-1, followed by 10 unknowns, and then 2 more FC-1. Collected data were input into the CALAMARI 9.0 (© P. Mueller) reduction protocol for U-Pb geochronology spreadsheet.

GeoSep Services (GSS) in Idaho analyzed sample TR-02 (EV2S). Isotopic analyses utilized a New Wave UP-213 laser ablation system along with a Agilent 7700x quadrupole Inductively Coupled Plasma-Mass Spectrometer (LA-ICP-MS) at the Washington State University GeoAnalytical Lab. Material was delivered to the plasma source by a stream of He and Ar gas. Each analysis cycle took ~30 seconds and consisted of a 6-second integration with the laser shutter closed to collect background measurements followed by a 24-second integration with the laser shutter open. Analyses were separated by a 20-second delay and measured the following isotopes: ^{202}Hg, ^{204}(Hg + Pb), ^{206}Pb, ^{207}Pb, ^{208}Pb, ^{232}Th, ^{235}U, and ^{238}U. U-Pb age standards were used during analysis for calibration purposes. Laser ablations consisted of 2 ablations of the FC-1 standard, 10 ablations of the zircon sample, and 2 more FC-1 ablations (Paces and Miller, 1993). FC-1 was used in order to correct the fractionation and drift errors that occurred, corrections were then calibrated against a known standard (Paces and Miller, 1993; Black et al., 2003). Collected analysis data were input into the GSS-ZrnUPb (© Geoseps Services, LLC) reduction protocol for U-Pb geochronology spreadsheet.

All remaining samples were analyzed by laser ablation ICP-MS using a Varian 810 Quadrupole ICP-MS coupled with a PhotonMachines Analyte.193 excimer laser at the University of Arkansas Stable Isotope Laboratory. Data reduction methods are outlined in Shaulis et al. (2010).

U-Pb analyses were sorted based on discordance, and those between <10% or >-5% reversely discordant were approved. These discordance values are arbitrary, but a widely accepted range to remove damaged grains from the data set (e.g., major Pb loss or large amounts of common Pb). After sorting based on discordance, analyses were chosen for each sample. For

ages <800 Ma, $^{206}Pb/^{238}U$ ages are used and for grain ages >800 Ma, $^{207}Pb/^{206}Pb$ ages were used. These ages were used to create probability density plots (PDP) in Isoplot 3.75 (Ludwig, 2012). The PDP show the relative probability of the ages of the grains. Cumulative age probability plots (CDP) were created using the analytical spreadsheet created by the Arizona Laserchron Center (Gehrels and Way, 2015) and show the cumulative age probability for each sample on a single graph.

Statistical analyses were performed in order to compare samples using the Kolmogorov-Smirnov (K-S) test (Gehrels and Way, 2015). The K-S test analyzes if there are significant differences between sample distributions and determines if samples are not the same based on a >95% confidence level, represented by the P-value (Gehrels and Way, 2015). These tests are based on the cumulative density functions (CDF) that create the CDP (Gehrels and Way, 2015). The K-S test compares the maximum vertical probability distances between the curves and a value based on the number of samples in the distribution and confidence level, which is referred to as the critical value (Gehrels and Way, 2015). If the distance between two sample CDFs is greater than the critical value, then the null hypothesis is rejected and detrital zircon samples did not originate from the same source (P-value <0.05). Therefore, the K-S test only indicates if populations are statistically different rather than whether the populations are the same (Guynn and Gehrels, 2010). The statistical analyses were completed using the analytical spreadsheet from the Arizona Laserchron Center (Gehrels, 2010).

3.4. XRD Analysis

Four samples were powdered in house at the University of Mississippi and then sent to Mississippi State for analysis. XRD analysis was performed at the Mississippi State University

Institute for Imaging and Analytical Technologies Lab using a Rigaku Ultima III X-Ray Diffraction System. XRD analysis was performed on two northern samples (TR-01; TR-04) and two southern samples (Pontotoc-1; Pontotoc-2) in order to compare the compositions between the southern bentonite, which was previously analyzed by Charles Swann and confirmed to be a bentonite, and the unknown northern sample. Pontotoc-1 and Pontotoc-2 were collected in May 2018 and are different from the southern samples that were collected in May 2016 and that are referred to in the other sections of this study.

4. RESULTS

4.1. Southern Site Stratigraphy

The southern sampling location is correlative to the previously mined bentonites in central Pontotoc County, MS. The outcrop is ~9 m below the K-Pg boundary and underlies the Owl Creek Fm. The southeast sampling site is ~4 m thick and descriptions covered a 200 cm section of the outcrop. The sandy-clay/clayey-sand is ~40 cm thick and contains mostly medium quartz grains in a brown clay matrix along with some concentrations of cm-scale clay aggregates and subangular sand grains (Fig. 3). Sample SE60 was taken from the upper portion of the sandy-clay/clay-sand. Above the sandy-clay/clayey-sand lies a sandy-clay layer that is ~20 cm thick and that contains mm-sized clay balls (Fig. 3). A fining upward brown silty-clay overlies with isolated fine sand grains in clay matrix grains and is ~120 cm thick (Fig. 3). Sample SE140 was collected from the middle portion of the silty-clay portion of the outcrop and sample SE200 from the upper boundary of the clay at the zone where pedogenic overprinting is prominent (Fig. 3).

Sampling moved to a ~5 m section of the northeast cut at the southern sampling location. The first sample (NE-S) was taken from the lower bounding sand described as an orange-brown silty, fine-grained, sand that is ~2.4 m thick (Fig. 3). The next sample (NE0) was collected from the base of a ~200 cm thick sandy clay section with clay rip ups (Fig. 3). The sandy-clay is poorly sorted with mostly very fine to coarse subangular to subrounded quartz grains. At the top

of the ~200 cm section, the sandy clay is grey to red, with some very fine sand grains and muscovite flakes, and shows MnO staining and bioturbation. Sample NE180 was collected from this portion of the sandy-clay.

4.2. Northern Site Stratigraphy

The Northern Sample location is in northeast Pontotoc County, MS off Tuscumbia Road and ~17.4 km away from the Southern Sample location (Fig. 1). This study will focus on the stratigraphy off the upper portion of the middle Ripley Fm, Chiwapa Sandstone Member, and clay interval to help constrain the deposition of the bentonites. The CSM limestone was included to correlate the northern and southern locations. The middle Ripley Fm at this location is an orange fine to medium poorly sorted sand with minor amounts of clay. The sand grains are subangular to subrounded and dominated by quartz in composition. Brown clay balls up to ~4 cm in diameter were observed along with ripple cross lamination, and trace fossils. The middle Ripley shares a sharp upper contact with the CSM. The CSM limestone is ~80 cm thick and a white sandy limestone (Fig. 3). Abundant fossils were found, including belemnites, brachiopods, echinoids, shell fragments, possible crab fragments, gastropods, shark teeth, and *Exogyra*. This is also the location where *Hardouina subquadrata* and *Sphenodiscus* were found during the 2018 sample collection and confirm the stratigraphic location within the CSM because the same fossils were found at the CSM type locality (Mellen, 1958). The CSM underlies a 2.2 m thick sand bed that is a highly weathered fine to medium sand with an abundant brown clay matrix (Fig. 3). The sand is subangular to subrounded, massive, contains minor mm-thick stringers of white/grey clay, and is very poorly sorted (Fig. 3). This sand bed shares a gradational contact with the overlying ~3.85 m thick grey bentonite (Fig. 3). Samples were collected from the bottom of the

exposure ~1 m above the bentonite/sand contact and ~1 m below the exposed ground surface (Fig. 3). The exposure consisted of two outcrops that were separated by ~15 m at the top of the bentonite and they converged at the base (Fig. 3). Samples TR-01 and TR-03 were collected at the top of the bentonite and samples TR-02 and TR-04 from near the base (Fig. 3).

4.3. Detrital Zircon Geochronology

A total of 1,291 U-Pb analyses were collected, and 649 ages yielded a discordance of >-5% and <10%. The samples are combined based on collection location in southern or northern Pontotoc County for presenting the data in the form of probability density plots (PDP) and cumulative age probability plots (CPD). The PDP are representations of the number and relative probabilities of the grain ages along with the potential source locations (Fig. 5, 6, 7, and 8). Cumulative probability age plots are a visual tool used to show the age data by graphically comparing the cumulative probability of the separate samples (Fig. 7 and 8). The potential source age range percentages for the southern, northern, and combined samples are summarized in Table 1. Age analysis shows an overall age range of 2,870 Ma (Mesoarchean) to 305 Ma (Late Pennsylvanian) and are categorized into nine different potential terranes. The possible age terranes are as follows: Superior (>2,500 Ma), Trans-Hudson/Penokean (~1,900–1,800 Ma), Yavapai-Mazatzal (~1,800–1,600 Ma), Mid-Continent Granite Rhyolite (MCGRP) (~1,600–1,350 Ma), Grenville/Midcontinent Rift (~1,350–900 Ma), Gondwanan Terranes (~900–500 Ma), Taconic (~490–440 Ma), Acadian (~420–350 Ma), and Alleghenian (~330–265 Ma) (Table 1, Fig. 5).

The northern and southern samples show similar age distributions but, the K-S results (P values > 0.05) show that the null hypothesis was rejected. The K-S statistical analysis confirmed

that grain ages of the seven southern samples were statistically not different and therefore could be combined into one complete Southern Sample. The same approach was used for the four samples that comprise the Northern Sample (Appendix B). K-S statistical analyses were used to compare the two samples in this study and ten other studies based on the previous work performed in the Superior and Mid-Continent region (Craddock et al., 2013; Konstantinou et al., 2014), Illinois Basin (Finzel, 2014; Kissock et al., 2018; Potter-McIntyre et al., 2018), Forest City Basin (Finzel, 2014; Kissock et al., 2018), and Cenomanian-Paleocene sediments in the MSE (Blum and Pecha, 2014) (Fig. 7, Appendix B).

4.4. Southern Sample Geochronology

The seven combined southern samples (n=376) have mostly Grenville-aged grains (80.1%, n=301). Acadian aged grains make up the next dominant group with 10.6% of the grains (n=40) coming from the 450–320 Ma age range. The remainder of the age groups in descending order are: MCGR (4.5%, n=17), Gondwanan Terranes (2.9%, n=11), Alleghanian (1.1%, n=4), Superior (0.5%, n=2), and Taconic (0.3%, n=1). The southern samples did not yield any results from the Yavapai-Mazatzal or Trans-Hudson/Penokean provinces (Table 1, Fig. 5). Although detailed sample descriptions for each sample were not recorded, heavy mineral separation yielded high amounts of kyanite within the southern samples.

4.1.1. Sample NE-S. This sample was collected from the lower bounding orange/brown silty sand (Fig. 3). U-Pb zircon analyses (n=25) for this sample range in age from 1,372.0 ± 91.6 Ma to 602.0 ± 12.0 Ma. Overall, 98 grains were sampled but only 25 grains fell within the required discordance values. The PDP for sample NE-S contains a dominant double peak at

~1,172 Ma and ~1,081 Ma in the Grenville age range along with two other age peaks at ~602 Ma (Gondwanan Terranes) and ~1,386 Ma (MCGRP) (Fig. 6).

4.4.2. Sample NE0. This sample was collected at the base of the sand clay in the northeastern trench (Fig. 3). U-Pb zircon analyses (n=21) for this sample range in age from 1,399.9 ± 71.8 Ma to 440.0 ± 12.5 Ma. A total of 57 grains were hit for this sample and only 21 fell within the required discordance range. The PDP for sample NE0 has a dominant double peak at ~1,167 Ma and ~1,036 Ma in the Grenville age range along with two other age peaks at ~444 Ma (Taconic) and ~698 Ma (Gondwanan Terranes).

4.4.3. Sample NE100. This sample was collected from the middle sandy clay within the northeastern trench (Fig. 3). U-Pb zircon analyses (n=76) for this sample range in age from 1,446.5 ± 29.5 Ma to 326.1 ± 10.1 Ma. The PDP for sample NE100 has a dominant double peak at ~1,176 Ma and ~1,033 Ma in the Grenville age range along with two other age peaks at ~337 Ma (Alleghanian) and ~428 Ma (Taconic/Acadian). Minor age occurrences also appear in the Gondwanan Terranes and MCGRP ranges (Fig. 6).

4.4.4. Sample NE180. This sample was collected from the grey to red clay near the top of the northeastern trench (Fig. 3). U-Pb zircon analyses (n=70) for this sample range in age from 1,410.0 ± 60.0 Ma to 332.1 ± 12.7 Ma. The PDP for sample NE180 has a dominant double peak at ~1,163 Ma and ~1,041 Ma in the Grenville age range along with two other age peaks at ~357 Ma (Acadian) and ~432 Ma (Taconic/Acadian). Minor age occurrences are present in the Gondwanan Terranes and MCGRP ranges (Fig. 6).

4.4.5. Sample SE60. This sample was collected from the top of the sandy-clay/clayey-sand (Fig. 3). U-Pb zircon analyses (n=57) for this sample range in age from 2,667.0 ± 37.7 Ma

to 304.7 ± 5.6 Ma. The PDP for sample SE60 has a dominant double peak at ~1,110 Ma and ~1,222 Ma in the Grenville age range along with three other age peaks at ~337 Ma (Alleghanian) and ~428 Ma (Taconic/Acadian), and ~599 Ma (Gondwanan Terranes). Sample SE60 does show a minor age occurrence in the Superior age range (>2,500 Ma) (Fig. 6).

4.4.6. Sample SE140. This silty-clay sample was collected from the middle portion of the southeastern trench (Fig. 3). U-Pb zircon analyses (n=83) for this sample range from 1,489.0 ± 18.4 Ma to 332.7 ± 11.1 Ma. The PDP for sample SE140 has a dominant double peak at ~1,040 Ma and ~1,182 Ma in the Grenville age range along with three other age peaks at ~342 Ma (Alleghanian/Acadian) and ~418 Ma (Acadian), and ~1,485 Ma (MCGRP) (Fig. 6).

4.4.7. Sample SE200. This sample was collected from the top of the clay close to where modern soil overprinting starts (Fig. 3). U-Pb zircon analyses (n=44) for this sample range from 1,337.0 ± 41.2 Ma to 349.0 ± 12.6 Ma. The PDP for sample SE200 has a dominant double peak at ~1,040 Ma and ~1,182 Ma in the Grenville age range along with three other age peaks at ~350 Ma (Acadian) and ~435 Ma (Acadian/Taconic), and ~680 Ma (Gondwanan Terranes) (Fig. 6).

4.5. Northern Sample Geochronology

The combined northern samples are dominantly Grenville in age (80.2%, n=219). The next highest percentage of analyses is the MCGRP at 9.9% (n=27) of the analyses. The remainder of the analyses in descending order are: Taconic (3.3%, n=9), Acadian (1.8%, n=5), Superior (1.5%, n=4), Yavapai-Mazatzal (1.5%, n=4), Gondwanan Terranes (1.1%, n=3), and Trans-Hudson/Penokean (0.7%, n=2). There were no analyses that were of Alleghanian age.

4.5.1. Sample TR-01. U-Pb zircon analyses (n=44) for this sample range in age from 2,870.2 ± 41.4 Ma to 338.1 ± 6.5 Ma. The PDP for sample TR-01 has a large Grenville peak at

~1,115 Ma along but does not exhibit the standard Grenville double peak. Four large age peak occur at ages less than Grenville, which differs from the other samples. The four peaks are at ~338 Ma (Acadian), ~446 Ma (Taconic), ~561 Ma, and ~612 Ma, which are both Gondwanan in age. Sample TR-01 does show a minor age occurrence in the Superior age range (>2,500 Ma) and contains the oldest grain found out of all 11 samples (Fig. 6).

4.5.2. Sample TR-02. U-Pb zircon analyses (n=86) for this sample range in age from 2,761.8 ± 34.2 Ma to 354.3 ± 116.6 Ma. The PDP for sample TR-02 has a dominant double peak at ~1,086 Ma and ~1,188 Ma along with two peaks at ~449 Ma (Taconic) and ~2,754 Ma (Superior) (Fig. 6).

4.5.3. Sample TR-03. U-Pb zircon analyses (n=62) for this sample range in age from 2,684.0 ± 63.3 Ma to 438.8 ± 10.3 Ma. The PDP for sample TR-03 has a dominant double peak at ~1,057 Ma and ~1,219 Ma along with two peaks at ~444 Ma (Taconic) and ~618 Ma (Gondwanan Terranes). Sample TR-03 does show a minor age occurrence in the Superior age range (>2,500 Ma) and contains grains in the MCGRP age range (Fig. 6).

4.5.4. Sample TR-04. U-Pb zircon analyses (n=81) for this sample range in age from 1,768.7 ± 63.3 Ma to 448.4 ± 8.9 Ma. The PDP for sample TR-03 has a subtle double peak at ~1,105 Ma and ~1,180 Ma along with an age peak at ~461 Ma (Taconic) and contains grains in the MCGR age range.

4.6. XRD Results

XRD results reveal that a large percentage of the northern and southern Samples are mainly quartz with other minor minerals (Table 2). The northern samples (TR-01 and TR-04) have a range of 56.9-49.8% quartz and a high kaolinite presence ranging from 21.9-17.2% (Table

2). Low amounts of expansive clays such as montmorillonite were measure in theses samples (6.2-3.6%) (Table 2; Fig. 9). The southern samples (Pontotoc-1 and Pontotoc-2) contain 46.0-36.6% quartz and a number of constituents that do and do not have expansive properties such as montmorillonite and illite, respectively. The southern samples show a much lower kaolinite abundance than the northern samples (Table 2, Fig. 9). The weight percentages of the southern samples are shown in Table 2. The XRD analysis images are compiled in Appendix C.

5. DISCUSSION

5.1. North American Igneous Provinces

The northern and southern Pontotoc bentonite samples predominantly contain Grenville-aged (~1,350–900 Ma) detrital zircons at ~80.1%. The next two largest age provinces represented in the data are the Acadian orogeny (~450320 Ma) at 6.9% and Mid Continent-Granite-Rhyolite (~1,600–1,350 Ma) at 6.8%. Smaller peaks in descending order are the Gondwanan Terranes (~900–500 Ma) at 2.2%, Taconic (~490–440 Ma) at 1.5%, and all containing less than 1% per province are the Superior (>2,500 Ma), Trans-Hudson/Penokean (~1,900–1,800 Ma), Yavapai-Mazatzal (~1,800–1,600 Ma), and Alleghanian (~330265 Ma).

5.1.1. Superior (>2,500 Ma). The Superior province in North America (Fig. 5) is the result of multiple episodes of subduction that led to the amalgamation of the world's largest Archean craton (e.g., Corfu and Davis, 1992; Boehm et al., 2000; David et al., 2003; Percival and Helmstaedt, 2004; Bickford et al., 2006). East-west trending belts of extensive and alternating metasedimentary and granite-greenstones along with high-grade plutonic terranes comprise the Superior province (Langford and Morin, 1976; Corfu and Davis, 1992, Calvert and Ludden, 1999, Bickford et al., 2015). Geochemical evidence shows that the Superior province decreases in age to the south (Calvert and Ludden, 1999).

5.1.2. Trans-Hudson/Penokean (~1,900–1,800 Ma). The Penokean orogen occurred between 1,880–1,820 Ma and outcrops in central Minnesota and Northern Wisconsin (Sims,

1996; Holm, 1999; Chandler et al., 2007). The lack of Penokean aged rocks in central Minnesota suggests previous removal due to tectonic and erosional influences exposing the Archean basement to which the orogeny was sutured (Holm, 1999). The Trans-Hudson orogen is a well-preserved Middle Proterozoic orogenic belt that stretches from central-northern United States and into Canada (Holm, 1999). Trans-Hudson aged rocks outcrop extensively in Saskatchewan in Southern Canada (Fig. 5; Van Schmus et al., 1987).

5.1.3. Yavapai-Mazatzal (~1,800–1,600 Ma). The Late Paleoproterozoic marks a time of large-scale crustal growth in southwestern North America. During this time three provinces (Mojave, Yavapai, and Mazatzal; Fig. 5), were accreted to the Wyoming Craton along its southern boundary (e.g., Bennett and Depaolo, 1987; Condie, 1992, Ramo et al., 2003; Whitmeyer and Karlstrom, 2007). Grains that fall within this age range are likely recycled from Pennsylvanian basins, which had also been recycled from Neoproterozoic and early Proterozoic sands (Craddock et al., 2013; Potter-McIntyre et al., 2018).

5.1.4. Mid-Continent Granite Rhyolite (~1,600–1,350 Ma). The Mid-Continent Granite Rhyolite Province (MCGRP) is a Precambrian basement terrane beneath southwestern Ontario extending south to Arkansas, east to Ohio, and west to Kansas, Oklahoma, and the Texas panhandle (Fig. 5; Van Schmus et al., 1996). The MCGRP in the east contains high-silica rhyolite to dacite with granite having U-Pb ages of ~1,470 Ma and the southern MCGRP has the same composition, however U-Pb ages are ~1,390–1,340 Ma westward and only show major episodes of magmatism in the south-central mid-continent region (Van Schmus et al., 1996; Bickford et al., 2015). These Precambrian basement rocks show no deformation and remain unmetamorphosed (Van Schmus et al., 1996).

5.1.5. Grenville (~1,350–900 Ma). The Grenville igneous province extends from northern Quebec in Canada to the southeastern United States and from the southwestern United States into northern Mexico (Fig. 5). The Grenville orogeny reflects late Mesoproterozoic convergence along the margin of Laurentia during the assembly of Rodinia (Whitmeyer and Karlstrom, 2007). The Appalachian Mesoproterozoic basement rocks that comprise the southeastern United States differ from Canadian Grenvillian rocks because the Appalachian massifs experienced Paleozoic metamorphism and deformation due to orogenesis (Tollo et al., 2004). Grenville-aged grains are common in Paleozoic sedimentary basins because of the recycling of the grains caused by the Paleozoic Taconic, Acadian, and Alleghanian orogenies and redeposition in different basins and the overall large amount of zircons that Grenvillian rocks contained (Park et al., 2010; Xie et al., 2016, 2018; Kissock et al., 2017; Potter-McIntyre et al., 2018).

5.1.6. Gondwanan Terranes (~900–500 Ma). Potential Neoproterozoic source terranes include the Carolina (Fig. 5; southern Appalachians; e.g., Dennis and Wright, 1997), Suwanee (Fig. 5; Florida; e.g., Barnett, 1975; Chowns and Williams, 1983; Duncan, 1998), and Sabine (Fig. 5; Texas-Louisiana; e.g., Mueller et al., 2014). Neoproterozoic terrane accretion is the result of the collision of Laurentia and Gondwana (Dennis and Wright, 1997; Mueller et al., 2014). The Carolina terrane is a volcanic island arc along the southern Appalachian orogen that consists of basalts and basaltic andesites intruded by mafic-ultramafic plutonic complexes (Dennis and Wright, 1997). In the northern Suwanee terrane, Paleozoic sedimentary packages are Gondwanan derived based on support from lithostratigraphy (Barnett, 1975; Chowns and Williams, 1983; Duncan, 1998), fossil assemblages (Cramer, 1973; Pojeta et al., 1976),

paleomagnetic data (Opdyke et al., 1987), and detrital zircon data (Mueller et al., 1994). The Sabine terrane is a continental crustal block underlying the Gulf Coastal Plain and within the Ouachita orogenic belt (Mueller et al., 2014). The composition of the Sabine terrane is poorly constrained because it lies under ~3.5km of sedimentary cover (Clift et al., 2018). However, Clift et al. (2018) suggest that the Sabine terrane is not an exotic terrane and but is an extension of the Mazatzal due to rifting.

5.1.7. Taconic (~490–440 Ma). Igneous activity related to the Taconic Orogeny occurred from the late Cambrian and into the early Silurian (e.g., Drake et al., 1989: Sinha et al., 1997; Miller et al., 2000). Taconic igneous rocks are characteristically different in the in the northern, central, and southern Appalachians (Fig. 5). Two distinct groups of igneous rocks make up the northern Appalachians: (1) mafic and ultramafic rocks occurring to the west and (2) gneissic domes that overlay other volcanic and plutonic rocks (e.g., Chidester, 1968; Naylor, 1967; Leo et al., 1984; Billings, 1956). Igneous rocks of the southern Appalachians include different granites and two suites of Blue Ridge gneisses and schists, a tonalitic and dioritic suite and mafic-ultramafic suite (Drake et al., 1989). Deformation in the southern Appalachians is hard to discern due to later Alleghanian activity and the small amount of well-preserved Ordovician rocks but is more prominent within the Blue Ridge and Piedmont than the Appalachian foreland basin (Drake et al., 1989).

5.1.8. Acadian (~420–350 Ma). The Acadian Orogeny spans from the late Silurian to early Carboniferous (Sevigny and Hanson, 1993; Miller et al., 2000) and characteristically includes flysch and molasse deposits, periods of volcanism, folding and faulting, pulses of plutonism, and several periods of metamorphism (Osberg et al., 1989). Volcanic activity of the

Acadian Orogeny primarily outcrops in New England and occurs in two belts: the Piscataquia volcanic belt (e.g., Rankin, 1968; Bradley, 1983; Hon et al., 1991) and the Coastal volcanic belt (e.g., Berry and Boucot, 1970; Gates, 1975; Shride, 1976). Acadian volcanics also appear in the Talladega belt in Alabama in the southern Appalachians (Osberg et al., 1989).

5.1.9. Alleghenian (~330–265 Ma). The Alleghanian Orogeny occurred from the Late Mississippian to Permian when Africa collided with North America and resulted in the progression of the southern and central Appalachians cratonward as a single crystalline thrust sheet, resulting in foreland basin deformation (Hatcher, 2010). The Alleghanian Orogeny is differentiated based on western and eastern characteristics. The western belt includes folds and thrust faults that continue into North American cratonic sedimentary rocks in the southern and central Appalachians (Hatcher et al., 2007). To the east, pre-Alleghanian metamorphic rocks make up a complex allochthonous belt (Hatcher et al., 2007; Mueller et al., 2014). Historic succession of the Alleghanian orogeny is recorded in the synorogenic clastic wedges that comprise the Appalachian foreland basin (Hatcher et al., 1989).

5.2. Detrital Zircon Provenance of the Ripley Formation Bentonites

North American zircon ages are well constrained according to the igneous province in which they originate. However, it is important to keep in consideration as detrital zircon ages are discussed that the likelihood of the detrital zircon being directly sourced from its origin is low. This is due to the repeated cycles of erosion, transport, and deposition that the zircon could have been subjected to. It is also possible that metamorphism could have altered the original ages of zircon, yielding a younger age that may represent the depositional history of the zircon.

It is also important to note that the four samples from northern Pontotoc were combined based on similar K-S analysis (P-value > 0.05) and the same approach was applied to the seven samples that comprise the southern sampling locality. The four northern samples are referred to as the Northern Sample and the seven southern samples comprise the Southern Sample. The K-S values support that the age spectra of the separate components of each sample are statistically similar. However, the P-values comparing the Northern and Southern Samples are not statistically compatible. This is likely due to four differences in detrital zircon ages between the Northern and Southern Samples. The first difference is an 8.8% difference in Acadian (~450–320 Ma) sourced grains between the Southern (1.8%; Table 1) and Northern Samples (10.6%; Table 1). The Northern Sample shows a larger percentage of Taconic (~490–440 Ma) aged grains at 3.3% compared to the 0.3% in the Southern Sample (Table 1). The MCGRP ages (~1,600–1,350 Ma) are more prominent in the Northern Sample (9.9%; Table 1) than Southern Sample (4.5%; Table 1). Finally, the southern sample shows no age spectra for the Yavapai-Mazatzal (~1,800–1,600 Ma) and Trans-Hudson/Penokean provinces (~1,900–1,800 Ma) compared to the northern sample (1.5% and 0.7% respectively; Table 1).

The Grenville double peaks (Fig. 7) represent the orogenic events that bound a period of Adirondian magmatism (1,180–1,080 Ma) (Gower and Krogh, 2002). The first orogenic event is the Elzeverian Orogeny (1,230–1,180 Ma) followed by the back-arc tectonics of the Adirondian magmatic period and finally the continental-continental collision of the Grenville orogeny (1,080–980 Ma) (Gower and Krogh, 2002). Zircons originating from Grenville basement rocks are rich in Zr and are prominent in the Appalachian foreland basin (e.g., Blum and Pecha, 2014; Moecher and Samson, 2006). The Grenville orogeny is not extensively exposed at the surface in

the southeastern United States, indicating that Cretaceous sediments deposited in the MSE sourced from the Appalachian-Ouachita fold thrust belt is likely to have a high Grenville signature and therefore the Grenville aged zircons were previously reworked before settling in the Appalachian foreland basin.

All Pontotoc samples and comparison samples show a dominant Grenville (~1,350–900 Ma) aged peak, however the Lake Superior region samples (Craddock et al., 2013; Konstantinou et al., 2014) do not show the distinct Grenville double peak (Fig. 8). Craddock et al. (2013) and Konstantinou et al. (2014) cited a prominent source in the northern part of the North American craton and since the Northern and Southern samples do not contain a higher amount of Archean grains then they are not recycled from the north.

The Southern Sample contains 1.1% Alleghanian derived detrital grains (Table 1) and are comparable to the Albian (~113–100.5 Ma), Cenomanian (100.5–93.9 Ma), and Paleocene (66–56 Ma) strata of Blum and Pecha (2014) and Finzel (2014; Fig. 8). Alleghanian aged grains within the Southern Sample suggest a sediment source from the Appalachian-Ouachita fold-thrust belt and basin that routed sediment from the Appalachians to the northeastern ME (Blum and Pecha, 2014). Alleghanian deformation extends from the Southern Appalachians into New England and, before the continental scale paleodrainage shift to the MSE, the Southern and New England Appalachians could have been sourcing the Albian and Cenomanian strata dated by Finzel (2014). Then the paleodrainage shift deposited the Cretaceous and Paleocene strata of this study and Blum and Pecha (2014) (Hatcher et al., 1989). Provenance of upper Cretaceous and Paleogene strata in the MSE are likely sourced from the Blue Ridge and Piedmont area of

the Southern Appalachians and show no source change during this time (Fig. 1; Pryor, 1960; Pryor and Glass, 1961).

A large Acadian age peak (~337 Ma; 10.6%) occurs in the Southern Sample along with a minor Taconic peak (~430 Ma; 0.3%). This is the opposite in the Northern Sample, which has a larger Taconic age peak (~447 Ma; 3.3%) and no Alleghanian aged grains. Acadian aged grains are present in the Pennsylvanian Illinois Basin deposits (Kissock et al., 2017; Potter-McIntyre et al., 2018), Albian and Cenomanian sandstone deposits (Blum and Pecha, 2014; Finzel, 2014), and Paleocene paleoriver deposits (Blum and Pecha, 2014) (Fig. 8). Acadian-aged zircons may been derived from recycling of Paleozoic strata, however, the southern sample contains elongate kyanite grains that likely correlate to the kyanite-staurolite amphibolite facies zones in the central-northern Appalachians suggesting direct sediment source from Appalachian Orogen or Appalachian foreland basin (Blum and Pecha, 2014; Osberg et al., 1989). Blum and Pecha (2014) similarly noted a range in kyanite abundances in Cenomanian and Paleocene GoM samples.

The Northern and Southern Samples show relatively small input from Gondwanan Terranes (1.1% and 2.9%; i.e., Sabine and Suwanee blocks) along with the Illinois Basin (Fig. 8; Kissock et al., 2017; Potter-McIntyre et al., 2018), Forest City Basin (Fig. 8; Kissock et al., 2017; Finzel, 2014), and the Cenomanian and Paleocene MSE samples (Fig. 8; Blum and Pecha, 2014). When the Gondwanan Terranes accreted to southeastern Laurentia, foreland intracratonic and pericratonic basins accumulated sediment from the Appalachian-Ouachita Orogenic Belt and Gondwanan sources therefore, it is expected to see Gondwanan Terrane zircon ages within these basins (Coleman and Cahan, 2012; Blum and Pecha, 2014) (Fig. 10). Blum and Pecha (2014)

suggest that Gondwanan Terrane grains are sourced from the Appalachian foreland basin based on the ~800–500 Ma age signature in samples from the Appalachian foreland basin in Becker et al. (2005).

All samples in Figure 8 show major to minor age peaks in MCGRP ages (~1,456–1,354 Ma). The Northern Sample contains 9.9% MCGRP grains with an age peak of ~1,426 Ma while the Southern Sample contains 4.5% MCGRP grains and contains two lower age peaks of ~1,354 Ma and ~1,490 Ma. The appearance of a high percentage MCGRP grains into the Ripley Fm would suggest two possible sediment sources: (1) Paleozoic intracratonic basins and (2) the exposed Precambrian rocks within the MCGRP (Van Schmus et al., 1996). Neoproterozoic and Paleozoic basins host sediments that have undergone recycling before deposition, leading to a wide age spectra (Archean to Cenozoic) of grains present in a single sample. The only outcrops of the MCGRP from which Mesoproterozoic grains may have originated are in the St. Francois Mountains (southeast Missouri), the highest points of the Arbuckle Mountains (south-central Oklahoma), and the Spavinaw Creek area (northeastern Oklahoma) (Van Schmus et al., 1996) because the remaining Precambrian basement terranes are buried beneath Phanerozoic sediments. Cenozoic subsidence and Quaternary southern tilting of the MSE resulted from the underlying Reelfoot Rift zone and would have created a direct sediment route from surrounding areas to the MSE. However, MCGRP aged grains from Oklahoma and Missouri would not have drained this way making the source for MCGRP aged zircons recycled sediment from the intracratonic basins (Fig. 10).

Superior and Wyoming aged grains show prominent peaks in the Northern Illinois Basin (Kissock et al., 2017), Forest City Basin (Kissock et al., 2017; Finzel, 2014), and the Paleo-

Tennessee Paleocene Wilcox Group samples (Blum and Pecha, 2014) (Fig. 8). A small population of Superior and Wyoming aged grains are observed in the Cenomanian Tuscaloosa Sample of Blum and Pecha (2014), the Paleocene Wilcox Tennessee and Mississippi paleo-River samples of Blum and Pecha (2014), and the southern Illinois Maastrichtian McNairy sandstones of Potter-McIntyre et al. (2018). The lack of Archean aged grains in the Blum and Pecha (2014) samples support that older aged grains are from recycled sources and are not directly sourced from the Minnesota, Wisconsin, and Canadian Superior regions (Fig. 8). Gleason et al. (2002) suggested an Ordovician shift from Archean Superior Province and MCGRP ages to a dominant Appalachian-Grenville in sediment influx of strata in western Oklahoma and central Arkansas. The Cenomanian Woodbine samples from Blum and Pecha (2014) show a large input of previously recycled sediment from the Ouachita fold and thrust belt and could therefore explain that the Superior signature in the Ripley Fm samples is a result of the sediment input from the same region (Blum and Pecha, 2014; Gleason et al., 2002).

This is also supported by the work of Finzel (2014) since Albian-Cenomanian Dakota Fm samples are geographically close to the Superior region. Finzel (2014) collected Albian-Cenomanian Dakota Fm samples from eastern Nebraska and Western Iowa that are statistically similar to the Northern Sample. If Cenomanian samples that are closer to the Superior and MCGRP regions do not contain strong age ranges from those provinces as well, then Superior and MCGRP age signatures are the result of sediment recycling and not direct sediment sourcing (e.g., Blum and Pecha, 2014; Finzel, 2014; Gleason et al., 2002). In addition, there is a complete absence of Yavapai-Mazatzal and Trans-Hudson/Penokean ages in the Southern Sample and only a small combined population in the Northern Sample comprising 2.2% of the sample. The

overall lack of Paleoproterozoic aged grains in the Northern and Southern samples reflects that there was likely no direct input into the north and northeastern MSE during Maastrichtian time from the south and southwestern North American igneous provinces from which these grains likely originated (Fig. 5 and 10). The small age population in the northern sample is attributed to recycling of Paleoproterozoic sediment into distal sources that then drained into the MSE.

The Southern Sample is statistically comparable to the Cenomanian Tuscaloosa Fm detrital zircon ages (P-value = 0.652) and the Paleo-Tennessee Paleocene Wilcox Group samples detrital zircon ages (P-value = 0.165) discussed by Blum and Pecha (2014). Data was compared from the Cenomanian and Paleogene rim of fluvial sediments on both sides of the MSE and Cretaceous sediments within the Alberta Oil Sands Areas within the Western Canada Sedimentary Basin (Blum and Pecha, 2014). The data support a westerly drainage system extending from the Appalachian Mountains into the Western Interior Seaway (WIS) continuing from the Permian through the Early Cretaceous. At the end of the Early Cretaceous, the retreat of the WIS rerouted all sediment drainage from west to east and the southern river systems joined the ancestral Mississippi River and other Appalachian-sourced systems (Blum and Pecha, 2014).

Finzel (2014) expanded on the work of Blum and Pecha (2014) by analyzing mid to Late Cretaceous midcontinent sediments in the Forest City Basin (FCB). These data suggest that foredeep Cordilleran foreland basin sediment was sourced from the Appalachians and traveled >2000 km across the midcontinent before being deposited and shifted to backbulge deposition after Albian time (Finzel, 2014). K-S statistical analysis shows that the Northern Sample is similar to the Albian-Cenomanian strata of the Dakota Fm in western Iowa and eastern Nebraska

(P-value = 0.083) (Finzel, 2014). The similarities in ages of the Albian-Cenomanian Dakota Fm and Maastrichtian Ripley Fm support that the Appalachian-Ouachita cordillera was a major sediment source for the FCB in the Cenomanian that shifted to the northeastern MSE during the Maastrichtian based on paleodrainage configurations from Blum and Pecha (2014) (Fig. 10). Since the Northern and Southern Samples are similar to both the work of Blum and Pecha (2014) and Finzel (2014), the Appalachian-Ouachita foreland basin and fold and thrust belt, Ripley Fm sediments are likely sourced from the same areas.

5.3. Stratigraphic Correlation and Depositional Environments of Ripley Formation Bentonites

The Late Cretaceous marked a time of accumulation of marine and non-marine siliciclastic and carbonate sedimentary rocks derived from the deltaic influx of sediment (Mancini et al., 1996), from the ancestral Mississippi River (Potter-McIntyre et al., 2018) and the Appalachian foreland basin (Blum and Pecha, 2014). Upper Cretaceous strata of the MSE and Gulf Coastal Plain (GCP) are horizontal and show no effects of tectonism (Mancini et al., 1996) but the syndepositional tectonic characteristics of the MSE (i.e., rifting and south plunging) are related to the reactivation of the Paleozoic Reelfoot Rift at the beginning of the Late Cretaceous (Cox and Van Arsdale, 1997). The Santonian to Maastrichtian MSE and GCP sedimentary rocks are composed of 270 m of nonmarine, marginal marine, and marine siliciclastics and carbonates that show a transgressive shoreline, shelf margin that is primarily siliciclastic, and a deeper basin deposits comprised of siliciclastic and shelf carbonates (Mancini et al., 1995; Russel and Keady, 1983).

The Demopolis Chalk and the older Ripley Fm units fall within the deeper basin environments (Mancini et al., 1996). The McNairy Sand and Chiwapa Sandstone Member of the

Ripley Fm belong to the shoreline and shelf margin environment along with the overlying Owl Creek Fm. Deposition of sediments in northeast and central Mississippi include a combination of marginal marine (i.e., fluvio-deltaic), shallow marine (i.e., upper and lower shoreface), and deeper marine (i.e., shelf) environments (Mancini et al., 1996; Pryor, 1960).

Pryor (1960) gives a detailed summary of the transgressive and regressive cycles that deposited the Ripley Fm. A marine transgression deposited the chalks and calcareous clays of the Selma Group as subsidence of the MSE continued. This was followed by a large influx of sediment from the Pennsylvanian sandstones of the Illinois Basin (Potter-McIntyre et al., 2018), and deposition of the McNairy Sand in the northern MSE and middle Ripley along the TN and MS Cretaceous margin. These coarse grained sands make up the middle Ripley that underlies the CSM observed at the northern and southern bentonite locations. The McNairy Sandstone deltaic deposits prograded to the south, filling the northern MSE until they covered the Coffee Fm and Selma Fm (Demopolis Chalk) deposited in a transitional marine environment. The prograding delta front combined with uplift in the northern MSE caused a swift regression of the MSE (Pryor, 1960). A transgression then resulted in the reworking of younger deltaic sediments and the deposition of the upper Ripley Fm. Deposition of the upper Ripley was then followed be a hiatus and then deposition of the Owl Creek Fm. The accumulation of the Pontotoc bentonites would have required a low energy environment between the reworking of the middle Ripley sands and the deposition of the overlying Owl Creek Fm. A low energy environment is represented by the increasing ratio of clay to sand in the Ripley Fm when moving from coarse clastic sediments in the northern MSE to the finer clastic material in the southern Ripley Fm into MS. Volcanic activity in the Late Cretaceous was mainly intrusive, but the Ripley Fm bentonites

recognized by Priddy (1943) and Mellen (1958) suggest that extrusive volcanics related to MSE Cretaceous and Paleogene/Neogene volcanism are responsible for producing the volcanic ash that comprises the previously mined bentonites. These bentonites are not laterally extensive within the MSE, indicating that there was not enough ejected tephra created by Late Cretaceous volcanic events to substantially infill a portion of the MSE (Pryor, 1960).

The end of the Late Cretaceous was marked by rapid regressions, which exposed the newly deposited sediments to erosion and weathering, resulting in the alteration and transport of the sediment, which might explain the scarceness of these bentonite lenses throughout Pontotoc County, MS (Pryor, 1960). The northern and southern bentonite beds are not the pure blue/greyish bentonites described by Priddy (1943). The bentonites mined in the 1940s underlie the sandy-limestone unit of the CSM, but the northern and southern location bentonites overly the CSM. The stratigraphic positions of the northern and southern bentonites were confirmed at the northern location based on the presence of a wide variety of macrofossils including: belemnites, brachiopods, echinoids, *Exogyra*, gastropods, shell fragments, and possible crab fragments. The two most important macrofossils recovered from the CSM, however, are *Hardouina* (echinoderm) and *Sphenodiscus* (cephalopod) (Priddy, 1943). The type locality of the CMS in Pontotoc County contained *Exogyra costata*, *Harduouina mortonis*, and *Sphenodiscus lenticularis* (Mellen, 1958). The presence of *Sphenodiscus lobatus* in strata in the northern GoM, northeastern Texas, Alabama, Mississippi is associated with the high stand systems tract noted by Haq et al. (1988), implying that the CSM was deposited in a transgressive setting (Larina et al., 2016). The type locality of the CSM contains *Sphenodiscus lenticularis*, while the ammonite found at the northern location was identified as *Sphenodiscus lobatus*. However,

Priddy (1943) recognizes the upper Ripley Fm to be *Sphenodiscus* bearing and not particular to the species.

The CSM would have had to be deposited in a nearshore-deltaic environment that had sediment input into system a capable of accumulating carbonates while mixing with clastic sediment. In a typical marine transgressive sequence, it would be expected to see sand above clay materials, which lie directly above the limestone facies, however, at the northern and southern sample locations in Pontotoc County, the sandy-limestone unit is overlain by fine to medium poorly sorted sands. This means that after the transgression that deposited the middle Ripley a regression would have occurred so rapidly that the landward deltaic sediments covered the CMS sandy limestone. After the deposition of McNairy strata and a pause in MSE subsidence, a rapid landward transgression of the sea resumed due to the reactivation of MSE subsidence (Pryor, 1960). Wavy bedding occurs in the lower bounding sand at the southern location. The wavy bedding was measured ~1 to 2 m beneath the sand/bentonite contact indicating that after deposition of the sandy limestone of the CMS was dominated by either shelf sediments, tidal areas, or depositional environments with energy levels that vary over time (Pryor, 1960).

The sand unit overlying the sandy fossiliferous limestone unit at the northern location does not show any signs of body fossils, but does show possible *Ophiomorpha* burrows ~3 m below the contact of the sandy-limestone and underlying sand. However, the southern location does contain a likely *Ophiomorpha* boxwork burrow network in the lower bounding sand to the bentonite. The burrows are likely *Ophiomorpha* due to the diameter and network architecture observed. The characteristic pelleted wall of the *Ophiomorpha* was poorly preserved (Fig. 3).

Ophiomorpha is a well-known trace fossil that is correlative to Mesozoic sand shallow marine facies that include near shore depositional environments such as lagoons, estuaries, intertidal zones, and shorefaces (Pollard et al., 1993) but has also been observed in deep offshore turbidite deposits (e.g. Crimes, 1977; Crimes et al., 1981). *Ophiomorpha* is recognized in non-marine facies from the Lower Cretaceous fluvio-deltaic and lacustrine strata in southern England (Kennedy and MacDugall, 1969). The combined presence of *Ophiomorpha* and wavy bedding is an indication of an energy change in the depositional environment after the deposition of the CMS. It is possible that as the Late Cretaceous seas were regressing due to the shift to sandy-clay deposits overlying the sandy limestone unite of the CSM. The MSE was continuously subsiding and allowing deltaic sands to accumulate while maintaining a higher water level. In addition, there is no other evidence that the *Ophiomorpha* formed in a turbidite deposit at this location.

Pryor and Glass (1961) studied the ideal depositional environments for clay accumulation during the Cretaceous and Paleogene/Neogene. The study found that the McNairy and Tuscaloosa Fm (Cretaceous) and overlying Eocene strata are mainly kaolinite, while the Owl Creek, Clayton, and Porters Creek Fms along with underlying Selma Fm strata (to the south) to the south are dominantly montmorillonite. X-ray diffraction performed on the four samples of this study show that the northern samples are predominantly kaolinitic while the southern samples contain primarily montmorillonite (Fig. 9, Appendix C). Pryor and Glass (1961) refer to the Ripley Fm as the McNairy Fm and Ripley Fm will be used forward in this discussion in place of the McNairy Fm.

The northern XRD samples of this study (TR-01, TR-04) contain quartz, kaolinite, illite, muscovite, and montmorillonite (Table 2A, 2B). Sample TR-01was collected at the top of the bentonite and contains, in decreasing weight percent, quartz (49.8%), kaolinite (21.9%), muscovite (13.9%), illite (10.8%), and montmorillonite (3.6%) (Table 2A, 2B). The sample collected from the lower portion of the bentonite (TR-04) is composed of quartz (56.8%), kaolinite (17.2%), illite (10.0%), muscovite (9.7%), and montmorillonite (6.2%). The similar percentages of kaolinite, illite, and montmorillonite in sample TR-04 compare to clays of the Coon Creek, northern Selma Fm (Demopolis Chalk and Sardis Fm) and southern Coffee Sands according to Pryor and Glass (1961). Sample TR-01 however has kaolinite, illite, and montmorillonite percentages that differ more than sample TR-04 and compare more to the kaolinite-rich clays of the Ripley Fm, Tuscaloosa Fm and Coffee Sand that uncomformably underlies the Demopolis Chalk (Fig. 2). The northern bentonite location is stratigraphically higher than the sandy-limestone of the CMS and supports the relationship between kaolinite and a fluvio-deltaic depositional environment in the upper Maastrichtian strata in northeast MS. This does not explain the relationship between the similar percentages of kaolinite, illite, and montmorillonite in sample TR-04. A possible explanation would be that there was a transition in depositional environments of the clays from a shallow marine shelf capable of accumulating fine ash material to a more fluvio-deltaic system that increased the input of clays into the system, but Pryor and Glass (1961) suggest that kalinite, illite, and montmorillonite are characteristic of offshore shelf environments.

Both southern samples (Pontotoc-1 and Pontotoc-2) contain a high percentage of montmorillonite (Table 2C, 2D). Sample Pontotoc-1 contains quartz (39.9%), montmorillonite

(20.4%), muscovite (14.1%), illite (12.3%), kaolinite (9.0%), and birnessite (4.1%) (Table 2C, 2D). The higher amount of montmorillonite than illite, and kaolinite in the southern sample compares to the montmorillonite rich clays described by Pryor and Glass (1961) in the Porters Creek, Clayton, Owl Creek Fm, and southern Selma Fms. Sample Pontotoc-2, was collected at the base of the southern bentonite and contains a slightly higher amount of quartz (46.0%) along with muscovite (16.5%), kaolinite (16.0%), illite (10.4%), montmorillonite (7.8%), birnessite (2.9%) (Table 2C, 2D). The similar percentages of kaolinite, illite, and montmorillonite collected at the base of the bentonite in the southern location suggest that the bentonite is comparable to a prodelta or shelf environment. The montmorillonite-rich bentonite collected at the top of the southern sample location did appear to have a more pure bentonite that has the more distinct grey color of purer bentonites in Pontotoc County (Priddy, 1943). The shift in clay composition from the base of the southern bentonite when compared to the depositional environment classifications of Pryor and Glass (1961) as shifting from a inner marine shelf environment to an outer marine shelf environment. The change in mineral composition coincides with the transgressions that occurred in the late Maastrichtian (Pryor, 1960; Mancini et al., 1996) and is further supported by the occurrence of the shallow marine *Ophiomorpha* in the lower bounding sand beneath the bentonite (Pollard et al., 1993). The amount of montmorillonite increases upward from the base of the bentonite (Table 2C, 2D) and can be attributed to the overall size difference in montmorillonite grains, which tend to be smaller compared to kaolinite and illite and is observed in a fining upward sequence at the southern location (Fig. 4) (Pryor and Glass, 1961). However, montmorillonite-rich clays occur largely in the Porters Creek, Clayton, Owl Creek, and southern Selma Fms, excluding the Ripley Fm from

the possibility of clay deposition in a shallow marine shoreface/delta-front zone. Therefore, two assumptions can be made: (1) the CMS portion of the Ripley Fm has a higher abundance of montmorillonite than is previously documented (Pryor, 1960; Pryor and Glass, 1961) or (2) the montmorillonite-rich southern samples are altered volcanic ash deposits as initially made known by Mellen (1958).

In order for ash deposits with clastic sediments to accumulate in marginal marine or shallow marine environments, there would have to be terrigenous clastic sediment, in this case from the Appalachian foreland basin along with minor input from the intracratonic basins, being mixed into the system but low enough energy to allow ~3.5 to 2 m of bentonites to accumulate in the northern and southern locations. No volcanogenic material corresponding from late Maastrichtian time was recovered from the northern and southern bentonite samples in this study. The Owl Creek Fm overlies the upper Ripley and if a shift from montmorillonite-rich clay to kaolinite-rich and back to montmorillonite clay occurred, this would suggest that a calmer period of fluvial input or erosion preceded the deposition of the Owl Creek which unconformably overlies the Ripley Fm (Fig. 2). Late Cretaceous sediment input into the MSE is likely sourced from the Appalachian foreland basin, which primarily contains dominant Grenville aged grains and Appalachian derived grains from the Blue Ridge and Piedmont regions with some input from the northern ancestral Mississippi (this study, Blum and Pecha, 2014; Potter-McIntyre et al., 2018; Pryor and Glass, 1961).

6. CONCLUSIONS

Sediment input into the northeastern Mississippi Embayment (MSE) during the Late Maastrichtian was likely sourced from the Appalachian foreland basin with minor input from the midcontinent region by routing sediment through the Reelfoot Rift trough at the apex the ancestral Mississippi River (Pryor and Glass, 1961; Blum and Pecha, 2014; Finzel, 2014; Potter-McIntyre et al., 2018). Appalachian foreland basin sourcing is based on the statistical similarities to the detrital zircon ages of Albian-Paleocene strata of the MSE and Forest City Basin (FCB) and the upper Maastrichtian strata of Pontotoc County, MS, which had not previously been analyzed in northeastern Mississippi (Blum and Pecha, 2014; Finzel 2014). The similar detrital zircon ages of this study compared to Albian-Cenomanian strata of the FCB support that sediment transported across the continent before the Early Cretaceous (Finzel, 2014).

The montmorillonite-rich southern location provides a multitude of evidence that the bentonites were deposited during a transgression based on lithostratigraphy, biostratigraphy, and mineralogical composition of the bentonites. The high abundance of heavy minerals such as muscovite and kyanite, along with the large number of Acadian and Alleghanian aged grains within the sample also support that sediment sources during the marine regression of upper Ripley strata followed the transgressive accumulation of middle Ripley strata are likely from the

Appalachian foreland basin and the Blue Ridge and Piedmont regions (Pryor; 1960; Blum and Pecha, 2014). The northern samples are kaolinite-rich, suggesting fluvial input into a shallow marine system (Pryor and Glass, 1961). The deposition of the Pontotoc bentonites would have had to occur after the reworking of middle Ripley strata and prior to the overlying Owl Creek Fm deposition during the late Maastrichtian in a low energy environment capable of accumulating Appalachian derived sediment or volcanic ash and weathering it.

Therefore, understanding the depositional environments in which the Pontotoc bentonites accumulated might reveal the occurrence of bentonite deposits elsewhere in the MSE and Gulf Coastal Plain and a younger volcanic event that occurred at the end of Maastrichtian time. If a younger volcanic event was responsible for the sediment supply of the upper Ripley Fm bentonites, then a younger source of volcanism may have occurred at the end of Maastrichtian time (~70-60 Ma) than what is already known. Also, if the bentonites are volcanic in origin then other bentonite deposits high in montmorillonite and of economic importance may be present throughout Pontotoc County, MS and other portions of the MSE.

REFERENCES

Alsalem, O.B., Fan, M., Zamora, J., Xie, X., Griffin, W.R., 2018. Erratum: Paleozoic sediment dispersal before and during the collision between Laurentia and Gondwana in the Fort Worth Basin: USA. Geosphere 14, 325–342. doi:10.1130/GES01480.1.

Barnett, R., 1975. Basement structure of Florida and its tectonic implications. Transactions Gulf Coast Association of Geological Societies 25, 122–142.

Becker, T.P., Thomas, W.A., Samson, S.D., Gehrels, G.E., 2005. Detrital zircon evidence of Laurentian crustal dominance in the lower Pennsylvanian deposits of the Alleghanian clastic wedge in eastern North America. Sedimentary Geology, 182, 59–86. doi:10.1016/j.sedgeo.2005.07.014.

Bennett, V.C., DePaolo, D.J., 1987. Proterozoic crustal history of the western United States as determined by neodymium isotopic mapping. Geologic Society of America Bulletin 99, 674–685. doi: 10.1130/0016-7606(1987)99<674:PCHOTW>2.0.CO;2.

Berry, W.B.N., Boucot, A.J., 1970. Correlation pf the North American Silurian rocks. Geological Society of America Special Paper 102, p. 289 p.

Bickford, M.E., Wooden, J.L., Bauer R.L., 2006. SHRIMP study of zircons from Early Archean rocks in the Minnesota River Valley: Implications for the tectonic history of the Superior Province. Bulletin of the Geological Society of America 118 (1–2), 94–108. doi:10.1130/B25741.1.

Bickford, M.E., Van Schmus, W.R., Karlstrom, K.E., Mueller, P.A., Kamenov, G.D., 2015. Mesoproterozoic-trans-Laurentian magmatism: A synthesis of continent-wide age distributions, new SIMS U-Pb ages, zircon saturation temperatures, and Hf and Nd isotopic compositions: Precambrian Research 265, 286–312. https://doi.org /10.1016/j .precamres.2014.11.024.

Billings, M.P., 1956. The geology of New Hampshire: Part II Bedrock geology: New Hampshire State Planning and Development Commission, 204 p.

Black, L.P., Kamo, S.L., Williams, I.S., Mundil, R., Davis, D.W., Korsch, R.J., Foudoulis, C., 2003. The application of SHRIMP to phanerozoic geochronology: a critical appraisal of four zircon standards. Chemical Geology 200, 171–188.

Blum, M., Pecha, M., 2014. Mid-cretaceous to paleocene North American drainage reorganization from detrital zircons: Geology 42, 607–610, doi:10.1130/G35513.1.

Boehm, C.O., Heaman, L.M., Creaser, R.A., Corkery, M.T., 2000. Discovery of pre–3.5 Ga exotic crust at the northwestern Superior Province margin, Manitoba. Geology 28, 75–78, doi: 10.1130/0091-7613(2000)028<0075:DOPGEC>2.3.CO;2.

Bradley, D.C. 1983. Tectonics of the Acadian orogeny in New England and adjacent Canada. Journal of Geology 91, pp. 381-400.

Calvert, A.J., Ludden, J.N., 1999. Archean Continental assembly in the southeastern Superior Province of Canada. Tectonics 18, 412-429.

Chandler, V.W., Boerboom, T.J., Jirsa, M.A., 2007. Penokean tectonics along a promontory embayment margin in east-central Minnesota. Precambrian Research 157, 26–49.

Chidester, A.H., 1968. Evolution of the ultramafic complexes of northwestern New England. In: Zen, E-an, White, W. S., Hadley, J. B., and Thompson, J. B., (Eds.), Studies of Appalachian Studies of Appalchain geology: Nothern and maritime: New York, Wiley Interscience, New York, pp. 343-354.

Chiu, S.-C.C., Chiu, J.M., Johnston, A.C., 1997. Seismicity of the southeastern margin of Reelfoot rift, central United States. Seismological Research Letters 68, 785–796.

Chowns, T., Williams, C., 1983. Pre-Cretaceous rocks beneath the Georgia coastal plain—regional implications. In: Gohn, G. (Eds.), Studies related to the Charleston, South Carolina, earthquake of 1886—tectonic and seismicity. U.S. Geological Survey Professional Paper 1313, pp. L1–L42.

Clift, P.D., Heinrich, P., Dunn, D., Jacobus, A., Blusztajn, J., 2018. The Sabine block, Gulf of Mexico: Promontory on the North American Margin?. Geology 46, 15-18.

Coleman, J.L. Jr., Cahan, S.M., 2012. Paleozoic Sedimentary Basins of the United States: U. S. Geological Survey Open File Report 2012-1111.

Condie, K.C., 1992. Proterozoic terranes and continental accretion in southwestern North America. In: Condie, K.C., (Ed.), Proterozoic crustal evolution: Amsterdam, Elsevier, pp. 447–480.

Corfu, F., Davis, D.W., 1992. A U-Pb geochronological framework for the western Superior Province, In: Thurston, P.C., Williams, H.R., Sutcliffe, R.H., and Stott, G.M. (Eds.), Geology of Ontario: Ontario Geological Survey Special Volume 4, Pt. 2, p. 1335–1346.

Cox, R.T., Van Arsdale, R.B., Harris, J. B., Larsen, D., 2001. Neotectonics of the southeastern Reelfoot rift zone margin, central United States, and implications for regional strain accommodation: Geology 29, 419–422. doi:10.1130/0091-7613(2001)029<0419:NOTSRR>2.0.CO;2.

Cox, R.T., Van Arsdale, R.B., 1997. Hotspot origin of the Mississippi embayment and its possible impact on contemporary seismicity. Engineering Geology 46, 201–216. doi:10.1016/S0013-7952(97)00003-3.

Craddock, J.P., Konstantinou. A., Vervoort J.D., Wirth K.R., Davidson, C., Finley-Blasi, L., Juda, N.A., E. Walker, 2013. Detrital Zircon Provenance of the Mesoproterozoic

Midcontinent Rift, Lake Superior Region, U.S.A. Journal of Geology 21 (1), 57–73. doi:10.1086/668635.

Cramer, F., 1973. Middle and Upper Silurian chitinozoan succession in Florida sub-surface. Paleontology 47, 279–288.

Crimes, T.P., 1977. Trace fossils of an Eocene deep-sea fan, northern Spain. In: Crimes, T.P. and Harper, J.C. (Eds.), Trace fossils 2. Geological Journal Special Issue 9, 71-90.

Crime, T.P., Goldring, R., Homewoodv, P., Van Stuijevenberg, J., Winkler, J., 1981. Trace fossil assemblages of deep-sea deposits, Gurnigel and Schlieren flysch (Cretaceous-Eocene), Switzerland. Eclogae geologica Helvetica 74, 953-995.

Csontos, R., Van Arsdale, R., Cox, R.T., Waldron, B., 2008. Reelfoot rift and its impact on Quaternary deformation in the central Mississippi River valley. Geosphere 4, 145-158. doi:10.1130/ges00107.1.

Cushing, E.M., E. H. Boswell, and R. L. Hosman, 1964. General geology of the Mississippi embayment: U.S. Geological Survey Professional Paper 448-B. 448 p.

Dart, R.L., Swolfs, H.S., 1998. Contour mapping of relic structures in the Precambrian basement of the Reelfoot Rift: North American Midcontinent. Tectonics 17, 235–249.

David, J., Parent, M., Stevenson, R., Nadeau, P., Godin, L., 2003. The Porpoise Cove supracrustal sequence, Inukjuak area: A unique example of Paleoarchean crust (ca. 3.8 Ga) in the Superior Province. Geological Association of Canada Program with Abstracts, v. 28, no. 355.

Dickinson, W.R., Gehrels, G.E., 2009. Use of U-Pb ages of detrital zircons to infer maximum depositional ages of strata: A test against a Colorado Plateau Mesozoic database. Earth and Planetary Science Letters 288, 115-125.

Dennis, A.J., Wright J.E., 1997. The Carolina terrance in northwestern South Carolin, U.S.A.: Late Precambrian-Cambrian deformation and metamorphism in a peri-Gondwanan oceanic arc. Tectonics 16, 460-473.

Dickinson, W.R., Gehrels, G.E., 2009. U-Pb ages of detrital zircons in Jurassic eolian and associated sandstones of the Colorado Plateau: Evidence for transcontinental dispersal and intraregional recycling of sediment. Geological Society of America Bulletin 121, 408–433, doi:10.1130/B26406.1.

Dockery, D.T., III, 2008. Mesozoic stratigraphic units in Mississippi: Mississippi Geology, v. 17, no. 1, p. 1-8.

Dockery, D.T., and D.E. Thompson, 2017. The Geology of Misisssissippi: University of Mississippi Press, Oxford MS, pp. 221-233.

Drake, A.A., Sinha, A.K., Laird, J., Guy, R.E., 1989. The Taconic orogen. In: Hatcher, R.D., Jr., et al., (Eds.), The Appalachian-Ouachita orogen in the United States: Boulder, Colorado, Geological Society of America, Geology of North America F-2, pp. 101-177.

Duncan, J., 1998. Geologic History of an Accreted Terrane: Paleozoic Stratigraphy of the North Florida Basin, Suwannee Terrane. Florida State University (dissertation (UMI#9905409)).

Ervin, C.P., McGinnis, L.D., 1975. Reelfoot rift: Reactivated precursor to the Mississippi embayment: Geological Society of America Bulletin 86, 287–1295. doi:10.1130/0016-7606(1975)86<1287:RRRPTT>2.0.CO;2.

Finzel, E.S., 2014, Detrital zircons from Cretaceous midcontinent strata reveal an Appalachian Mountains–Cordilleran foreland basin connection: Lithosphere 6, 378–382. doi:10.1130/l400.1.

Gates, O., 1975. Geological map and cross-section of the Eastport Quadrangle, Washington County, Maine: Maine Geological Survey. Geologic Map Series 3, 62,500.

Geoseps Services, LLC., 2019. GSS Zircon U-Pb Dating Methodology, p. 1-6.

Gleason, J.D., Finney, S.C., Gehrels, G.E., 2002. Paleotectonic implications of a Mid- to Late Ordovician provenance shift, as recorded in sedimentary strata of the Ouachita and southern Appalachian mountains. Journal of Geology 110, 291–304. doi:10.1086/339533.

Garrote, J., Cox, R. T., Swann, C., Ellis, M., 2006. Tectonic geomorphology of the southeastern Mississippi Embayment in northern Mississippi, USA. Geological Society of America Bulletin 118 (9–10), 1160–1170. doi:10.1130/B25721.1.

Gehrels, G., 2010. K-S Test (2010), from https://docs.google.com/document/d/1MYwm8GcdYFOsfNV62B6PULb_-g2r1AS3vmm4gHMOFxg/preview.

Gehrels, G., Way, I., 2015. Cumulative age probability plots (2010), from https://docs.google.com/document/d/1MYwm8GcdYFOsfNV62B6PULb_-g2r1AS3vmm4gHMOFxg/preview.

Gower, C., Krogh, T.E., 2002. A U–Pb geochronological review of the Proterozoic history of the eastern Grenville Province: Canadian Journal of Earth Sciences 39, 795-829.

Guynn, J., Gehrels, G., 2010. Comparison of Detrital Zircon Age Distributions Using the K-S Test. University of Arizona, 1-16. Online version at: https://docs.google.com/document/d/1MYwm8GcdYFOsfNV62B6PULb_-g2r1AS3vmm4gHMOFxg/preview.

Haq, B.L., Hardenbol, J., Vail, P.R., 1988. Mesozoic and Cenozoic chronostratigraphy and cycles of sea-level change. In: Sea - level changes an integrated approach (Eds.), Wilgus, C.K., Hastings, B.S., Ross, C.A., Posamentier, H.W., Van Wagoner, J.C., Kendall, C.G. St. C.), p. 71 – 108 (SEPM Special Publication 42) .

Hatcher, R.D., Jr., Thomas, W.A., Geiser, P.A., Snoke, A.W., Mosher, S., Wiltschko, D.V., 1989. Alleghanian orogen. In: Hatcher, R.D., Jr., et al., (Eds.), The Appalachian-Ouachita orogen in the United States: Boulder, Colorado, Geological Society of America, Geology of North America F-2, pp. 233–318.

Hatcher, R.D. Jr., Bream, B.R., Merschat, A.J., 2007. Tectonic map of the southern and centra; Appalachians, USA. In: Hatcher, R.D. Jr., Carlson, M.P., McBride, J.H., Martínez Catalán, J.R. (Eds.), Memoir 200: The 4-D Framework of Continental Crust. Geological Society of America, pp. 595-632.

Hatcher, R.D. Jr., 2010. The Appalachian orogen: a brief summary. In: Tollo, R., Bartholomew, M., Hibbard, J., Karabinos, P. (Eds.), Memoir 206: From Rodinia to Pangea: the lithotectonic record of the Appalachian region. Geological Society of America, pp. 1–20.

Hildenbrand, T.G., 1985. Rift structure of the northern Mississippi Embayment from the analysis of gravity and magnetic data. Journal of Geophysical Research 90, 12,607–12,622.

Holm, D.K., 1999. A geodynamic model for Paleoproterozoic post-tectonic magma geneisis in the southern Trans-Hudson (Black Hills, South Dakota) and Penokean (southern Lake Superior) orogens: Rock Mountain Geolgoy, v. 34, no 2, p.183-194, doi:10.2113/34.2.183.

Hon, R., Fitzgeral, Sargent, J.P., Schwartz, W.D, 1991. Silurian-Early Devonianmafic rocks of the Piscataquis volcanic belt in Northern Maine. Atlantic Geology 28, 163-170.

Howe, J.R., 1985. Tectonics, sedimentation, and hydrocarbon potential of the Reelfoot Aulocogen [Master's thesis]: Norman, University of Oklahoma, 109 p.

Howe, J.R., Thompson, T.L., 1984. Tectonics, sedimentation, and hydrocarbon potential of the Reelfoot Rift. Oil and Gas Journal 82, 179–190.

Kane, M.F., Hildenbrand, T.G., Hendricks, J.D., 1981. Model for the tectonic evolution of the Mississippi Embayment and its contemporary seismicity: Geology 9, 563–568. doi: 10.1130/0091-7613(1981)9<563:MFTTEO>2.0.CO;2.

Kennedy, W.J., MacDougall, J.D.S., 1969. Crustacean burrows in the Weald Clay (Lower Cretaceous) of south-eastern England and their environmental significance. Palaeontology 12, 459-471.

Kissock, J.K., Finzel, E.S., Malone, D.H., Craddock, J.P., 2017, Lower – Middle Pennsylvanian strata in the North American midcontinent record the interplay between erosional unroofing of the Appalachians and eustatic sea-level rise. Geosphere 14, 141–161, doi:10.1130/GES01512.1.

Konstantinou, A., Wirth, K.R., Vervoort, J.D., Malone, D.H., Davidson, C., and Craddock, J.P., 2014. Provenance of quartz arenites of the early Paleozoic Mid-Continent region, USA. Journal of Geology 122, 201–216.

Langford, F.F., J.A. Morin, 1976, The development of the Superior province of northwestern Ontario by merging island arcs, Journal of American Science 276, 1023-1034.

Larina, E., Garb, M., Landman, N., Dastas, N., Thibault, N., Edawds, L., Phillips, G., Rovelli, R., Myers, C., and Naujokaityte, J., 2016. Upper Maastrichtian ammonite biostratigraphy of the Gulf Coastal Plain (Mississippi Embayment, southern USA). Cretaceous Research 60, 128-151.

Leier, A.L., Gehrels, G.E., 2011. Continentalscale detrital zircon provenance signatures in Lower Cretaceous strata, western North America. Geology 39, 399–402, doi:10.1130/G31762.1.

Leo. G.W., Zartman, R.E., and Brookins, D.G., 1984. Glastonbury Gneiss and mantling rocks (a modified Ordovician dome) in south-central Massachusetts and north-central Connecticut. Geochemistry, petrogenesis, and isotopic age: U.S. Geological Survey Professional Paper 1295, p. 45.

Ludwig, K.R., 2012. Isoplot 3.75. Berkley Geochronology Center. from http://www.bgc.org/isoplot_etc/isoplot.html.

Mancini, E.A., Puckett, T.M., Tew, B.H., 1996. Integrated biostratigraphic and sequence stratigraphic framework for Upper Cretaceous strata of the eastern Guld Coastal Plain, USA. Cretaceous Research 17, 645-669.

May, S.R., Gray, G.G., Summa, L.L., Stewart, N.R., Gehrels, G.E., Pecha, M., 2013. Detrital zircon geochronology from the Bighorn Basin, Wyoming, USA: Implications for tectonostratigraphic evolution and paleogeography. Geological Society of America Bulletin, 125, 403–1422, doi:10.1130/B30824.1.

Miller, C.F., Hatcher, R.D. Jr., Ayers, J.C., Coath, C.D., Harrison, T.M., 2000. Age and zircon inheritance of easter Blue Ridge plutons, southwestern North Carolina and northeastern Georgia, with implications for magma history and evolution of the southern Appalachian Oroge. American Journal of Science 300, 142-172.

Mellen F.F., 1958. Cretaceous Shelf Sediments of Mississippi: Mississippi Geological Survey Bulletin 54, 16-25.

Moecher, D.P., Samson, S.D., 2006. Differential zircon fertility of source terranes and natural bias in the detrital zircon record: Implications for sedimentary provenance analysis. Earth and Planetary Science Letters 247, 252–266.

Mueller, P.A., Heatherington, A., Shuster, R., Wooden, J., Nutman, A., Williams, I., 1994. Precambrian zircons from the Florida basement: a Gondwanan connection. Geology 22, 119–122.

Mueller, P.A., Heatherington, A.L., Foster, D.A., Thomas, W.A., Wooden, J.L., 2014. The Suwannee suture : Significance for Gondwana-Laurentia terrane transfer and formation of Pangaea. Gondwana Research 26, 365–373, doi:10.1016/j.gr.2013.06.018.

Mueller, P., 2017, LA-ICP-MS Data reduction Protocol for U-Pb Geochronology of Zircon and Titanite: University of Florida GeoPlasmaLab, Gainsville, Florida, USA.

Naylor, R.S., 1967. A field and geochronologic study of mantled gneiss domes in general New England [Ph.D thesis]: Pasadena, California Institute of Technology, p. 123.

Nelson, K.D., Zhang, J., 1991. A COCORP deep reflection profile across the buried Reelfoot rift, south-central United States: Tectonophysics 197, 271–293. doi: 10.1016/0040-1951(91)90046-U.

Opdyke, N., Jones, D., MacFadden, B., Smith, D., Mueller, P., Shuster, R., 1987. Florida as an exotic terrane: paleomagnetic and geochronologic investigation of lower Paleozoic rocks from the subsurface of Florida. Geology 15, 900–903.

Osberg, P.H., Tull, J.F., Robinson, P., Hon, R., Butler J.R., 1989. The Acadian orogen. In: Hatcher, R.D. Jr., et al., (Eds.), The Appalachian-Ouachita orogen in the United States. Boulder, Colorado, Geological Society of America, Geology of North America F-2, pp. 179–232.

Paces, J.B., Miller, J.D., 1993. Precise U-Pb age of Duluth Complex and related mafic intrusions, northeastern Minnesota: Geochronological insights into physical, petrogenetic, paleomagnetic, and tectonomagmatic processes associated with the 1.1 GA midcontinent rift system. Journal of Geophysical Research 98, 13,997-14,103.

Park, H., Rickenbaker, A., Bachmann-Krug, D., Gehrels, G.E., 2010. Application of Foreland Basin Detrital-Zircon Geochronology to the Reconstruction of the Southern and Central Appalachian Orogen. The Journal of Geology 118, 23–44. doi:10.1086/648400.

Pojeta, J., Kriz, J., Berdan, J.M., 1976. Silurian–Devonian pelecypods and Paleozoic stratigraphy of sub-surface rocks in Florida and Georgia and related Silurian pelecypods from Bolivia and Turkey. U.S. Geological Survey Professional Paper 879, 32 p.

Pollard, J.E., Goldring, R., and Buck, S.G., 1993. Ichnofabrics containing Ophiomorpha: significance in shallow-water facies interpretation. Journal of the Geological Society, London, 150, 149-164.

Potter-Mcintyre, S.L., Breeden, J.R., Malone, D.H., 2018. A Maastrichtian birth of the Ancestral Mississippi River system : Evidence from the U-Pb detrital zircon geochronology of the McNairy: Cretaceous Research, 71–79. doi:10.1016/j.cretres.2018.05.010.

Priddy. R.R., 1943. Pontotoc County Mineral Resources: Mississippi Geological Survey Bulletin 54, 16-25.

Pryor, W.A., 1960. Cretaceous Sedimentation in the Upper Mississippi Embayment. AAPG Bulletin 44, 1473-1504.

Pryor, W.A., Glass, H.D., 1961. Cretaceous-Tertiary Clay Mineralogy of the Upper Mississippi Embayment. Journal of Sedimentary Petrology 31, 38-51.

Tapani Ramo, O., McLemore, V.T., Hamilton, M.A., Kosunen, P.J., Heizler, M., Haapala, I., 2003. Intermittent 1630-1220 Ma magmatism in central Mazatzal province: New geochronologic piercing points and some tectonic implications: Geology 31, 335-338.

Rankin, D.W., 1968. Volcanism related to tectonism in the Piscataquis Volcanic belt, an island arc of early Devonian age in tnorth-central Maine. In: Zen, E., White, W.S., Hadley, J.B., Thompson, J.B. Jr. (Eds.), Studies of Appalachain geology: North maritime: New York, Interscience Publishers, pp. 355-370.

Reed, J.C., Wheeler, J.O., Tucholke, B.E., compilers, 2004. Geologic Map of North America: Decade of North American Geology Continental: Geological Society of America, Boulder. Scale Map 001, 5,000,000.

Russell, E.E., Keady, D.M., 1983. Notes on Upper Cretaceous lithostratigraphy of the eastern Mississippi Embayment. In Upper Cretaceous lithostratigraphy and biostratigraphy in northeast Mississippi, southwest Tennessee, and northwest Alabama ,shelf chalks and coastal clastics. Society of Economic Paleontologists and Mineralogists, Gulf Coast Section Guidebook, 1–15.

Sinha, A.K., 1997. Lead isotope mapping of crustal reservoirs within the Grenville superterrane: Geological Society of America, Abstracts with programs, v. 29, no. 3, p. 69.

Salvador, A., 1991. Origin and development of the Gulf of Mexico Basin, *in* The Geology of North America: Boulder, Colorado, The Gological Society of America, pp. 389–444.

Sevigny, J.H., Hanson, G.N., 1993. Orogenic evolution of the New England Appalachians of southwestern Connecticut: Geological Society of America Bulletin 105, 1591-1605.

Shaulis, B., Lapen, T.J., Toms, A., 2010. Signal linearity of an extended range pulse counting detector: Applications to accurate and precise U - Pb dating of zircon by laser ablation quadrupole ICP - MS. Geochemistry Geophysics Geosystems 11, 1–12, doi:10.1029/2010GC003198.

Shride, A.F., 1976. Stratigraphy and correlation of Newbury volcanic complex, northeastern Massachusetts, In: Page, L.R. (Ed.), Contributions to the stratigraphy of New England: Geological Society of America Memoir 148, 147-177.

Sims, P.K. 1996. Early Proterozoic Penokean orogen. In: Sims, P.K., Carter, L.M.H. (Eds.), Archean and Proterozoic geology of the Lake Superior region, USA. United States Geological Survey Professional Paper 1556, pp. 28–30.

Stark, J.T., 1997. The East Continent Rift Complex: Evidence and conclusions. In: Ojakangas, R.W., et al. (Eds.), Middle Proterozoic to Cambrian rifting: Mid-North America: Geological Society of America Special Paper 312, 253–266.

Swann, C. T., Dew, J. J., 2009. Geology of the Troy, Miss., 7.5 Minute Topographic Quadrangle Chickasaw and Pontotoc Counties Mississippi: Mississippi Mineral Resources Institute Open - File Report 09-2S, 4-11.

Thomas, W.A., 1985. The Appalachian-Ouachita connection: Paleozoic orogenic belt at the southern margin of North America. Annual Review of Earth and Planetary Sciences 13, 175–199. doi:10.1146/annurev.ea.13.050185.001135.

Thomas, W.A., 1991. The Appalachian-Ouachita rifted margin of southeastern North America. Geological Society of America Bulletin 103, 415– 431. doi: 10.1130/0016-7606(1991)103<0415:TAORMO>2.3.CO;2.

Tollo, R.P., Corriveau, L., McLelland, J., Bartholomew, M.J., 2004. Proterozoic tectonic evolution of the Grenville orogeny in North America: An introduction. In: Tollo, R.P., et al. (Eds.), Memoir 197: Proterozoic Tectonic Evolution of the Grenville Orogen in North America: Boulder Colorado: Geological Society of America, pp. 1-18.

Van Schmus, W.R., Bickford, M.E., Zietz, I., 1987,. Early and middle Proterozoic provinces in the central United States. In: Kroner, A. (Ed.), Proterozoic lithosphere evolution, Washington, D.C., American Geophysical Union, Geodynamics Series 17, 273 p.

Van Schmus, W.R., Bickford, M.E., Turek, A., 1996. Proterozoic geology of the east-central midcontinent basement. In: Van der Pluijm, B.A., Catacosinos, P.A. (Eds.), Basements and basins of eastern North America. Geological Society of America Special Paper 308, 7–32.

Walker, J.D., Geissman, J.W., Bowring, S.A., Babcock, L.E., compilers, 2018, Geologic Time Scale v. 5.0: Geological Society of America, https://doi.org/10.1130/2018.CTS005R3C. ©2018 The Geological Society of America.

Whitmeyer S.J., Karlstrom, K.E., 2007. Tectonic model for the Proterozoic growth of North America: Geosphere 3, 220–259.

Xie, X., O'Connor, P.M., Alsleben, H., 2016. Carboniferous sediment dispersal in the Appalachian–Ouachita juncture: provenance of selected late Mississippian sandstones in the Black Warrior Basin, Mississippi, United States. Sedimentary Geology 342, 191–201.

Xie, X., Buratowski, G., Manger, W.L., Worth, F., 2018. U-Pb detrital-zircon geochronology of the Middle Bloyd Sandstone (Morrowan) of northern Arkansas (U.S.A.). Implications for early Pennsylvanian sediment dispersal in the Laurentian foreland. Journal of Sedimentary Research 88, 795–810.

APPENDIX A: TABLES AND FIGURES

North American Age Provinces	Northern Samples n = 273	Southern Samples n = 376	Combined n = 649
Alleghanian (330-265 Ma)	0.0%	1.1%	0.6%
Acadian (450-320 Ma)	1.8%	10.6%	6.9%
Taconic (490-440 Ma)	3.3%	0.3%	1.5%
Gondwanan Terranes (900-500 Ma)	1.1%	2.9%	2.2%
Grenville (1350-900 Ma)	80.2%	80.1%	80.1%
MC-Granite-Rhyolite (1600-1350 Ma)	9.9%	4.5%	6.8%
Yavapi-Mazatzal (1800-1600 Ma)	1.5%	0.0%	0.6%
Trans-Hudson/Penokean (1900-1800 Ma)	0.7%	0.0%	0.3%
Superior (>2500 Ma)	1.5%	0.5%	0.9%

TABLE 1—North American Igneous Province age distribution and percentages for the Northern and Southern samples.

Northern Location XRD Analysis			
TR-01		TR-04	
Constituent	Weight %	Constituent	Weight %
Quartz	49.8	Quartz	56.9
Kaolinite	21.9	Kaolinite	17.2
Muscovite	13.9	Illite	10.0
Illite	10.8	Muscovite	9.7
Montmorillonite (Ca, Na rich)	3.6	Montmorillonite (Ca, Na rich)	6.2
Southern Location XRD Analysis			
Pontotoc-1		Pontotoc-2	
Constituent	Weight %	Constituent	
Quartz	39.9	Quartz	46.0
Montmorillonite (Na rich)	15.5	Muscovite	16.5
Muscovite	14.1	Kaolinite	16.4
Illite	12.3	Illite	10.4
Kaolinite	9.0	Montmorillonite (Ca, Na rich)	7.8
Montmorillonite (Ca, Na rich)	4.9	Birnessite	2.9
Birnessite	4.1		

TABLE 2—XRD analysis results for two northern samples (A and B) and two southern samples (C and D.)

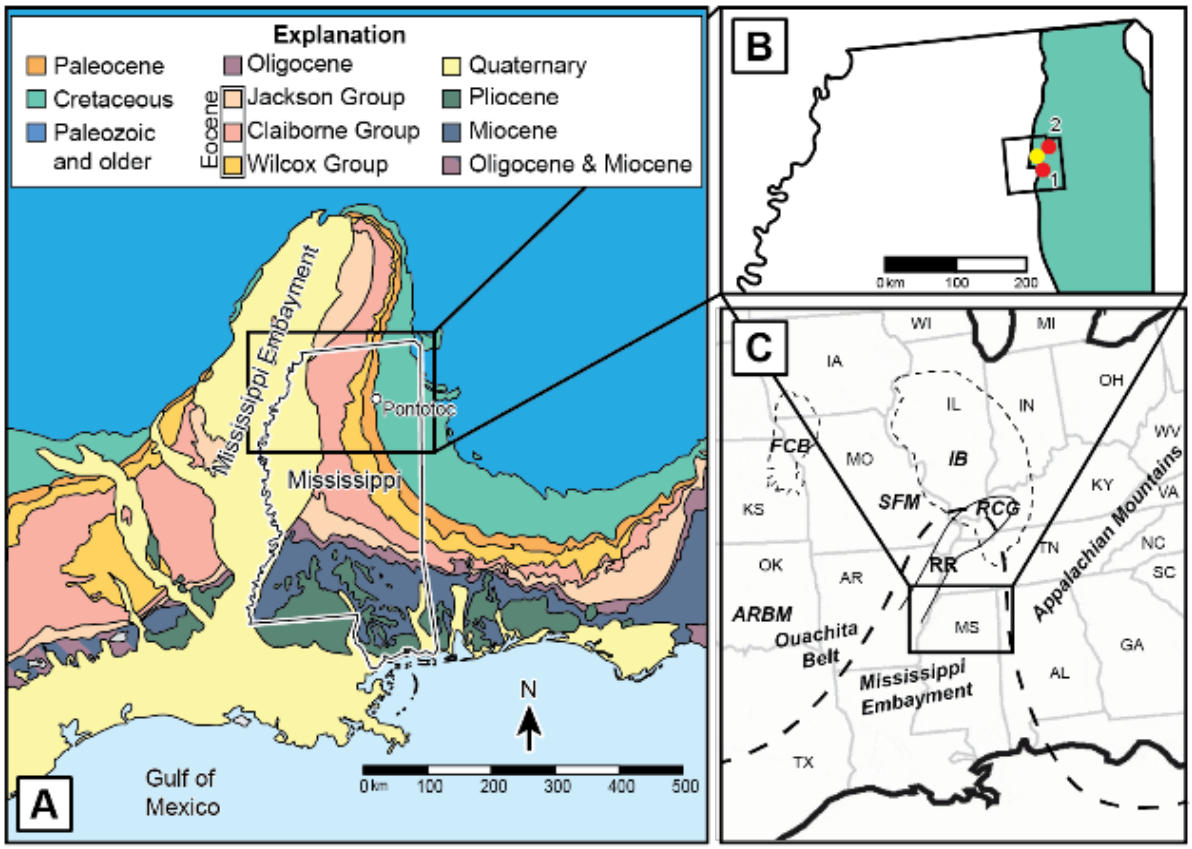

Figure 1—Cretaceous outcrops, basin locations, and structural maps of the Mississippi Embayment and central United States. **A.** Mississippi Embayment outcrops with the location of Pontotoc County, MS. **B.** Locations of (1) southern sample location dots and (2) northern sample location are marked by red dots while the previously mined bentonite location is marked by a yellow dot. **C.** Basin and structures of the central and eastern United States. ARBM-Arbuckle Mountains; FCB-Forest City Basin; IB-Illinois Basin; RCG-Rough Creek Graben; RR-Reelfoot Rift.

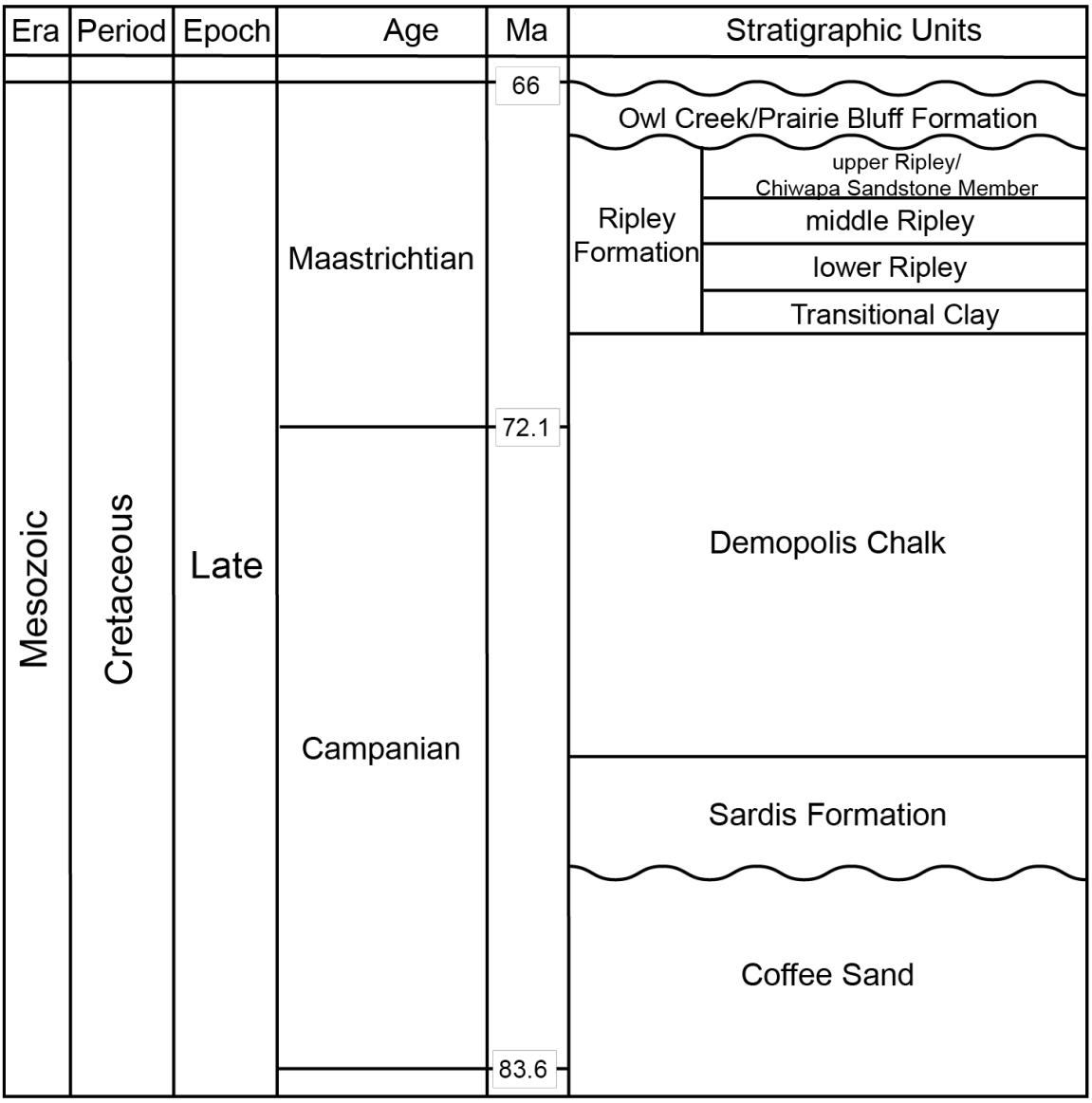

Figure 2—Generalized stratigraphic column of the late Cretaceous units of northeastern Mississippi. Modified from Swann and Dew (2009), Walker et al. (2018), and Dockery (2008).

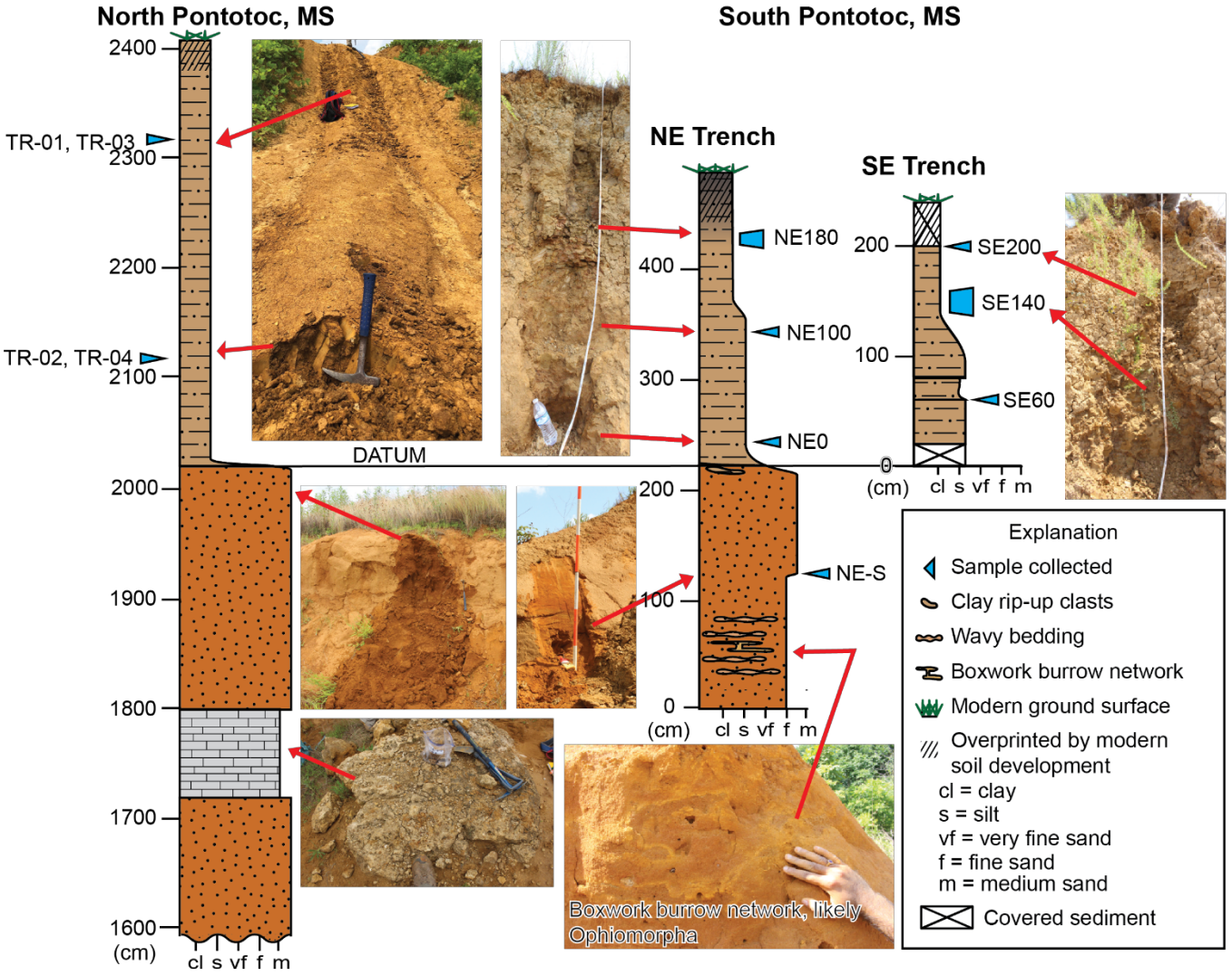

Figure 3—Stratigraphic correlation diagram of the Northern and Southern sample locations. Corresponding pictures to the lithological unit are placed alongside the stratigraphic column and the red arrows indicate specific locations within the image and stratigraphic column.

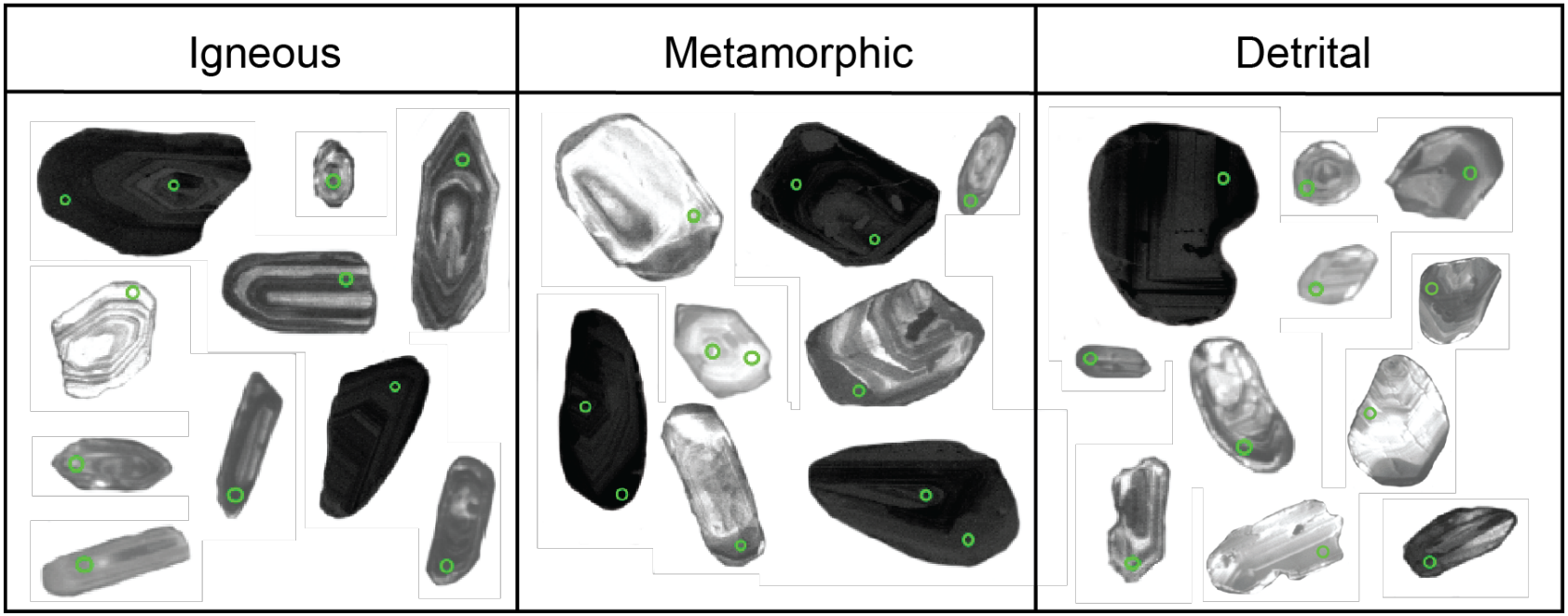

Figure 4—A range of detrital zircon morphologies and the zonation CL images grains from all 11 samples. The ~20 μm laser ablation spots are indicated by green circles on the individual grains

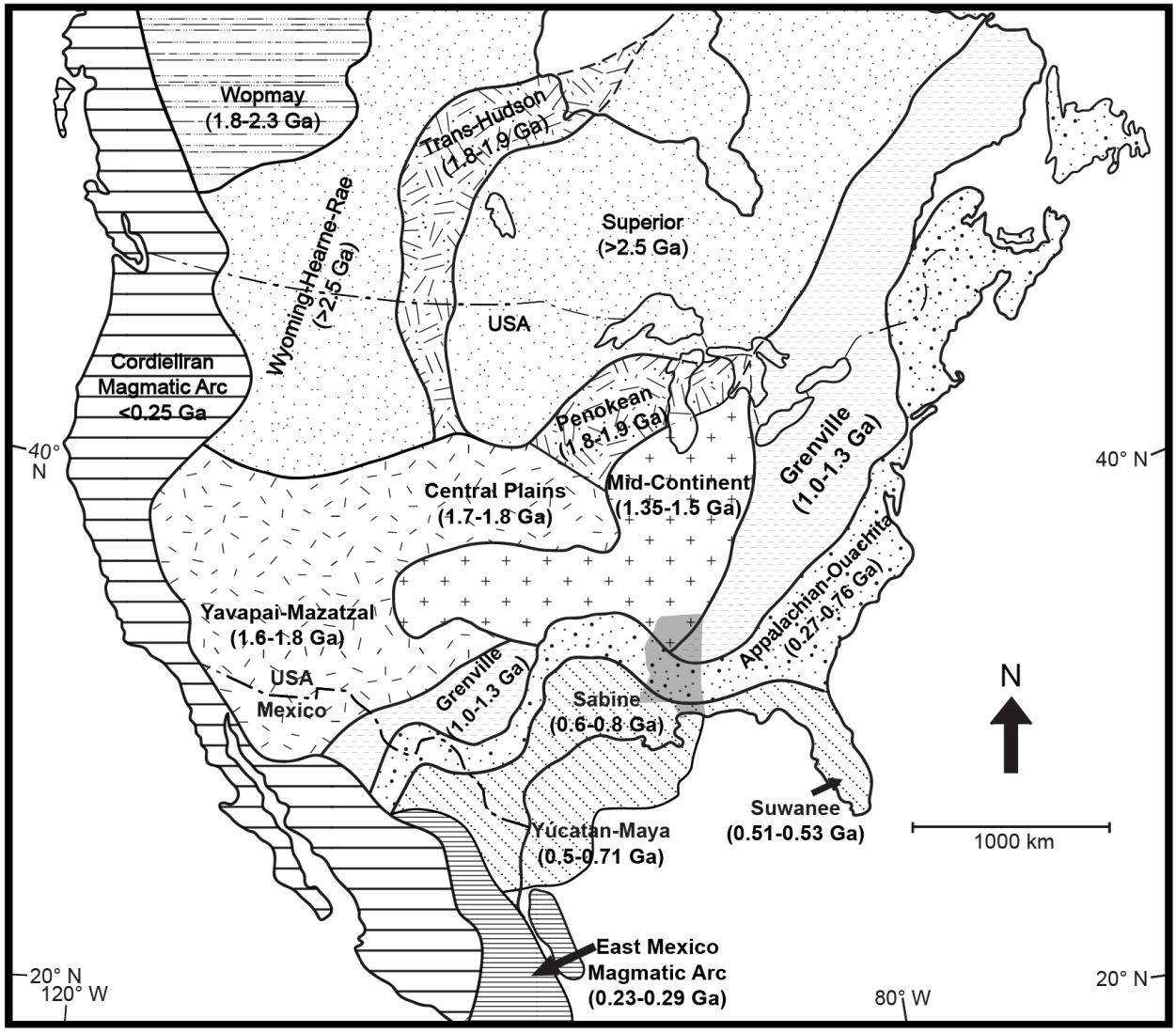

Figure 5—Igneous provinces of North America. Modified from Dickinson and Gehrels (2009) and Alsalem et al. (2018).

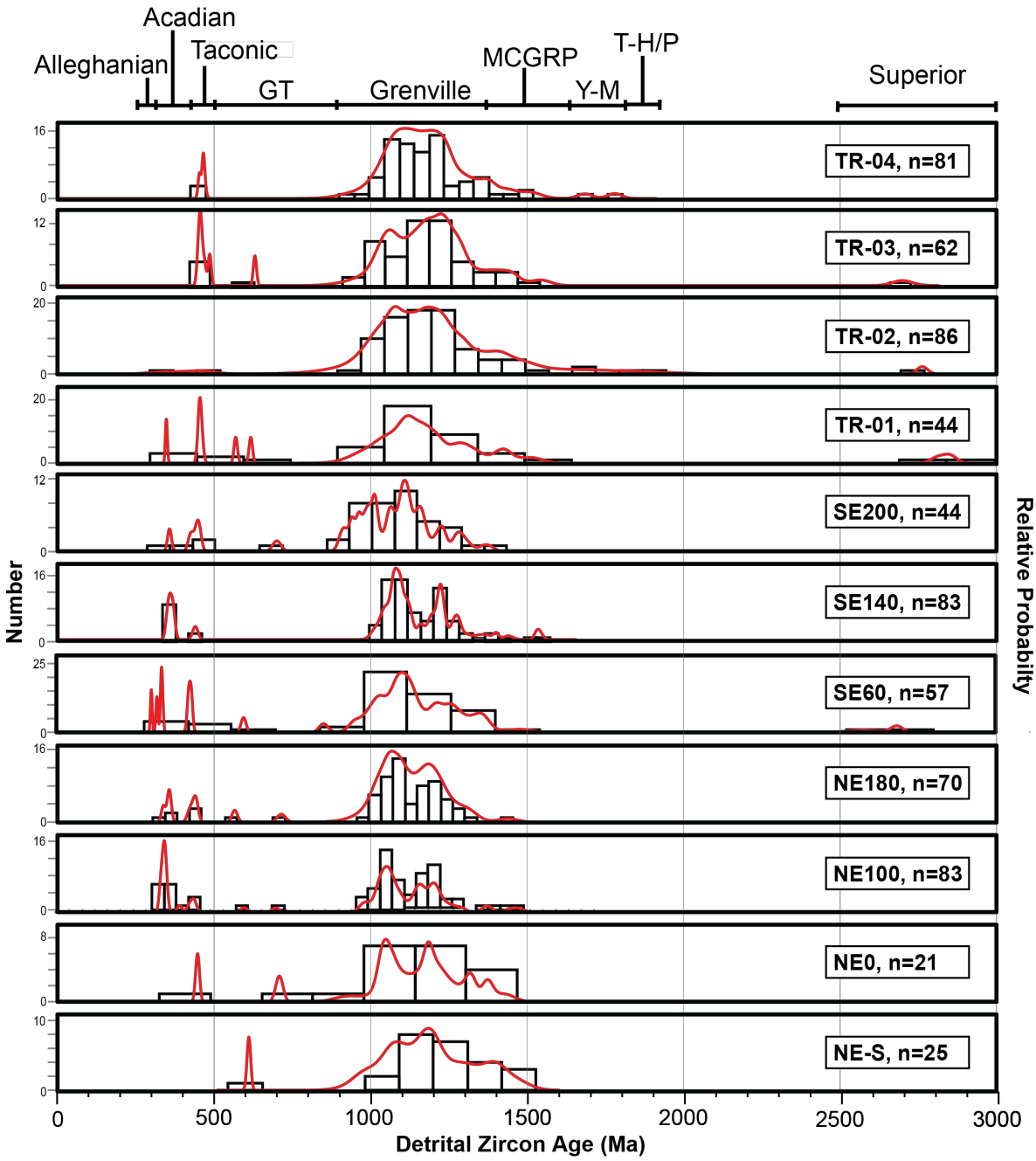

Figure 6—Stacked Probability Density Plots of the 11 northern and southern samples.

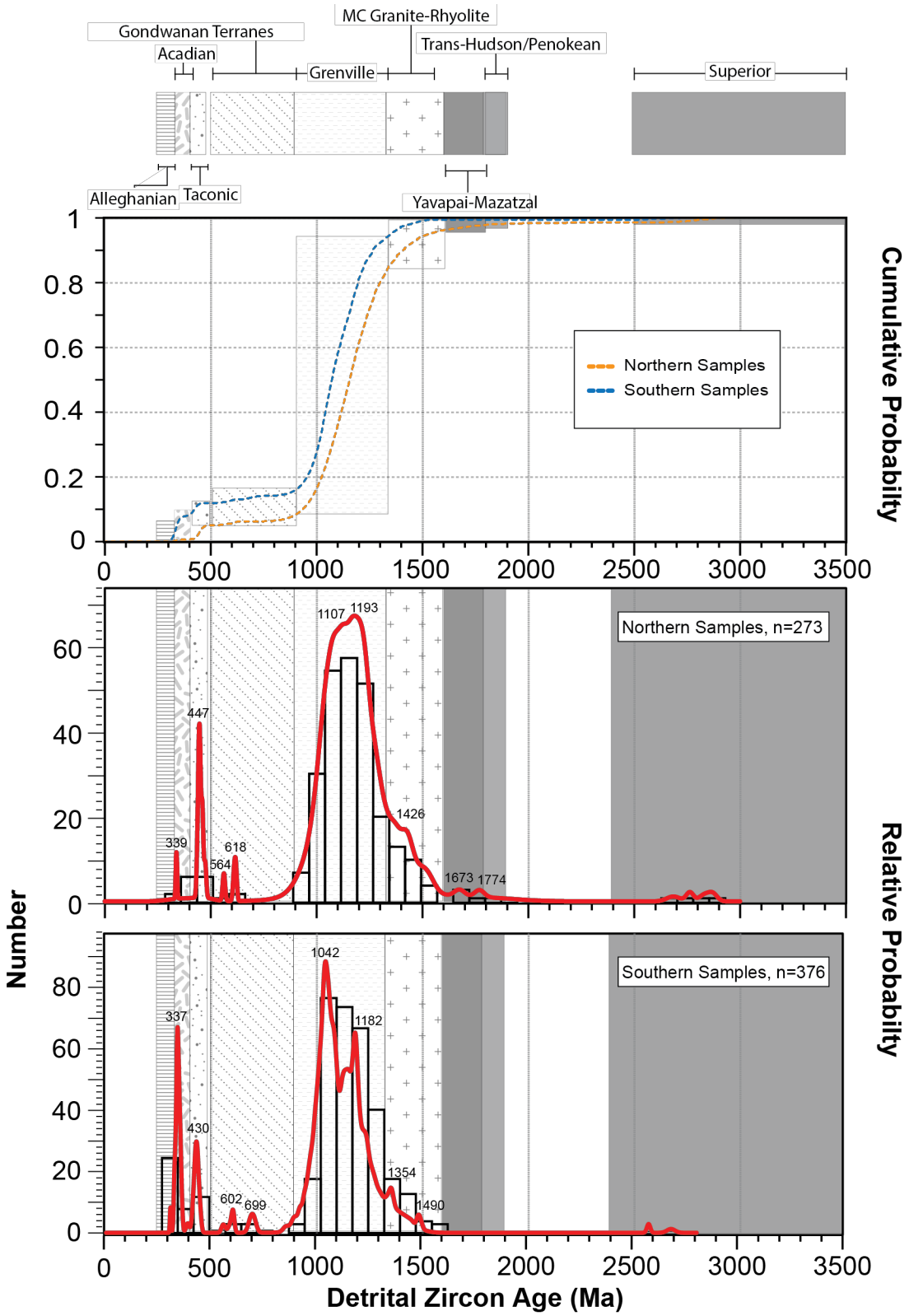

Figure 7—Cumulative and Probability density plots of the Northern and Southern Ripley Fm bentonites.

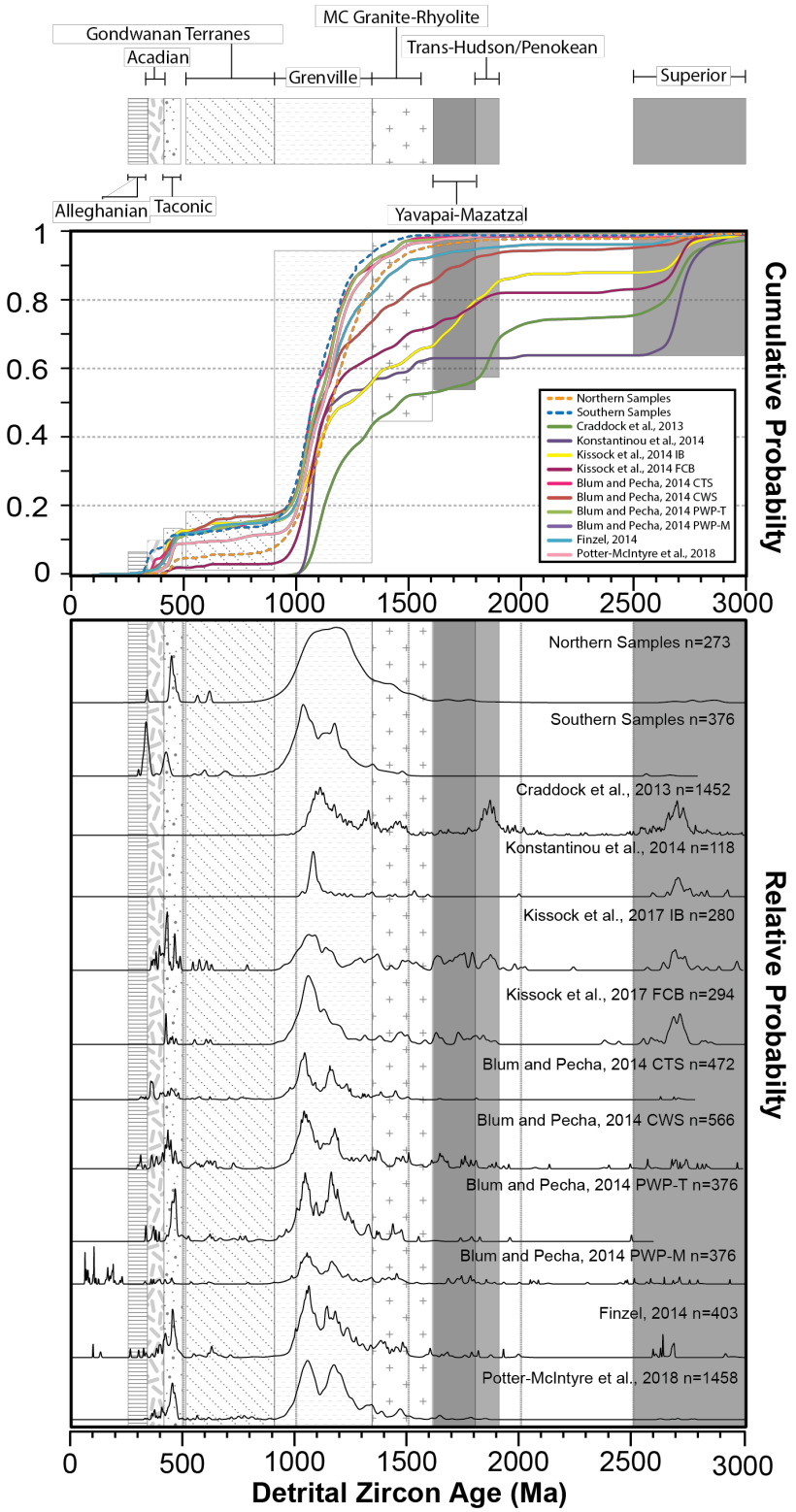

Figure 8—Age probability diagrams of the Northern and Southern Ripley Fm. bentonites with potential source regions and comparable data from the Superior region, Illinois Basin, Forest City Basin, and MSE.

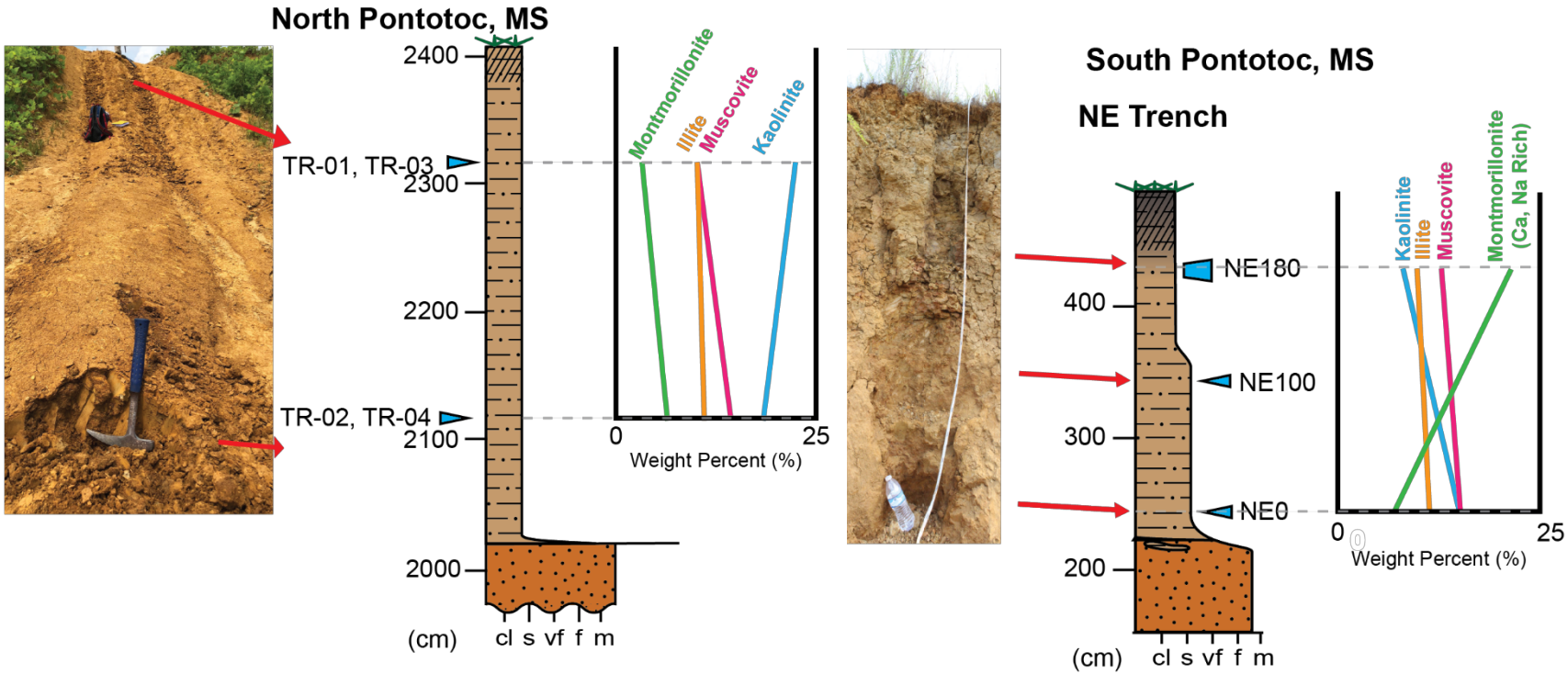

Figure 9—XRD results for the Northern and Southern locations.

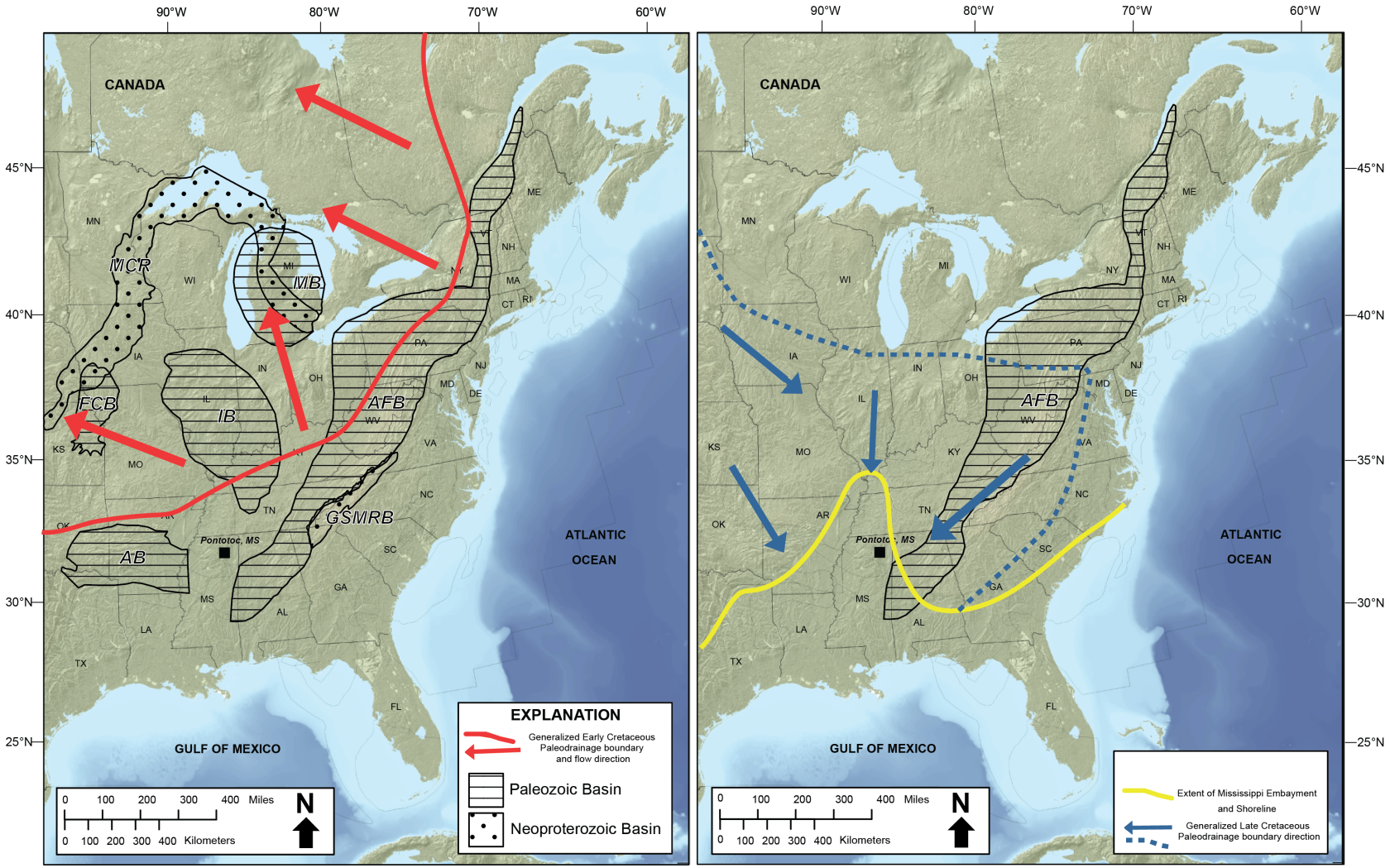

Figure 10—A. Map of the Paleozoic and Neoproterozoic basins of eastern North America. AB=Arkoma Basin, AFB=Appalachian Foreland Basin, FCB=Forest City Basin, GSMRB=Great Smokey Mountain Rift Basin, MB=Michigan Basin, MCR=Mid-Continent Rift. Modified from Coleman and Cahan (2012). **B.** Map of North America showing the Late Cretaceous mid continent paleodrainge boundary and flow directions. Modified from Coleman and Cahan (2012).

APPENDIX B: U-PB GEOCHRONOLOGIC DATA

Northern Sample Data

Grain Number	Chosen Age	Err. 2σ	Analysis Type	*207Pb 235U bcalculated	Rel. Err. *2σ bcalculated	206Pb 238U	Rel. Err. 2σ	RHO (error corr.)	207Pb 206Pb	Rel. Err. 2σ	206Pb 238U age	Err. 2σ	207Pb 206Pb age	Err. 2σ	Disc. (%)
EV3S_TR-01.34	**338.1**	**6.5**	206Pb/238Pb	1.58673	5.7	0.15167	4.1	0.89	0.05341	3.4	338.1	6.5	346.2	77.6	2.3
EV3B.TR-01.30	**444.6**	**13.4**	206Pb/238Pb	2.19314	2.5	0.18789	2.2	0.64	0.05688	7.6	444.6	13.4	487.0	167.0	8.7
EV3B.TR-01.11	**445.5**	**10.2**	206Pb/238Pb	1.83434	5.7	0.16564	2.8	0.26	0.05634	5.7	445.5	10.2	465.7	125.2	4.3
EV3S_TR-01.40	**451.5**	**12.5**	206Pb/238Pb	1.29351	3.9	0.12699	1.8	0.07	0.05674	3.0	451.5	12.5	481.5	65.7	6.2
EV3S_TR-01.14	**562.1**	**11.2**	206Pb/238Pb	1.74048	3.7	0.16648	2.2	0.28	0.05820	5.0	562.1	11.2	537.4	108.7	-4.6
EV3S_TR-01.52	**610.7**	**11.3**	206Pb/238Pb	2.02714	3.6	0.18742	2.2	0.58	0.06181	4.4	610.7	11.3	667.5	93.6	8.5
EV3S_TR-01.37	**953.0**	**93.4**	207Pb/206Pb	2.52792	3.8	0.21505	2.5	0.49	0.07085	4.6	862.6	40.5	953.0	93.4	9.5
EV3S_TR-01.45	**973.7**	**97.4**	207Pb/206Pb	3.00536	3.2	0.24379	2.1	0.42	0.07157	4.8	948.8	20.2	973.7	97.4	2.6
EV3B.TR-01.15	**1007.8**	**86.0**	207Pb/206Pb	1.98369	3.2	0.18498	1.8	0.36	0.07278	4.2	952.5	18.2	1007.8	86.0	5.5
EV3B.TR-01.36	**1053.9**	**81.1**	207Pb/206Pb	2.33122	3.2	0.17916	2.3	0.56	0.07446	4.0	959.2	18.1	1053.9	81.1	9.0
EV3S_TR-01.30	**1009.6**	**83.6**	207Pb/206Pb	1.92369	3.5	0.17985	1.9	0.42	0.07284	4.1	970.2	19.5	1009.6	83.6	3.9
EV3S_TR-01.11	**1038.9**	**54.3**	207Pb/206Pb	1.89459	3.0	0.17124	2.2	0.62	0.07390	2.7	970.8	13.1	1038.9	54.3	6.6
EV3S_TR-01.13	**1090.4**	**75.2**	207Pb/206Pb	1.90173	4.0	0.17361	2.7	0.73	0.07582	3.8	992.7	20.2	1090.4	75.2	9.0
EV3S_TR-01.21	**1064.2**	**95.1**	207Pb/206Pb	15.23436	2.7	0.53773	1.9	0.44	0.07484	4.7	1002.8	51.5	1064.2	95.1	5.8
EV3S_TR-01.50	**1077.0**	**64.7**	207Pb/206Pb	1.47329	6.6	0.14781	3.0	0.19	0.07532	3.2	1013.3	21.5	1077.0	64.7	5.9
EV3B.TR-01.37	**1105.6**	**44.5**	207Pb/206Pb	1.64715	3.8	0.16044	2.0	0.17	0.07640	2.2	1017.3	16.2	1105.6	44.5	8.0
EV3B.TR-01.18	**1128.3**	**79.6**	207Pb/206Pb	2.55290	8.6	0.19824	4.0	0.30	0.07727	4.0	1021.6	23.4	1128.3	79.6	9.5
EV3B.TR-01.07	**1119.5**	**40.9**	207Pb/206Pb	2.17461	2.4	0.19517	1.7	0.51	0.07694	2.1	1024.7	21.0	1119.5	40.9	8.5
EV3S_TR-01.24	**1075.1**	**217.5**	207Pb/206Pb	1.05398	11.3	0.11160	8.0	0.86	0.07525	10.8	1035.1	40.2	1075.1	217.5	3.7
EV3S_TR-01.29	**1136.0**	**64.5**	207Pb/206Pb	3.36068	4.1	0.25738	2.5	0.43	0.07758	3.2	1066.1	18.8	1136.0	64.5	6.2
EV3S_TR-01.02	**1185.2**	**46.8**	207Pb/206Pb	1.74894	3.8	0.16625	2.0	0.31	0.07952	2.4	1082.7	15.5	1185.2	46.8	8.6
EV3S_TR-01.27	**1088.7**	**51.6**	207Pb/206Pb	2.14579	4.8	0.19286	2.4	0.35	0.07576	2.6	1082.8	17.1	1088.7	51.6	0.5
EV3S_TR-01.51	**1140.0**	**58.0**	207Pb/206Pb	1.97853	2.8	0.18459	2.0	0.30	0.07774	2.9	1092.0	19.6	1140.0	58.0	4.2
EV3B.TR-01.14	**1141.2**	**60.9**	207Pb/206Pb	1.10973	24.6	0.09982	8.9	-0.91	0.07778	3.1	1094.1	18.5	1141.2	60.9	4.1
EV3B.TR-01.25	**1075.1**	**142.2**	207Pb/206Pb	2.16911	6.4	0.18814	3.3	-0.05	0.07525	7.1	1107.0	34.5	1075.1	142.2	-3.0
EV3B.TR-01.40	**1160.9**	**86.1**	207Pb/206Pb	2.31715	3.0	0.20088	1.7	0.54	0.07855	4.3	1123.3	25.1	1160.9	86.1	3.2
EV3S_TR-01.47	**1168.1**	**57.3**	207Pb/206Pb	2.11408	3.5	0.19252	2.2	0.35	0.07884	2.9	1123.4	17.9	1168.1	57.3	3.8
EV3S_TR-01.06	**1160.0**	**65.0**	207Pb/206Pb	2.08428	3.4	0.19251	2.0	0.36	0.07853	3.3	1134.9	20.6	1160.0	65.0	2.2

EV3S_TR-01.46	**1188.1**	**67.0**	207Pb/206Pb	1.81662	4.7	0.16864	2.3	-0.01	0.07964	3.4	1135.0	22.4	1188.1	67.0	4.5
EV3S_TR-01.26	**1214.0**	**89.4**	207Pb/206Pb	1.68593	2.8	0.16163	1.9	0.44	0.08069	4.5	1136.9	25.2	1214.0	89.4	6.4
EV3B.TR-01.06	**1216.9**	**41.0**	207Pb/206Pb	1.74862	4.2	0.16376	2.3	0.57	0.08081	2.1	1149.3	17.7	1216.9	41.0	5.6
EV3B.TR-01.39	**1284.6**	**49.0**	207Pb/206Pb	2.60038	3.6	0.20887	2.1	0.61	0.08366	2.5	1180.1	18.8	1284.6	49.0	8.1
EV3B.TR-01.08	**1317.9**	**156.0**	207Pb/206Pb	1.82758	2.5	0.17228	2.2	0.63	0.08510	8.0	1204.6	41.1	1317.9	156.0	8.6
EV3S_TR-01.31	**1224.2**	**78.7**	207Pb/206Pb	0.38660	4.4	0.05251	1.7	0.21	0.08111	4.0	1212.3	22.6	1224.2	78.7	1.0
EV3B.TR-01.26	**1326.1**	**61.3**	207Pb/206Pb	0.40975	4.6	0.05273	2.3	0.01	0.08547	3.2	1217.0	25.2	1326.1	61.3	8.2
EV3S_TR-01.36	**1321.4**	**65.4**	207Pb/206Pb	1.79732	2.5	0.15529	1.4	0.32	0.08526	3.4	1255.7	28.5	1321.4	65.4	5.0
EV3S_TR-01.57	**1264.0**	**63.0**	207Pb/206Pb	2.46474	3.2	0.21591	2.1	0.33	0.08279	3.2	1260.2	24.0	1264.0	63.0	0.3
EV3S_TR-01.18	**1306.5**	**119.8**	207Pb/206Pb	0.67013	7.3	0.08070	2.9	0.13	0.08460	6.2	1330.3	35.1	1306.5	119.8	-1.8
EV3S_TR-01.03	**1459.2**	**102.5**	207Pb/206Pb	2.00527	2.8	0.18288	1.6	0.54	0.09161	5.4	1343.2	29.4	1459.2	102.5	8.0
EV3S_TR-01.56	**1430.9**	**47.1**	207Pb/206Pb	1.71110	3.0	0.15697	1.8	0.29	0.09025	2.5	1386.9	20.6	1430.9	47.1	3.1
EV3S_TR-01.44	**1412.9**	**56.8**	207Pb/206Pb	0.54195	7.3	0.06587	2.8	0.08	0.08941	3.0	1406.4	26.4	1412.9	56.8	0.5
EV3S_TR-01.28	**1522.1**	**71.1**	207Pb/206Pb	1.91054	2.8	0.18290	1.7	0.43	0.09470	3.8	1476.4	33.4	1522.1	71.1	3.0
EV3B.TR-01.28	**2829.9**	**47.6**	207Pb/206Pb	2.51977	4.0	0.20907	2.6	0.33	0.20046	2.9	2649.1	52.7	2829.9	47.6	6.4
EV3S_TR-01.20	**2870.2**	**41.4**	207Pb/206Pb	2.04450	12.4	0.18449	8.0	0.40	0.20548	2.5	2773.9	43.8	2870.2	41.4	3.4
EV3S_TR-02.155	**354.3**	**116.6**	206Pb/238Pb	5.878858	7.184	0.22434	2.5	0.80	0.053600	5.2	325.7	8.3	354.3	116.6	8.1
EV3S_TR-02.146	**464.1**	**91.0**	206Pb/238Pb	1.648713	3.809	0.16096	2.3	0.59	0.056297	4.1	447.8	9.3	464.1	91.0	3.5
EV3S_TR-02.182	**941.6**	**149.2**	207Pb/206Pb	1.702687	2.776	0.16081	1.9	0.64	0.070454	7.3	917.1	31.9	941.6	149.2	2.6
EV3B.TR-02.23	**1011.6**	**72.1**	207Pb/206Pb	1.725214	3.330	0.16514	1.9	0.08	0.072917	3.6	921.5	18.4	1011.6	72.1	8.9
EV3S_TR-02.145	**1049.4**	**62.1**	207Pb/206Pb	2.055885	4.990	0.13279	5.3	-0.29	0.074290	3.1	962.1	21.0	1049.4	62.1	8.3
EV3S_TR-02.163	**995.0**	**70.8**	207Pb/206Pb	2.148259	4.312	0.19460	2.3	0.29	0.072321	3.5	971.1	21.1	995.0	70.8	2.4
EV3S_TR-02.156	**983.2**	**82.3**	207Pb/206Pb	0.382929	5.756	0.05181	2.6	0.44	0.071905	4.0	972.9	20.5	983.2	82.3	1.0
EV3S_TR-02.141	**1035.4**	**65.2**	207Pb/206Pb	1.828274	7.783	0.17022	6.1	0.77	0.073779	3.2	975.2	22.1	1035.4	65.2	5.8
EV3B.TR-02.22	**1089.0**	**74.0**	207Pb/206Pb	1.810602	5.140	0.17616	2.6	0.16	0.075770	3.7	985.3	17.1	1089.0	74.0	9.5
EV3S_TR-02.161	**1082.8**	**74.8**	207Pb/206Pb	1.704691	5.796	0.16111	2.4	0.34	0.075535	3.7	985.5	20.5	1082.8	74.8	9.0
3235AZ1_1	**1028.9**	**275.0**	207Pb/206Pb	1.67778	0.21361	0.16546	0.0	0.09	0.07350	0.0	987.1	55.3	1028.9	275.0	4.1
3235AZ1_111	**993.5**	**205.9**	207Pb/206Pb	1.65495	0.16578	0.16609	0.0	0.24	0.07230	0.0	990.5	47.3	993.5	205.9	0.3
EV3S_TR-02.136	**1097.0**	**71.6**	207Pb/206Pb	1.670680	4.007	0.15244	3.5	0.85	0.076072	3.6	995.7	22.6	1097.0	71.6	9.2
EV3S_TR-02.153	**1071.6**	**121.0**	207Pb/206Pb	0.389595	4.282	0.05292	2.1	0.39	0.075116	6.0	997.3	24.9	1071.6	121.0	6.9
3235AZ1_14	**1083.3**	**260.1**	207Pb/206Pb	1.74627	0.23347	0.16763	0.0	0.32	0.07560	0.0	999.0	63.6	1083.3	260.1	7.8
EV3S_TR-02.134	**1029.3**	**64.0**	207Pb/206Pb	1.844311	7.289	0.17844	4.3	0.16	0.073556	3.2	1006.3	21.1	1029.3	64.0	2.2

3235AZ1_47	**986.7**	**273.6**	207Pb/206Pb	1.68543	0.21325	0.16972	0.0	0.07	0.07200	0.0	1010.5	51.2	986.7	273.6	-2.4
EV3B.TR-02.15	**1055.9**	**72.8**	207Pb/206Pb	2.028605	3.689	0.18383	1.8	0.19	0.074532	3.6	1014.0	18.2	1055.9	72.8	4.0
EV3S_TR-02.178	**1073.2**	**43.6**	207Pb/206Pb	2.123052	5.785	0.19102	2.7	0.00	0.075176	2.2	1016.3	16.7	1073.2	43.6	5.3
EV3B.TR-02.26	**1129.1**	**79.9**	207Pb/206Pb	1.939184	5.964	0.17933	3.3	0.26	0.077308	4.0	1022.4	21.8	1129.1	79.9	9.5
EV3S_TR-02.166	**1080.4**	**35.5**	207Pb/206Pb	2.145227	6.216	0.18703	3.0	0.46	0.075445	1.8	1031.1	16.0	1080.4	35.5	4.6
EV3S_TR-02.132	**1086.1**	**103.1**	207Pb/206Pb	2.825846	7.591	0.22514	3.2	-0.03	0.075662	5.1	1031.2	23.2	1086.1	103.1	5.1
EV3B.TR-02.27	**1116.0**	**53.7**	207Pb/206Pb	1.831951	3.787	0.17187	2.3	0.20	0.076800	2.7	1032.1	21.0	1116.0	53.7	7.5
3235AZ1_17	**1044.4**	**277.4**	207Pb/206Pb	1.78362	0.23931	0.17456	0.0	0.11	0.07410	0.0	1037.2	45.1	1044.4	277.4	0.7
3235AZ1_37	**1076.7**	**160.6**	207Pb/206Pb	1.81353	0.14738	0.17466	0.0	0.32	0.07530	0.0	1037.7	46.2	1076.7	160.6	3.6
EV3B.TR-02.33	**1124.4**	**64.1**	207Pb/206Pb	1.980096	2.830	0.18118	1.8	0.66	0.077126	3.2	1043.5	19.8	1124.4	64.1	7.2
EV3B.TR-02.21	**1056.2**	**108.2**	207Pb/206Pb	2.113883	3.388	0.18607	2.0	0.08	0.074544	5.4	1046.0	25.3	1056.2	108.2	1.0
3235AZ1_119	**1069.2**	**205.3**	207Pb/206Pb	1.82512	0.17850	0.17643	0.0	0.26	0.07503	0.0	1047.5	61.8	1069.2	205.3	2.0
EV3S_TR-02.133	**1067.4**	**157.6**	207Pb/206Pb	1.809628	5.156	0.17346	2.4	0.24	0.074961	7.8	1058.5	42.1	1067.4	157.6	0.8
EV3B.TR-02.25	**1157.7**	**119.3**	207Pb/206Pb	1.945230	9.310	0.17423	4.6	0.18	0.078428	6.0	1063.3	32.5	1157.7	119.3	8.2
3235AZ1_116	**1135.9**	**233.6**	207Pb/206Pb	1.92200	0.20632	0.17970	0.0	0.04	0.07760	0.0	1065.3	51.1	1135.9	233.6	6.2
3235AZ1_68	**1130.3**	**639.5**	207Pb/206Pb	1.91846	0.59871	0.17988	0.0	0.07	0.07740	0.0	1066.3	78.1	1130.3	639.5	5.7
EV3S_TR-02.180	**1136.5**	**64.8**	207Pb/206Pb	2.009845	6.591	0.18265	2.9	0.19	0.077596	3.3	1071.6	20.1	1136.5	64.8	5.7
EV3B.TR-02.32	**1178.8**	**41.9**	207Pb/206Pb	3.124515	5.139	0.23507	2.7	0.23	0.079266	2.1	1073.4	17.9	1178.8	41.9	8.9
EV3S_TR-02.179	**1192.2**	**131.9**	207Pb/206Pb	1.770030	2.865	0.17076	1.8	0.65	0.079808	6.7	1081.4	29.2	1192.2	131.9	9.3
EV3B.TR-02.14	**1197.9**	**74.7**	207Pb/206Pb	1.828488	4.915	0.17183	2.7	-0.07	0.080035	3.8	1087.9	17.9	1197.9	74.7	9.2
3235AZ1_48	**1077.3**	**157.3**	207Pb/206Pb	1.91459	0.15062	0.18434	0.0	0.32	0.07530	0.0	1090.6	49.0	1077.3	157.3	-1.2
EV3S_TR-02.151	**1212.6**	**84.7**	207Pb/206Pb	2.104434	5.438	0.18834	2.7	0.24	0.080636	4.3	1094.6	24.3	1212.6	84.7	9.7
3235AZ1_29	**1173.6**	**216.6**	207Pb/206Pb	2.02323	0.20614	0.18561	0.0	0.20	0.07910	0.0	1097.6	66.2	1173.6	216.6	6.5
3235AZ1_103	**1211.8**	**493.5**	207Pb/206Pb	2.08087	0.51000	0.18724	0.0	0.07	0.08060	0.0	1106.4	63.3	1211.8	493.5	8.7
EV3S_TR-02.139	**1151.9**	**58.6**	207Pb/206Pb	1.270595	8.897	0.12543	3.5	0.05	0.078198	3.0	1106.7	22.1	1151.9	58.6	3.9
EV3S_TR-02.150	**1222.3**	**107.4**	207Pb/206Pb	1.814255	4.182	0.16651	2.5	0.41	0.081036	5.5	1112.4	27.8	1222.3	107.4	9.0
3235AZ1_81	**1196.5**	**197.6**	207Pb/206Pb	2.08711	0.19659	0.18926	0.0	0.22	0.08000	0.0	1117.4	61.1	1196.5	197.6	6.6
EV3S_TR-02.129	**1235.5**	**105.7**	207Pb/206Pb	2.683994	4.020	0.21721	2.3	0.41	0.081584	5.4	1120.6	28.8	1235.5	105.7	9.3
EV3S_TR-02.177	**1211.9**	**125.5**	207Pb/206Pb	2.182429	6.178	0.19158	3.1	0.16	0.080609	6.4	1126.9	28.0	1211.9	125.5	7.0
3235AZ1_72	**1170.5**	**199.3**	207Pb/206Pb	2.08693	0.18698	0.19175	0.0	0.14	0.07890	0.0	1130.9	62.4	1170.5	199.3	3.4
EV3B.TR-02.30	**1255.6**	**56.3**	207Pb/206Pb	2.139626	2.112	0.18945	1.9	0.65	0.082424	2.9	1132.1	18.4	1255.6	56.3	9.8
EV3S_TR-02.121	**1203.2**	**84.7**	207Pb/206Pb	1.746649	4.696	0.17183	2.7	0.35	0.080254	4.3	1140.5	29.7	1203.2	84.7	5.2

EV3B.TR-02.18	**1182.9**	**162.9**	207Pb/206Pb	2.373181	3.235	0.20436	2.9	0.76	0.079433	8.2	1143.0	38.1	1182.9	162.9	3.4
3235AZ1_25	**1242.4**	**322.2**	207Pb/206Pb	2.18989	0.33036	0.19400	0.0	0.10	0.08190	0.0	1143.0	83.9	1242.4	322.2	8.0
EV3B.TR-02.07	**1207.3**	**68.6**	207Pb/206Pb	1.742121	8.502	0.16184	3.5	0.38	0.080419	3.5	1144.3	24.5	1207.3	68.6	5.2
EV3S_TR-02.162	**1198.6**	**84.1**	207Pb/206Pb	1.720366	4.306	0.16518	2.2	0.50	0.080063	4.3	1146.3	24.1	1198.6	84.1	4.4
3235AZ1_53	**1276.0**	**145.4**	207Pb/206Pb	2.23824	0.15806	0.19490	0.0	0.19	0.08330	0.0	1147.9	43.4	1276.0	145.4	10.0
3235AZ1_58	**1271.7**	**625.0**	207Pb/206Pb	2.23412	0.69517	0.19498	0.0	0.11	0.08310	0.0	1148.3	104.3	1271.7	625.0	9.7
3235AZ1_49	**1256.7**	**216.8**	207Pb/206Pb	2.22050	0.23697	0.19528	0.0	0.10	0.08250	0.0	1149.9	43.6	1256.7	216.8	8.5
3235AZ1_15	**1249.4**	**302.7**	207Pb/206Pb	2.21977	0.33326	0.19595	0.0	0.19	0.08220	0.0	1153.5	78.5	1249.4	302.7	7.7
EV3B.TR-02.04	**1209.6**	**85.7**	207Pb/206Pb	0.593725	5.018	0.07019	2.4	0.17	0.080514	4.4	1172.7	26.2	1209.6	85.7	3.1
3235AZ1_36	**1130.9**	**338.2**	207Pb/206Pb	2.15340	0.35644	0.20185	0.0	0.06	0.07740	0.0	1185.2	51.0	1130.9	338.2	-4.8
3235AZ1_23	**1162.6**	**327.8**	207Pb/206Pb	2.19323	0.34250	0.20232	0.0	0.07	0.07860	0.0	1187.8	70.2	1162.6	327.8	-2.2
3235AZ1_97	**1142.4**	**246.6**	207Pb/206Pb	2.17745	0.26420	0.20293	0.0	0.16	0.07780	0.0	1191.0	54.8	1142.4	246.6	-4.3
EV3S_TR-02.137	**1226.3**	**48.3**	207Pb/206Pb	1.751954	3.608	0.16703	2.4	0.35	0.081199	2.5	1195.0	25.4	1226.3	48.3	2.5
EV3B.TR-02.17	**1297.7**	**41.9**	207Pb/206Pb	2.541973	4.153	0.21272	2.3	0.28	0.084223	2.2	1198.7	31.3	1297.7	41.9	7.6
3235AZ1_77	**1304.6**	**357.6**	207Pb/206Pb	2.38272	0.42294	0.20446	0.0	0.08	0.08450	0.0	1199.2	67.6	1304.6	357.6	8.1
3235AZ1_96	**1316.6**	**195.4**	207Pb/206Pb	2.41868	0.24407	0.20627	0.0	0.33	0.08500	0.0	1208.9	71.9	1316.6	195.4	8.2
EV3S_TR-02.152	**1222.4**	**91.2**	207Pb/206Pb	2.057602	4.350	0.18507	2.4	0.30	0.081041	4.6	1212.9	25.4	1222.4	91.2	0.8
3235AZ1_61	**1267.1**	**148.5**	207Pb/206Pb	2.38060	0.18151	0.20825	0.0	0.29	0.08290	0.0	1219.5	48.2	1267.1	148.5	3.8
3235AZ1_5	**1167.0**	**167.4**	207Pb/206Pb	2.27393	0.18790	0.20931	0.0	0.35	0.07880	0.0	1225.1	70.2	1167.0	167.4	-5.0
3235AZ1_99	**1277.0**	**219.2**	207Pb/206Pb	2.42505	0.27470	0.21106	0.0	0.20	0.08330	0.0	1234.4	45.0	1277.0	219.2	3.3
3235AZ1_90	**1300.7**	**155.4**	207Pb/206Pb	2.47078	0.19435	0.21244	0.0	0.26	0.08440	0.0	1241.8	51.3	1300.7	155.4	4.5
EV3B.TR-02.16	**1353.1**	**80.4**	207Pb/206Pb	1.750570	3.963	0.17035	1.9	0.42	0.086668	4.2	1243.3	26.5	1353.1	80.4	8.1
3235AZ1_27	**1248.2**	**251.9**	207Pb/206Pb	2.41445	0.30104	0.21326	0.0	0.14	0.08210	0.0	1246.2	59.9	1248.2	251.9	0.2
3235AZ1_109	**1274.1**	**194.4**	207Pb/206Pb	2.46678	0.26439	0.21501	0.0	0.45	0.08320	0.0	1255.5	86.7	1274.1	194.4	1.5
3235AZ1_89	**1296.3**	**228.1**	207Pb/206Pb	2.57928	0.29056	0.22227	0.0	0.19	0.08420	0.0	1293.9	70.9	1296.3	228.1	0.2
EV3B.TR-02.13	**1419.3**	**94.7**	207Pb/206Pb	2.263427	5.535	0.19171	3.0	0.35	0.089709	5.0	1299.3	30.6	1419.3	94.7	8.5
EV3S_TR-02.158	**1434.3**	**109.9**	207Pb/206Pb	2.067706	5.006	0.17966	2.8	0.13	0.090414	5.8	1304.8	35.0	1434.3	109.9	9.0
EV3S_TR-02.131	**1447.3**	**158.8**	207Pb/206Pb	1.372522	5.976	0.13818	2.8	0.34	0.091033	8.3	1309.0	38.2	1447.3	158.8	9.6
3235AZ1_69	**1391.9**	**196.0**	207Pb/206Pb	2.76891	0.26216	0.22709	0.0	0.17	0.08840	0.0	1319.2	69.2	1391.9	196.0	5.2
EV3S_TR-02.122	**1417.0**	**56.9**	207Pb/206Pb	2.141594	4.264	0.19354	2.8	0.32	0.089597	3.0	1375.0	29.6	1417.0	56.9	3.0
EV3B.TR-02.11	**1497.5**	**81.4**	207Pb/206Pb	1.830219	4.487	0.16825	2.5	0.44	0.093476	4.3	1400.8	35.7	1497.5	81.4	6.5
3235AZ1_31	**1532.5**	**221.3**	207Pb/206Pb	3.20704	0.34415	0.24426	0.0	0.12	0.09523	0.0	1408.8	78.6	1532.5	221.3	8.1

3235AZ1_76	**1497.7**	**214.9**	207Pb/206Pb	3.48224	0.38719	0.27016	0.0	0.24	0.09350	0.0	1541.6	83.5	1497.7	214.9	-2.9
3235AZ1_6	**1661.7**	**206.1**	207Pb/206Pb	3.89801	0.42770	0.27704	0.0	0.19	0.10205	0.0	1576.4	67.4	1661.7	206.1	5.1
3235AZ1_93	**1679.7**	**205.0**	207Pb/206Pb	3.96328	0.43381	0.27895	0.0	0.19	0.10305	0.0	1586.1	68.5	1679.7	205.0	5.6
3235AZ1_12	**1838.2**	**205.2**	207Pb/206Pb	4.56836	0.42337	0.29483	0.0	0.20	0.11238	0.0	1665.6	125.8	1838.2	205.2	9.4
3235AZ1_64	**1881.0**	**271.0**	207Pb/206Pb	5.48504	0.82476	0.34570	0.0	0.25	0.11507	0.0	1914.0	122.1	1881.0	271.0	-1.8
EV3S_TR-02.125	**2761.8**	**34.2**	207Pb/206Pb	0.583585	4.478	0.07202	2.1	0.20	0.192284	2.1	2727.8	52.1	2761.8	34.2	1.2
EV3S_TR-03.04	**438.8**	**10.3**	206Pb/238Pb	2.49568	5.6	0.20915	2.8	-0.07	0.05673	5.93	438.8	10.3	481.0	131.0	8.8
EV3S_TR-03.75	**444.2**	**12.7**	206Pb/238Pb	2.24207	5.9	0.19167	2.9	0.24	0.05606	5.14	444.2	12.7	454.7	114.0	2.3
EV3S_TR-03.89	**445.8**	**9.3**	206Pb/238Pb	1.63121	2.7	0.15743	1.9	0.24	0.05639	3.19	445.8	9.3	467.6	70.7	4.7
EV3S_TR-03.107	**456.2**	**12.5**	206Pb/238Pb	1.53662	3.8	0.15187	2.5	0.25	0.05692	5.60	456.2	12.5	488.5	123.5	6.6
EV3S_TR-03.60	**474.5**	**9.8**	206Pb/238Pb	1.12126	3.0	0.06645	2.7	0.62	0.05703	5.93	474.5	9.8	492.9	130.8	3.7
EV3S_TR-03.07	**618.6**	**10.2**	206Pb/238Pb	2.36410	3.2	0.20671	2.1	0.26	0.06204	2.53	618.6	10.2	675.4	54.0	8.4
EV3S_TR-03.24	**991.2**	**103.7**	207Pb/206Pb	2.73950	3.0	0.22864	1.9	0.11	0.07219	5.10	915.0	19.5	991.2	103.7	7.7
EV3S_TR-03.86	**961.2**	**123.4**	207Pb/206Pb	1.75930	3.8	0.17188	2.0	0.37	0.07113	6.04	939.9	26.1	961.2	123.4	2.2
EV3S_TR-03.80	**1036.7**	**67.6**	207Pb/206Pb	2.03118	3.5	0.18065	2.2	0.22	0.07383	3.35	963.0	16.0	1036.7	67.6	7.1
EV3S_TR-03.114	**966.0**	**138.7**	207Pb/206Pb	1.72433	2.4	0.16852	2.0	0.60	0.07130	6.79	972.7	31.6	966.0	138.7	-0.7
EV3S_TR-03.108	**1019.1**	**50.3**	207Pb/206Pb	0.57557	5.1	0.07334	2.8	0.08	0.07319	2.48	982.5	21.4	1019.1	50.3	3.6
EV3S_TR-03.70	**1108.4**	**78.8**	207Pb/206Pb	2.09013	6.8	0.19457	3.1	0.10	0.07651	3.95	1000.1	19.1	1108.4	78.8	9.8
EV3S_TR-03.66	**1071.1**	**51.4**	207Pb/206Pb	2.43198	4.5	0.21351	2.5	0.33	0.07510	2.56	1000.7	13.1	1071.1	51.4	6.6
EV3S_TR-03.100	**1024.2**	**57.9**	207Pb/206Pb	1.53315	7.8	0.14077	4.9	0.30	0.07337	2.86	1003.6	20.9	1024.2	57.9	2.0
EV3S_TR-03.113	**1047.2**	**40.5**	207Pb/206Pb	2.18470	5.0	0.18966	2.9	0.34	0.07421	2.01	1004.0	18.5	1047.2	40.5	4.1
EV3S_TR-03.45	**1037.0**	**98.4**	207Pb/206Pb	2.05167	3.6	0.18004	2.2	0.21	0.07384	4.87	1012.2	28.4	1037.0	98.4	2.4
EV3S_TR-03.02	**1055.8**	**82.7**	207Pb/206Pb	3.20807	3.2	0.24431	1.8	0.29	0.07453	4.11	1013.2	21.4	1055.8	82.7	4.0
EV3S_TR-03.87	**1048.1**	**67.2**	207Pb/206Pb	1.53950	5.8	0.15697	3.0	0.19	0.07424	3.33	1015.7	20.4	1048.1	67.2	3.1
EV3S_TR-03.121	**1033.9**	**91.8**	207Pb/206Pb	1.56748	2.9	0.14662	3.3	0.77	0.07372	4.54	1022.2	25.9	1033.9	91.8	1.1
EV3S_TR-03.85	**1047.9**	**71.9**	207Pb/206Pb	2.37413	2.9	0.19242	2.2	0.52	0.07424	3.57	1022.4	18.8	1047.9	71.9	2.4
EV3S_TR-03.82	**1140.3**	**185.5**	207Pb/206Pb	2.40843	4.3	0.20178	2.8	0.28	0.07774	9.33	1026.7	34.3	1140.3	185.5	10.0
EV3S_TR-03.91	**1085.9**	**92.0**	207Pb/206Pb	2.04122	3.4	0.18444	2.0	0.26	0.07565	4.59	1030.0	22.1	1085.9	92.0	5.1
EV3S_TR-03.56	**1146.2**	**116.0**	207Pb/206Pb	2.32722	4.4	0.20315	2.6	0.33	0.07798	5.84	1033.2	29.9	1146.2	116.0	9.9
EV3S_TR-03.26	**1141.7**	**49.5**	207Pb/206Pb	1.58592	2.8	0.15116	1.8	0.46	0.07780	2.49	1036.8	18.4	1141.7	49.5	9.2
EV3S_TR-03.116	**1095.7**	**159.2**	207Pb/206Pb	1.66706	7.5	0.15779	6.4	0.92	0.07602	7.95	1037.6	36.2	1095.7	159.2	5.3
EV3S_TR-03.30	**1144.4**	**80.4**	207Pb/206Pb	2.06592	3.4	0.19433	2.0	0.24	0.07790	4.04	1041.3	24.2	1144.4	80.4	9.0

EV3S_TR-03.40	**1114.2**	**82.4**	207Pb/206Pb	2.21925	2.5	0.20086	1.9	0.43	0.07673	4.13	1044.8	23.1	1114.2	82.4	6.2
EV3S_TR-03.111	**1167.7**	**35.3**	207Pb/206Pb	1.61846	5.2	0.17066	2.8	0.39	0.07882	1.78	1059.8	18.4	1167.7	35.3	9.2
EV3S_TR-03.61	**1171.8**	**52.2**	207Pb/206Pb	0.60063	5.9	0.07638	2.1	0.17	0.07899	2.63	1074.7	19.7	1171.8	52.2	8.3
EV3S_TR-03.18	**1133.5**	**58.0**	207Pb/206Pb	1.77700	5.4	0.16743	2.4	0.37	0.07748	2.91	1085.1	19.0	1133.5	58.0	4.3
EV3S_TR-03.109	**1142.1**	**61.4**	207Pb/206Pb	1.77114	6.0	0.17336	3.0	0.10	0.07781	3.09	1088.1	24.9	1142.1	61.4	4.7
EV3S_TR-03.90	**1203.6**	**68.4**	207Pb/206Pb	0.55669	3.5	0.07160	2.1	0.43	0.08027	3.47	1091.2	20.6	1203.6	68.4	9.3
EV3S_TR-03.62	**1216.5**	**77.2**	207Pb/206Pb	1.97580	2.9	0.18142	2.0	0.45	0.08079	3.92	1099.9	26.2	1216.5	77.2	9.6
EV3S_TR-03.14	**1198.6**	**70.2**	207Pb/206Pb	2.79904	2.3	0.21308	1.6	0.41	0.08006	3.56	1106.2	20.7	1198.6	70.2	7.7
EV3S_TR-03.93	**1208.7**	**57.1**	207Pb/206Pb	1.75029	6.7	0.16219	4.5	0.60	0.08048	2.90	1124.4	24.1	1208.7	57.1	7.0
EV3S_TR-03.09	**1225.2**	**62.2**	207Pb/206Pb	2.22366	4.5	0.19536	2.1	0.22	0.08115	3.17	1135.2	22.4	1225.2	62.2	7.3
EV3S_TR-03.29	**1123.8**	**69.6**	207Pb/206Pb	2.87825	4.8	0.23139	2.5	0.10	0.07710	3.49	1144.8	20.7	1123.8	69.6	-1.9
EV3S_TR-03.69	**1144.6**	**142.4**	207Pb/206Pb	2.18922	4.2	0.19502	3.2	0.69	0.07791	7.17	1146.1	32.3	1144.6	142.4	-0.1
EV3S_TR-03.15	**1168.7**	**105.5**	207Pb/206Pb	2.06650	3.5	0.18720	2.0	0.28	0.07886	5.33	1147.0	24.8	1168.7	105.5	1.9
EV3S_TR-03.68	**1231.5**	**59.2**	207Pb/206Pb	0.67238	3.7	0.07460	2.0	0.24	0.08142	3.02	1148.5	34.0	1231.5	59.2	6.7
EV3S_TR-03.08	**1258.6**	**88.1**	207Pb/206Pb	0.86149	3.1	0.10071	1.7	0.57	0.08255	4.51	1150.4	21.8	1258.6	88.1	8.6
EV3S_TR-03.76	**1139.8**	**103.5**	207Pb/206Pb	0.55144	5.0	0.07134	3.0	0.25	0.07772	5.20	1156.1	29.3	1139.8	103.5	-1.4
EV3S_TR-03.97	**1221.3**	**72.1**	207Pb/206Pb	0.44338	6.6	0.05671	2.5	0.16	0.08099	3.67	1157.5	29.3	1221.3	72.1	5.2
EV3S_TR-03.41	**1224.8**	**57.6**	207Pb/206Pb	1.86152	4.3	0.17595	2.4	0.36	0.08114	2.93	1164.3	19.7	1224.8	57.6	4.9
EV3S_TR-03.77	**1129.6**	**100.9**	207Pb/206Pb	2.10496	5.3	0.19642	2.8	0.28	0.07732	5.07	1164.6	28.3	1129.6	100.9	-3.1
EV3S_TR-03.83	**1217.9**	**53.9**	207Pb/206Pb	1.85068	8.9	0.17265	3.6	0.08	0.08085	2.74	1166.7	20.2	1217.9	53.9	4.2
EV3S_TR-03.103	**1274.2**	**36.7**	207Pb/206Pb	0.60012	4.4	0.07016	2.8	0.58	0.08321	1.88	1168.0	19.3	1274.2	36.7	8.3
EV3S_TR-03.39	**1200.3**	**48.0**	207Pb/206Pb	3.17715	2.5	0.23285	1.7	0.18	0.08013	2.43	1179.9	20.2	1200.3	48.0	1.7
EV3S_TR-03.55	**1271.2**	**83.8**	207Pb/206Pb	2.55104	5.2	0.22514	2.9	0.26	0.08308	4.29	1192.2	28.5	1271.2	83.8	6.2
EV3S_TR-03.06	**1268.0**	**65.1**	207Pb/206Pb	2.90556	2.6	0.23247	2.0	0.40	0.08295	3.33	1211.3	23.4	1268.0	65.1	4.5
EV3S_TR-03.71	**1288.6**	**77.7**	207Pb/206Pb	1.77042	4.2	0.16783	2.1	0.38	0.08383	3.99	1212.2	25.8	1288.6	77.7	5.9
EV3S_TR-03.03	**1350.3**	**123.7**	207Pb/206Pb	0.40158	4.1	0.05293	1.5	0.08	0.08654	6.41	1224.3	31.6	1350.3	123.7	9.3
EV3S_TR-03.43	**1234.6**	**73.1**	207Pb/206Pb	0.44831	5.3	0.05817	2.3	0.25	0.08155	3.72	1227.7	26.9	1234.6	73.1	0.6
EV3S_TR-03.65	**1260.1**	**85.4**	207Pb/206Pb	1.76892	5.3	0.15956	2.8	0.20	0.08261	4.37	1247.5	28.6	1260.1	85.4	1.0
EV3S_TR-03.46	**1401.3**	**60.1**	207Pb/206Pb	1.73080	5.0	0.17001	3.0	0.35	0.08887	3.13	1270.4	29.6	1401.3	60.1	9.3
EV3S_TR-03.54	**1249.8**	**102.3**	207Pb/206Pb	2.08550	6.8	0.18633	3.5	0.29	0.08218	5.23	1309.0	33.9	1249.8	102.3	-4.7
EV3S_TR-03.47	**1357.5**	**96.3**	207Pb/206Pb	2.66892	3.1	0.21782	2.6	0.40	0.08686	5.00	1310.9	32.4	1357.5	96.3	3.4
EV3S_TR-03.23	**1358.3**	**65.2**	207Pb/206Pb	2.77683	4.6	0.21748	2.9	0.57	0.08690	3.38	1327.4	22.9	1358.3	65.2	2.3

EV3S_TR-03.28	**1430.1**	**99.9**	207Pb/206Pb	1.65481	3.7	0.15940	2.3	0.22	0.09022	5.24	1341.8	30.5	1430.1	99.9	6.2
EV3S_TR-03.05	**1439.3**	**49.2**	207Pb/206Pb	0.55093	5.7	0.07043	2.4	0.10	0.09065	2.58	1347.4	24.8	1439.3	49.2	6.4
EV3S_TR-03.01	**1532.7**	**60.6**	207Pb/206Pb	2.22171	2.5	0.20010	1.6	0.35	0.09523	3.22	1409.1	23.3	1532.7	60.6	8.1
EV3S_TR-03.57	**2684.0**	**63.3**	207Pb/206Pb	1.86887	5.7	0.17383	3.1	0.22	0.18342	3.83	2575.2	50.5	2684.0	63.3	4.1
EV3S_TR-04.72	**448.4**	**8.9**	206Pb/238Pb	2.65976	2.7	0.22487	1.7	0.41	0.05689	4.6	448.4	8.9	487.3	101.9	8.0
EV3S_TR-04.24	**460.5**	**8.0**	206Pb/238Pb	1.89093	3.6	0.17889	2.0	0.26	0.05620	3.7	460.5	8.0	460.4	81.3	0.0
EV3S_TR-04.56	**462.8**	**11.7**	207Pb/206Pb	2.14666	4.4	0.18614	2.5	0.28	0.05696	4.3	462.8	11.7	490.1	94.1	5.6
EV3S_TR-04.75	**919.7**	**89.7**	207Pb/206Pb	2.98341	3.5	0.22169	2.3	0.44	0.06970	4.4	871.1	15.6	919.7	89.7	5.3
EV3S_TR-04.46	**1036.9**	**73.4**	207Pb/206Pb	2.22643	3.3	0.19905	2.1	0.32	0.07383	3.6	940.0	16.0	1036.9	73.4	9.3
EV3S_TR-04.18	**1045.8**	**76.9**	207Pb/206Pb	1.80345	5.1	0.16997	2.7	0.24	0.07416	3.8	945.7	16.1	1045.8	76.9	9.6
EV3S_TR-04.36	**1047.0**	**62.6**	207Pb/206Pb	2.33613	3.8	0.19867	2.6	0.11	0.07420	3.1	987.8	18.9	1047.0	62.6	5.6
EV3B.TR-04.13	**1055.3**	**84.2**	207Pb/206Pb	1.83880	4.1	0.17565	2.9	0.31	0.07451	4.2	988.4	28.4	1055.3	84.2	6.3
EV3S_TR-04.70	**1068.1**	**65.7**	207Pb/206Pb	1.79486	2.6	0.17361	1.8	0.38	0.07499	3.3	989.3	14.7	1068.1	65.7	7.4
EV3B.TR-04.61	**1054.6**	**81.6**	207Pb/206Pb	0.59904	6.6	0.07191	2.5	-0.11	0.07448	4.1	993.1	18.6	1054.6	81.6	5.8
EV3S_TR-04.12	**1050.7**	**57.5**	207Pb/206Pb	4.74771	2.9	0.31836	2.3	0.59	0.07434	2.9	994.8	21.1	1050.7	57.5	5.3
EV3S_TR-04.61	**1004.7**	**133.2**	207Pb/206Pb	2.30067	3.1	0.20610	2.0	0.28	0.07267	6.6	995.1	27.5	1004.7	133.2	1.0
EV3B.TR-04.42	**1008.6**	**188.1**	207Pb/206Pb	0.64119	5.2	0.07136	3.0	0.12	0.07281	9.3	996.5	41.8	1008.6	188.1	1.2
EV3S_TR-04.13	**967.6**	**75.8**	207Pb/206Pb	1.77562	4.8	0.16958	2.4	0.14	0.07135	3.7	1000.0	21.9	967.6	75.8	-3.4
EV3B.TR-04.01	**1100.3**	**99.8**	207Pb/206Pb	2.53599	3.7	0.20872	2.9	0.50	0.07620	5.0	1000.5	33.8	1100.3	99.8	9.1
EV3B.TR-04.53	**1056.9**	**122.0**	207Pb/206Pb	2.30077	6.9	0.19689	3.4	0.24	0.07457	6.1	1002.2	25.2	1056.9	122.0	5.2
EV3B.TR-04.49	**1042.9**	**92.9**	207Pb/206Pb	2.22806	4.0	0.19538	2.5	0.41	0.07405	4.6	1008.0	26.3	1042.9	92.9	3.3
EV3S_TR-04.17	**1119.9**	**102.2**	207Pb/206Pb	2.18195	4.8	0.19672	2.5	0.05	0.07695	5.1	1012.0	25.5	1119.9	102.2	9.6
EV3S_TR-04.44	**1003.6**	**58.7**	207Pb/206Pb	2.47018	2.8	0.21350	1.9	0.26	0.07263	2.9	1012.0	23.4	1003.6	58.7	-0.8
EV3S_TR-04.29	**1099.9**	**121.7**	207Pb/206Pb	2.41550	3.3	0.22323	1.9	0.22	0.07618	6.1	1012.2	22.8	1099.9	121.7	8.0
EV3S_TR-04.09	**1047.8**	**83.6**	207Pb/206Pb	1.99957	3.6	0.17923	2.5	0.31	0.07423	4.1	1014.3	23.2	1047.8	83.6	3.2
EV3S_TR-04.27	**1070.5**	**97.1**	207Pb/206Pb	1.80208	22.0	0.12122	6.9	0.71	0.07508	4.8	1019.9	22.0	1070.5	97.1	4.7
EV3B.TR-04.33	**1088.0**	**103.0**	207Pb/206Pb	1.79265	5.3	0.17169	3.2	0.34	0.07573	5.1	1021.4	29.8	1088.0	103.0	6.1
EV3B.TR-04.27	**1130.0**	**83.0**	207Pb/206Pb	1.83777	4.2	0.17235	2.6	0.33	0.07734	4.2	1025.0	24.7	1130.0	83.0	2.1
EV3S_TR-04.53	**1124.9**	**59.7**	207Pb/206Pb	0.58304	4.2	0.06623	3.8	0.80	0.07714	3.0	1026.1	16.8	1124.9	59.7	8.8
EV3B.TR-04.11	**1090.3**	**73.0**	207Pb/206Pb	1.85298	2.9	0.17702	2.9	0.30	0.07582	3.6	1028.9	25.6	1090.3	73.0	5.6
EV3S_TR-04.69	**1068.0**	**50.9**	207Pb/206Pb	1.38177	4.8	0.14000	4.2	0.85	0.07498	2.5	1031.9	17.1	1068.0	50.9	3.4
EV3B.TR-04.23	**1117.7**	**60.7**	207Pb/206Pb	2.46909	7.8	0.17706	5.5	-0.35	0.07687	3.0	1041.6	22.3	1117.7	60.7	6.8

EV3S_TR-04.77	**1152.2**	**54.8**	207Pb/206Pb	1.79152	4.1	0.16786	1.9	0.22	0.07821	2.8	1041.8	19.5	1152.2	54.8	9.6
EV3B.TR-04.12	**1093.1**	**84.8**	207Pb/206Pb	1.80916	3.4	0.17306	2.7	0.30	0.07592	4.2	1043.2	28.0	1093.1	84.8	4.6
EV3B.TR-04.10	**1092.9**	**68.2**	207Pb/206Pb	0.45705	5.6	0.05189	3.1	0.20	0.07592	3.4	1050.7	28.0	1092.9	68.2	3.9
EV3S_TR-04.47	**1082.7**	**56.7**	207Pb/206Pb	1.59807	3.4	0.15698	1.8	0.16	0.07553	2.8	1051.0	21.7	1082.7	56.7	2.9
EV3S_TR-04.63	**1166.3**	**103.0**	207Pb/206Pb	1.90436	3.9	0.17186	1.9	0.14	0.07877	5.2	1052.0	24.3	1166.3	103.0	9.8
EV3S_TR-04.23	**1112.5**	**72.0**	207Pb/206Pb	3.97053	3.0	0.28036	2.2	0.55	0.07666	3.6	1060.9	19.5	1112.5	72.0	4.6
EV3S_TR-04.32	**1179.3**	**97.5**	207Pb/206Pb	0.58938	9.2	0.06893	3.5	0.08	0.07929	4.9	1061.0	25.7	1179.3	97.5	10.0
EV3S_TR-04.51	**1135.1**	**59.4**	207Pb/206Pb	2.41482	3.2	0.20842	2.3	0.30	0.07754	3.0	1065.9	22.8	1135.1	59.4	6.1
EV3B.TR-04.29	**1119.0**	**53.0**	207Pb/206Pb	1.91219	3.0	0.18027	2.4	0.53	0.07693	2.7	1068.4	23.2	1119.0	53.0	4.6
EV3S_TR-04.07	**1162.5**	**56.2**	207Pb/206Pb	1.82303	5.0	0.16947	3.0	0.35	0.07862	2.8	1073.1	21.0	1162.5	56.2	7.7
EV3B.TR-04.31	**1098.3**	**59.3**	207Pb/206Pb	1.83749	5.4	0.17625	2.7	0.10	0.07612	3.0	1078.2	22.2	1098.3	59.3	1.8
EV3B.TR-04.18	**1072.1**	**67.6**	207Pb/206Pb	2.00293	3.4	0.17912	2.2	0.18	0.07514	3.4	1078.8	22.9	1072.1	67.6	-0.6
EV3B.TR-04.37	**1156.9**	**102.1**	207Pb/206Pb	2.14657	6.0	0.18075	3.3	0.02	0.07840	5.1	1080.2	26.4	1156.9	102.1	6.6
EV3B.TR-04.19	**1171.7**	**44.6**	207Pb/206Pb	1.88720	3.3	0.18217	2.3	0.33	0.07898	2.3	1094.2	22.0	1171.7	44.6	6.6
EV3B.TR-04.51	**1198.6**	**69.4**	207Pb/206Pb	2.09410	2.8	0.18922	2.0	0.31	0.08007	3.5	1094.6	20.3	1198.6	69.4	8.7
EV3B.TR-04.54	**1206.3**	**49.8**	207Pb/206Pb	1.72941	6.0	0.16821	2.7	0.19	0.08038	2.5	1104.7	19.3	1206.3	49.8	8.4
EV3S_TR-04.02	**1167.3**	**87.4**	207Pb/206Pb	1.06263	24.1	0.07502	5.4	1.04	0.07881	4.4	1106.3	24.6	1167.3	87.4	5.2
EV3S_TR-04.59	**1140.8**	**49.0**	207Pb/206Pb	2.06533	5.3	0.19540	3.1	0.40	0.07776	2.5	1106.3	18.7	1140.8	49.0	3.0
EV3B.TR-04.50	**1203.5**	**57.0**	207Pb/206Pb	1.72816	5.2	0.16926	2.8	0.46	0.08027	2.9	1117.1	20.3	1203.5	57.0	7.2
EV3S_TR-04.83	**1214.7**	**82.2**	207Pb/206Pb	1.81406	2.1	0.16587	1.9	0.32	0.08072	4.2	1118.1	22.9	1214.7	82.2	8.0
EV3B.TR-04.62	**1150.9**	**115.1**	207Pb/206Pb	0.39745	4.0	0.05125	1.9	0.11	0.07816	5.8	1120.2	30.2	1150.9	115.1	2.7
EV3S_TR-04.54	**1229.7**	**68.6**	207Pb/206Pb	1.83516	2.9	0.17254	1.8	0.27	0.08134	3.5	1120.5	22.8	1229.7	68.6	8.9
EV3S_TR-04.73	**1216.6**	**55.1**	207Pb/206Pb	1.70088	5.0	0.17254	2.3	0.27	0.08080	2.8	1122.5	19.9	1216.6	55.1	7.7
EV3S_TR-04.33	**1199.1**	**78.7**	207Pb/206Pb	1.95576	4.6	0.17890	2.6	0.16	0.08009	4.0	1128.7	27.4	1199.1	78.7	5.9
EV3B.TR-04.59	**1145.4**	**87.1**	207Pb/206Pb	1.63835	3.5	0.15655	2.2	0.28	0.07794	4.4	1140.6	28.5	1145.4	87.1	0.4
EV3B.TR-04.15	**1221.1**	**83.4**	207Pb/206Pb	1.11780	6.3	0.10851	4.3	0.60	0.08098	4.2	1141.5	30.7	1221.1	83.4	6.5
EV3S_TR-04.66	**1174.0**	**45.9**	207Pb/206Pb	2.92874	4.4	0.23794	2.7	0.22	0.07908	2.3	1143.8	14.0	1174.0	45.9	2.6
EV3B.TR-04.48	**1262.3**	**73.7**	207Pb/206Pb	1.69153	5.6	0.14797	5.4	0.90	0.08271	3.8	1150.5	26.3	1262.3	73.7	8.9
EV3S_TR-04.58	**1112.3**	**99.0**	207Pb/206Pb	0.38899	3.4	0.05266	1.7	0.14	0.07666	5.0	1150.6	33.0	1112.3	99.0	-3.4
EV3S_TR-04.16	**1207.9**	**103.9**	207Pb/206Pb	4.08595	17.4	0.21362	4.6	1.07	0.08044	5.3	1157.7	26.3	1207.9	103.9	4.2
EV3S_TR-04.45	**1224.4**	**64.7**	207Pb/206Pb	1.70220	3.1	0.16998	2.5	0.48	0.08112	3.3	1170.2	22.3	1224.4	64.7	4.4
EV3B.TR-04.07	**1278.4**	**56.3**	207Pb/206Pb	1.02719	5.0	0.10728	3.9	0.59	0.08339	2.9	1174.6	26.1	1278.4	56.3	8.1

EV3B.TR-04.21	**1196.9**	**55.5**	207Pb/206Pb	0.54291	5.1	0.06667	2.5	0.34	0.08000	2.8	1174.7	25.3	1196.9	55.5	1.9
EV3S_TR-04.85	**1209.9**	**48.9**	207Pb/206Pb	2.66104	3.6	0.22000	2.1	0.10	0.08053	2.5	1175.9	17.5	1209.9	48.9	2.8
EV3B.TR-04.24	**1238.0**	**35.0**	207Pb/206Pb	2.25575	1.9	0.20024	1.9	0.58	0.08170	1.8	1176.6	20.3	1238.0	35.0	5.0
EV3B.TR-04.16	**1193.9**	**99.1**	207Pb/206Pb	2.16318	3.5	0.19373	2.9	0.15	0.07987	5.0	1178.6	31.1	1193.9	99.1	1.3
EV3S_TR-04.57	**1229.9**	**57.5**	207Pb/206Pb	0.58462	5.0	0.07444	2.6	0.51	0.08135	2.9	1205.8	23.5	1229.9	57.5	2.0
EV3S_TR-04.60	**1220.5**	**62.4**	207Pb/206Pb	2.00731	2.6	0.18722	1.8	0.42	0.08096	3.2	1208.0	22.1	1220.5	62.4	1.0
EV3B.TR-04.02	**1299.3**	**116.9**	207Pb/206Pb	0.40349	4.1	0.05255	3.3	0.12	0.08429	6.0	1215.9	36.3	1299.3	116.9	6.4
EV3S_TR-04.50	**1293.3**	**64.5**	207Pb/206Pb	1.16036	23.4	0.08866	22.8	0.70	0.08403	3.3	1220.4	25.6	1293.3	64.5	5.6
EV3S_TR-04.43	**1290.6**	**57.2**	207Pb/206Pb	1.80611	4.6	0.17119	2.8	0.10	0.08391	2.9	1247.4	21.4	1290.6	57.2	3.3
EV3S_TR-04.37	**1369.0**	**62.9**	207Pb/206Pb	1.69427	3.2	0.16560	2.1	0.35	0.08739	3.3	1252.7	21.4	1369.0	62.9	8.5
EV3S_TR-04.78	**1369.6**	**39.8**	207Pb/206Pb	1.89141	3.0	0.17540	2.0	0.46	0.08741	2.1	1256.5	18.5	1369.6	39.8	8.3
EV3B.TR-04.04	**1285.3**	**86.9**	207Pb/206Pb	1.81508	2.5	0.17003	2.8	0.48	0.08369	4.5	1260.3	33.9	1285.3	86.9	1.9
EV3S_TR-04.84	**1376.5**	**76.6**	207Pb/206Pb	2.10798	4.5	0.18940	2.2	0.40	0.08773	4.0	1281.9	24.8	1376.5	76.6	6.9
EV3S_TR-04.71	**1333.4**	**48.1**	207Pb/206Pb	1.71483	3.2	0.16586	1.6	0.21	0.08579	2.5	1307.5	20.1	1333.4	48.1	1.9
EV3S_TR-04.14	**1341.0**	**73.6**	207Pb/206Pb	1.65088	3.8	0.16780	2.4	0.36	0.08613	3.8	1312.5	24.9	1341.0	73.6	2.1
EV3S_TR-04.38	**1431.6**	**48.7**	207Pb/206Pb	2.58448	3.0	0.21450	1.9	0.15	0.09029	2.6	1353.2	24.1	1431.6	48.7	5.5
EV3S_TR-04.65	**1410.0**	**88.4**	207Pb/206Pb	4.05678	8.1	0.30219	8.9	0.93	0.08927	4.6	1376.0	33.1	1410.0	88.4	2.4
EV3B.TR-04.35	**1507.5**	**71.7**	207Pb/206Pb	2.36546	4.8	0.18704	3.0	0.33	0.09397	3.8	1401.1	34.2	1507.5	71.7	7.1
EV3S_TR-04.21	**1490.5**	**66.2**	207Pb/206Pb	1.83826	4.0	0.17146	2.3	0.40	0.09313	3.5	1480.4	26.3	1490.5	66.2	0.7
EV3S_TR-04.22	**1673.8**	**47.6**	207Pb/206Pb	3.31502	2.8	0.25816	2.0	-0.02	0.10272	2.6	1593.2	31.4	1673.8	47.6	4.8
EV3S_TR-04.11	**1768.7**	**44.1**	207Pb/206Pb	1.23664	8.6	0.11480	5.3	0.76	0.10816	2.4	1781.7	35.9	1768.7	44.1	-0.7

Southern Sample Data

Grain Number	Chosen Age	Err. 2σ	Analysis Type	$^{*207}Pb/^{235}U$ [b]calculated	Rel. Err. *2σ [b]calculated	$^{206}Pb/^{238}U$	Rel. Err. 2σ	RHO (error corr.)	$^{207}Pb/^{206}Pb$	Rel. Err. 2σ	$^{206}Pb/^{238}U$ age	Err. 2σ	$^{207}Pb/^{206}Pb$ age	Err. 2σ	Disc. (%)
EV3S_NE-S.14	**602.0**	**12.0**	$^{206}Pb/^{238}Pb$	1.64818	6.5	0.15990	3.5	0.16	0.06124	3.1	602.0	12.0	647.7	66.6	7.1
EV3B.NE-S.02	**972.2**	**74.1**	$^{207}Pb/^{206}Pb$	2.68552	4.4	0.20950	2.4	0.04	0.07152	3.6	886.7	34.4	972.2	74.1	8.8
EV3S_NE-S.32	**971.0**	**116.4**	$^{207}Pb/^{206}Pb$	2.03708	19.5	0.14934	11.5	0.61	0.07147	5.7	911.2	23.4	971.0	116.4	6.2
EV3S_NE-S.13	**1062.0**	**138.3**	$^{207}Pb/^{206}Pb$	0.61387	8.4	0.07016	3.3	0.27	0.07476	6.9	956.2	30.8	1062.0	138.3	10.0
EV3S_NE-S.60	**1067.9**	**137.7**	$^{207}Pb/^{206}Pb$	0.53502	4.2	0.05348	3.5	0.56	0.07498	6.8	979.3	37.1	1067.9	137.7	8.3
EV3S_NE-S.38	**1063.8**	**60.4**	$^{207}Pb/^{206}Pb$	2.25991	6.6	0.19604	3.6	0.16	0.07482	3.0	1007.2	22.1	1063.8	60.4	5.3
EV3B.NE-S.37	**1056.8**	**86.6**	$^{207}Pb/^{206}Pb$	1.86493	5.3	0.16932	3.8	0.55	0.07457	4.3	1011.9	24.7	1056.8	86.6	4.3
EV3S_NE-S.15	**1099.7**	**73.8**	$^{207}Pb/^{206}Pb$	0.82653	3.2	0.09788	2.1	0.38	0.07618	3.7	1011.9	19.2	1099.7	73.8	8.0
EV3S_NE-S.18	**1059.6**	**87.2**	$^{207}Pb/^{206}Pb$	1.71591	2.8	0.15853	1.6	0.21	0.07467	4.3	1044.2	19.7	1059.6	87.2	1.4
EV3S_NE-S.21	**1126.5**	**93.3**	$^{207}Pb/^{206}Pb$	2.66718	5.2	0.22392	2.9	0.22	0.07721	4.7	1055.9	22.7	1126.5	93.3	6.3
EV3S_NE-S.49	**1136.2**	**100.1**	$^{207}Pb/^{206}Pb$	1.77564	5.6	0.16931	3.5	0.30	0.07758	5.0	1058.6	31.9	1136.2	100.1	6.8
EV3B.NE-S.32	**1193.9**	**86.9**	$^{207}Pb/^{206}Pb$	1.77088	27.2	0.18175	21.8	0.91	0.07987	4.4	1080.0	23.3	1193.9	86.9	9.5
EV3B.NE-S.19	**1175.2**	**83.8**	$^{207}Pb/^{206}Pb$	1.80706	5.8	0.16915	3.0	0.26	0.07912	4.2	1112.3	23.2	1175.2	83.8	5.3
EV3B.NE-S.35	**1173.7**	**72.9**	$^{207}Pb/^{206}Pb$	2.92759	3.8	0.22738	1.9	0.65	0.07906	3.7	1114.4	23.2	1173.7	72.9	5.1
EV3S_NE-S.33	**1180.9**	**73.6**	$^{207}Pb/^{206}Pb$	1.49624	5.6	0.15183	2.8	0.20	0.07935	3.7	1132.1	22.7	1180.9	73.6	4.1
EV3S_NE-S.47	**1189.3**	**61.0**	$^{207}Pb/^{206}Pb$	1.64696	4.2	0.15541	2.5	0.63	0.07969	3.1	1139.8	25.8	1189.3	61.0	4.2
EV3S_NE-S.48	**1262.7**	**95.4**	$^{207}Pb/^{206}Pb$	2.12515	3.6	0.19341	2.5	0.53	0.08272	4.9	1168.5	35.2	1262.7	95.4	7.5
EV3S_NE-S.61	**1200.3**	**82.8**	$^{207}Pb/^{206}Pb$	1.69614	6.6	0.16407	4.1	0.24	0.08013	4.2	1175.4	33.4	1200.3	82.8	2.1
EV3S_NE-S.19	**1279.9**	**83.3**	$^{207}Pb/^{206}Pb$	1.81630	5.0	0.17109	2.5	-0.17	0.08346	4.3	1216.2	26.5	1279.9	83.3	5.0
EV3S_NE-S.40	**1293.0**	**88.0**	$^{207}Pb/^{206}Pb$	0.57434	8.6	0.07149	3.6	0.12	0.08402	4.5	1217.7	28.6	1293.0	88.0	5.8
EV3S_NE-S.41	**1396.9**	**66.0**	$^{207}Pb/^{206}Pb$	2.40851	4.4	0.20791	2.6	0.26	0.08867	3.4	1285.5	33.8	1396.9	66.0	8.0
EV3S_NE-S.20	**1346.9**	**103.1**	$^{207}Pb/^{206}Pb$	2.38926	4.5	0.20763	2.4	0.34	0.08639	5.3	1302.6	34.2	1346.9	103.1	3.3
EV3S_NE-S.02	**1398.7**	**112.8**	$^{207}Pb/^{206}Pb$	1.65830	4.9	0.14215	2.7	0.73	0.08875	5.9	1323.6	39.8	1398.7	112.8	5.4
EV3S_NE-S.55	**1462.0**	**87.0**	$^{207}Pb/^{206}Pb$	2.99333	5.1	0.23664	3.3	0.47	0.09174	4.6	1369.2	40.5	1462.0	87.0	6.3
EV3B.NE-S.26	**1372.0**	**91.6**	$^{207}Pb/^{206}Pb$	2.17336	9.5	0.18138	3.2	0.40	0.08752	4.8	1409.7	29.9	1372.0	91.6	-2.7
EV2S_NE0.01	**444.0**	**12.5**	$^{206}Pb/^{238}Pb$	1.75976	9.1	0.16694	4.2	0.03	0.05654	3.7	444.0	12.5	473.8	82.7	6.3
EV2S_NE0.22	**699.9**	**23.1**	$^{206}Pb/^{238}Pb$	1.73641	3.7	0.17015	3.3	0.78	0.06356	6.0	699.9	23.1	726.9	126.8	3.7

EV2S_NE0.10	**919.6**	**97.4**	$^{207}Pb/^{206}Pb$	0.56756	5.8	0.06867	3.3	0.43	0.06970	4.7	931.7	28.8	919.6	97.4	-1.3
EV2S_NE0.18	**1030.8**	**69.3**	$^{207}Pb/^{206}Pb$	3.41460	8.5	0.20051	3.8	-1.20	0.07361	3.4	951.1	26.4	1030.8	69.3	7.7
EV2B_NE0.09	**1021.7**	**30.5**	$^{207}Pb/^{206}Pb$	1.66846	2.8	0.16513	3.0	0.87	0.07328	1.5	985.2	27.4	1021.7	30.5	3.6
EV2S_NE0.45	**1083.8**	**110.2**	$^{207}Pb/^{206}Pb$	2.32925	6.0	0.19842	3.2	0.22	0.07557	5.5	995.4	30.8	1083.8	110.2	8.2
EV2S_NE0.37	**1075.2**	**70.1**	$^{207}Pb/^{206}Pb$	2.78576	4.1	0.22752	3.1	0.47	0.07525	3.5	999.6	21.3	1075.2	70.1	7.0
EV2S_NE0.32	**1039.9**	**39.8**	$^{207}Pb/^{206}Pb$	1.80385	2.9	0.16229	2.2	0.54	0.07394	2.0	1008.5	19.2	1039.9	39.8	3.0
EV2S_NE0.20	**1041.8**	**47.5**	$^{207}Pb/^{206}Pb$	1.61363	4.3	0.15899	3.0	0.61	0.07401	2.4	1013.0	31.3	1041.8	47.5	2.8
EV2S_NE0.48	**1120.6**	**110.2**	$^{207}Pb/^{206}Pb$	1.67042	3.1	0.16030	2.1	0.22	0.07698	5.5	1047.9	27.9	1120.6	110.2	6.5
EV2B_NE0.18	**1165.5**	**27.6**	$^{207}Pb/^{206}Pb$	1.96331	2.1	0.18085	2.7	0.86	0.07873	1.4	1071.6	26.5	1165.5	27.6	8.1
EV2B_NE0.06	**1093.9**	**120.3**	$^{207}Pb/^{206}Pb$	1.92565	6.1	0.18387	5.0	0.43	0.07596	6.0	1088.1	50.2	1093.9	120.3	0.5
EV2B_NE0.03	**1151.0**	**69.0**	$^{207}Pb/^{206}Pb$	1.98201	3.8	0.18394	3.0	0.50	0.07815	3.5	1088.5	30.4	1151.0	69.0	5.4
EV2S_NE0.25	**1201.9**	**105.7**	$^{207}Pb/^{206}Pb$	1.00496	6.1	0.11468	3.5	0.33	0.08020	5.4	1109.6	34.2	1201.9	105.7	7.7
EV2S_NE0.46	**1198.5**	**88.0**	$^{207}Pb/^{206}Pb$	1.73993	6.2	0.16698	3.3	0.48	0.08006	4.5	1150.9	85.2	1198.5	88.0	4.0
EV2S_NE0.50	**1203.7**	**85.4**	$^{207}Pb/^{206}Pb$	0.86002	7.0	0.08737	4.9	0.28	0.08027	4.3	1160.9	26.9	1203.7	85.4	3.6
EV2B_NE0.14	**1299.2**	**32.3**	$^{207}Pb/^{206}Pb$	2.32868	2.9	0.20038	3.0	0.84	0.08429	1.7	1177.3	32.2	1299.2	32.3	9.4
EV2S_NE0.51	**1280.1**	**65.6**	$^{207}Pb/^{206}Pb$	2.18382	4.9	0.19731	2.5	0.47	0.08346	3.4	1181.4	22.7	1280.1	65.6	7.7
EV2S_NE0.08	**1190.9**	**57.4**	$^{207}Pb/^{206}Pb$	0.51848	4.6	0.05731	3.5	0.39	0.07975	2.9	1234.8	53.9	1190.9	57.4	-3.7
EV2S_NE0.56	**1350.9**	**33.4**	$^{207}Pb/^{206}Pb$	0.53480	6.6	0.05745	2.7	0.38	0.08657	1.7	1298.8	25.4	1350.9	33.4	3.9
EV2S_NE0.36	**1399.9**	**71.8**	$^{207}Pb/^{206}Pb$	2.05086	4.5	0.15340	2.9	0.78	0.08880	3.7	1321.5	36.6	1399.9	71.8	5.6
NE100_02	**326.1**	**10.1**	$^{206}Pb/^{238}Pb$	0.38017	3.5	0.05189	3.2	0.91	0.05314	1.4	326.1	10.1	334.5	31.9	2.5
NE100_40	**327.7**	**12.7**	$^{206}Pb/^{238}Pb$	0.38689	4.3	0.05215	4.0	0.93	0.05380	1.6	327.7	12.7	362.5	35.6	9.6
NE100_35	**330.7**	**12.7**	$^{206}Pb/^{238}Pb$	0.38946	4.2	0.05263	3.9	0.93	0.05366	1.6	330.7	12.7	356.5	35.6	7.2
NE100_113	**333.6**	**12.7**	$^{206}Pb/^{238}Pb$	0.39379	4.3	0.05312	3.9	0.92	0.05377	1.7	333.6	12.7	361.0	38.2	7.6
NE100_54	**337.1**	**12.8**	$^{206}Pb/^{238}Pb$	0.39776	4.2	0.05368	3.9	0.93	0.05374	1.6	337.1	12.8	360.0	35.3	6.4
NE100_76	**337.3**	**12.9**	$^{206}Pb/^{238}Pb$	0.39855	4.2	0.05372	3.9	0.93	0.05381	1.6	337.3	12.9	362.5	35.7	6.9
NE100_09	**337.6**	**11.0**	$^{206}Pb/^{238}Pb$	0.39664	3.6	0.05376	3.3	0.92	0.05351	1.4	337.6	11.0	350.0	31.9	3.5
NE100_46	**339.1**	**13.2**	$^{206}Pb/^{238}Pb$	0.40208	4.3	0.05400	4.0	0.93	0.05400	1.6	339.1	13.2	370.5	35.8	8.5
NE100_45C	**340.2**	**13.1**	$^{206}Pb/^{238}Pb$	0.40442	4.3	0.05419	3.9	0.93	0.05412	1.6	340.2	13.1	376.0	36.1	9.5
NE100_45R	**340.6**	**13.1**	$^{206}Pb/^{238}Pb$	0.40279	4.3	0.05426	3.9	0.93	0.05384	1.6	340.6	13.1	364.0	36.4	6.4
NE100_10	**340.8**	**10.9**	$^{206}Pb/^{238}Pb$	0.40180	3.6	0.05429	3.3	0.92	0.05367	1.4	340.8	10.9	357.0	32.4	4.5
NE100_07	**345.7**	**11.3**	$^{206}Pb/^{238}Pb$	0.40535	3.6	0.05509	3.4	0.92	0.05336	1.4	345.7	11.3	344.0	31.4	-0.5
NE100_97	**385.8**	**15.2**	$^{206}Pb/^{238}Pb$	0.46909	4.4	0.06168	4.1	0.92	0.05516	1.7	385.8	15.2	418.5	38.4	7.8

NE100_75	**416.1**	**15.7**	$^{206}Pb/^{238}Pb$	0.51645	4.2	0.06669	3.9	0.92	0.05617	1.6	416.1	15.7	459.0	36.3	9.3
NE100_78	**429.3**	**16.1**	$^{206}Pb/^{238}Pb$	0.53089	4.2	0.06887	3.9	0.93	0.05591	1.6	429.3	16.1	448.5	35.0	4.3
NE100_95C	**431.7**	**16.9**	$^{206}Pb/^{238}Pb$	0.53753	4.4	0.06927	4.1	0.93	0.05628	1.6	431.7	16.9	463.0	35.2	6.8
NE100_112	**586.9**	**22.1**	$^{206}Pb/^{238}Pb$	0.79751	4.3	0.09532	3.9	0.92	0.06068	1.6	586.9	22.1	627.5	34.9	6.5
NE100_33	**685.6**	**23.4**	$^{206}Pb/^{238}Pb$	1.18707	5.0	0.11222	3.6	0.73	0.07672	3.4	685.6	23.4	1113.5	68.2	5.3
NE100_98	**963.5**	**32.0**	$^{207}Pb/^{206}Pb$	1.45130	4.5	0.14779	4.2	0.94	0.07122	1.6	888.5	34.7	963.5	32.0	7.8
NE100_71	**966.0**	**32.1**	$^{207}Pb/^{206}Pb$	1.45378	4.2	0.14788	3.9	0.93	0.07130	1.6	889.0	32.2	966.0	32.1	8.0
NE100_04	**1010.0**	**27.8**	$^{207}Pb/^{206}Pb$	1.52168	3.6	0.15146	3.3	0.93	0.07287	1.4	909.1	28.3	1010.0	27.8	10.0
NE100_21	**1013.0**	**29.7**	$^{207}Pb/^{206}Pb$	1.54101	3.6	0.15314	3.3	0.91	0.07298	1.5	918.5	28.1	1013.0	29.7	9.3
NE100_108	**1018.5**	**33.4**	$^{207}Pb/^{206}Pb$	1.57544	4.4	0.15616	4.0	0.93	0.07317	1.7	935.4	35.1	1018.5	33.4	8.2
NE100_63C	**1008.0**	**32.5**	$^{207}Pb/^{206}Pb$	1.57129	4.3	0.15654	3.9	0.93	0.07280	1.6	937.5	34.4	1008.0	32.5	7.0
NE100_53	**1010.5**	**31.8**	$^{207}Pb/^{206}Pb$	1.57740	4.2	0.15697	3.9	0.93	0.07288	1.6	939.9	34.1	1010.5	31.8	7.0
NE100_81	**992.5**	**31.7**	$^{207}Pb/^{206}Pb$	1.56355	4.2	0.15698	3.9	0.93	0.07224	1.6	939.9	34.3	992.5	31.7	5.3
NE100_96	**961.0**	**33.0**	$^{207}Pb/^{206}Pb$	1.54630	4.3	0.15767	4.0	0.93	0.07113	1.6	943.8	34.9	961.0	33.0	1.8
NE100_01	**1024.5**	**28.6**	$^{207}Pb/^{206}Pb$	1.60210	3.6	0.15834	3.3	0.92	0.07338	1.4	947.5	29.5	1024.5	28.6	7.5
NE100_24	**1043.5**	**29.5**	$^{207}Pb/^{206}Pb$	1.62075	3.6	0.15869	3.3	0.91	0.07407	1.5	949.5	29.1	1043.5	29.5	9.0
NE100_93	**1025.0**	**32.4**	$^{207}Pb/^{206}Pb$	1.61553	4.9	0.15960	4.6	0.95	0.07341	1.6	954.5	41.0	1025.0	32.4	6.9
NE100_08	**1013.5**	**29.4**	$^{207}Pb/^{206}Pb$	1.60917	3.7	0.15991	3.4	0.92	0.07299	1.5	956.2	30.4	1013.5	29.4	5.7
NE100_107	**1010.5**	**31.7**	$^{207}Pb/^{206}Pb$	1.60860	4.3	0.16009	4.0	0.93	0.07288	1.6	957.2	35.9	1010.5	31.7	5.3
NE100_20	**1040.5**	**27.8**	$^{207}Pb/^{206}Pb$	1.64011	3.6	0.16079	3.3	0.92	0.07398	1.4	961.1	29.5	1040.5	27.8	7.6
NE100_16	**1042.5**	**27.7**	$^{207}Pb/^{206}Pb$	1.64564	3.7	0.16119	3.4	0.93	0.07404	1.4	963.4	30.6	1042.5	27.7	7.6
NE100_32	**1076.0**	**27.8**	$^{207}Pb/^{206}Pb$	1.69060	3.8	0.16287	3.5	0.93	0.07529	1.4	972.7	31.7	1076.0	27.8	9.6
NE100_106	**1066.5**	**34.8**	$^{207}Pb/^{206}Pb$	1.69057	4.4	0.16364	4.0	0.92	0.07493	1.7	976.9	36.5	1066.5	34.8	8.4
NE100_23	**1034.0**	**28.5**	$^{207}Pb/^{206}Pb$	1.66671	3.6	0.16392	3.3	0.92	0.07374	1.4	978.5	29.9	1034.0	28.5	5.4
NE100_37	**1066.0**	**31.4**	$^{207}Pb/^{206}Pb$	1.69569	4.2	0.16416	3.9	0.93	0.07492	1.6	979.8	35.4	1066.0	31.4	8.1
NE100_92	**1037.0**	**31.1**	$^{207}Pb/^{206}Pb$	1.68304	4.3	0.16529	4.0	0.93	0.07385	1.5	986.1	36.7	1037.0	31.1	4.9
NE100_104	**1058.5**	**31.4**	$^{207}Pb/^{206}Pb$	1.70606	4.3	0.16579	4.0	0.93	0.07463	1.6	988.9	36.8	1058.5	31.4	6.6
NE100_89	**1101.0**	**33.3**	$^{207}Pb/^{206}Pb$	1.74629	4.3	0.16613	4.0	0.92	0.07624	1.7	990.7	36.3	1101.0	33.3	10.0
NE100_52	**1061.5**	**31.8**	$^{207}Pb/^{206}Pb$	1.71662	4.3	0.16656	4.0	0.93	0.07475	1.6	993.1	36.3	1061.5	31.8	6.4
NE100_94	**1027.5**	**31.4**	$^{207}Pb/^{206}Pb$	1.69519	4.3	0.16726	4.1	0.93	0.07351	1.6	997.0	37.4	1027.5	31.4	3.0
NE100_91	**1037.0**	**31.3**	$^{207}Pb/^{206}Pb$	1.70339	4.3	0.16731	4.0	0.93	0.07384	1.6	997.2	37.1	1037.0	31.3	3.8
NE100_100	**1048.0**	**33.2**	$^{207}Pb/^{206}Pb$	1.73766	4.3	0.16973	3.9	0.92	0.07425	1.6	1010.6	36.8	1048.0	33.2	3.6

NE100_50	**1035.5**	**31.4**	$^{207}Pb/^{206}Pb$	1.72995	4.3	0.17005	4.0	0.93	0.07378	1.6	1012.4	37.5	1035.5	31.4	2.2
NE100_79	**1115.0**	**31.1**	$^{207}Pb/^{206}Pb$	1.82843	4.2	0.17274	3.9	0.93	0.07677	1.6	1027.1	37.4	1115.0	31.1	7.9
NE100_38	**1129.0**	**30.7**	$^{207}Pb/^{206}Pb$	1.84267	4.3	0.17287	4.1	0.93	0.07731	1.5	1027.9	38.5	1129.0	30.7	9.0
NE100_15	**1083.0**	**27.8**	$^{207}Pb/^{206}Pb$	1.81528	3.6	0.17427	3.3	0.92	0.07555	1.4	1035.6	31.8	1083.0	27.8	4.4
NE100_51	**1050.5**	**31.3**	$^{207}Pb/^{206}Pb$	1.78741	4.3	0.17436	4.0	0.93	0.07435	1.6	1036.1	38.4	1050.5	31.3	1.4
NE100_65	**1139.0**	**30.9**	$^{207}Pb/^{206}Pb$	1.86926	4.3	0.17449	4.0	0.93	0.07770	1.6	1036.7	38.1	1139.0	30.9	9.0
NE100_85	**1122.5**	**31.2**	$^{207}Pb/^{206}Pb$	1.85907	4.3	0.17497	4.0	0.93	0.07706	1.6	1039.4	38.1	1122.5	31.2	7.4
NE100_58	**1167.0**	**31.0**	$^{207}Pb/^{206}Pb$	1.93280	4.1	0.17787	3.8	0.93	0.07881	1.6	1055.3	37.1	1167.0	31.0	9.6
NE100_101C	**1130.5**	**31.9**	$^{207}Pb/^{206}Pb$	1.90389	4.3	0.17849	4.0	0.93	0.07736	1.6	1058.7	38.8	1130.5	31.9	6.4
NE100_06	**1139.0**	**28.5**	$^{207}Pb/^{206}Pb$	1.91448	3.4	0.17871	3.1	0.91	0.07770	1.4	1059.9	30.6	1139.0	28.5	6.9
NE100_12	**1148.0**	**31.0**	$^{207}Pb/^{206}Pb$	1.93405	3.6	0.17971	3.2	0.90	0.07806	1.6	1065.3	31.8	1148.0	31.0	7.2
NE100_11	**1139.5**	**27.2**	$^{207}Pb/^{206}Pb$	1.92644	3.6	0.17975	3.4	0.93	0.07773	1.4	1065.6	32.9	1139.5	27.2	6.5
NE100_34	**1130.0**	**30.9**	$^{207}Pb/^{206}Pb$	1.92708	4.5	0.18068	4.2	0.94	0.07736	1.6	1070.6	41.3	1130.0	30.9	5.3
NE100_115	**1179.0**	**31.3**	$^{207}Pb/^{206}Pb$	1.97801	4.3	0.18094	4.0	0.93	0.07929	1.6	1072.1	39.5	1179.0	31.3	9.1
NE100_29	**1199.0**	**28.7**	$^{207}Pb/^{206}Pb$	2.01144	3.6	0.18216	3.3	0.92	0.08008	1.5	1078.7	33.2	1199.0	28.7	10.0
NE100_109	**1181.5**	**30.7**	$^{207}Pb/^{206}Pb$	1.99554	4.3	0.18230	4.0	0.93	0.07939	1.6	1079.5	39.5	1181.5	30.7	8.6
NE100_47	**1198.5**	**32.6**	$^{207}Pb/^{206}Pb$	2.03165	4.2	0.18402	3.9	0.92	0.08007	1.7	1088.8	39.1	1198.5	32.6	9.1
NE100_72	**1154.0**	**31.2**	$^{207}Pb/^{206}Pb$	1.98814	4.1	0.18416	3.8	0.93	0.07830	1.6	1089.6	38.4	1154.0	31.2	5.6
NE100_61	**1183.5**	**31.3**	$^{207}Pb/^{206}Pb$	2.02376	4.3	0.18470	4.0	0.93	0.07947	1.6	1092.6	39.7	1183.5	31.3	7.7
NE100_66	**1214.5**	**31.1**	$^{207}Pb/^{206}Pb$	2.08534	4.1	0.18737	3.8	0.92	0.08072	1.6	1107.1	38.2	1214.5	31.1	8.8
NE100_77	**1181.5**	**30.7**	$^{207}Pb/^{206}Pb$	2.05088	4.3	0.18738	4.0	0.93	0.07938	1.6	1107.1	40.3	1181.5	30.7	6.3
NE100_68	**1180.5**	**31.1**	$^{207}Pb/^{206}Pb$	2.05392	4.4	0.18775	4.1	0.93	0.07934	1.6	1109.1	41.6	1180.5	31.1	6.0
NE100_13	**1170.0**	**27.6**	$^{207}Pb/^{206}Pb$	2.04372	3.6	0.18783	3.4	0.92	0.07892	1.4	1109.6	34.2	1170.0	27.6	5.2
NE100_62	**1182.5**	**31.4**	$^{207}Pb/^{206}Pb$	2.05724	4.4	0.18786	4.1	0.93	0.07942	1.6	1109.8	41.6	1182.5	31.4	6.2
NE100_90	**1228.5**	**31.3**	$^{207}Pb/^{206}Pb$	2.11550	4.2	0.18871	3.9	0.93	0.08131	1.6	1114.3	40.0	1228.5	31.3	9.3
NE100_116	**1244.0**	**31.1**	$^{207}Pb/^{206}Pb$	2.18698	4.3	0.19357	4.0	0.93	0.08194	1.6	1140.6	41.3	1244.0	31.1	8.3
NE100_25	**1267.5**	**27.6**	$^{207}Pb/^{206}Pb$	2.22784	3.6	0.19482	3.4	0.92	0.08294	1.4	1147.4	35.3	1267.5	27.6	9.5
NE100_103	**1353.0**	**30.1**	$^{207}Pb/^{206}Pb$	2.52190	4.2	0.21104	3.9	0.93	0.08667	1.6	1234.3	44.2	1353.0	30.1	8.8
NE100_28	**1341.0**	**27.0**	$^{207}Pb/^{206}Pb$	2.59732	3.8	0.21872	3.5	0.93	0.08613	1.4	1275.0	40.5	1341.0	27.0	4.9
NE100_44	**1418.0**	**30.4**	$^{207}Pb/^{206}Pb$	2.73921	4.3	0.22160	4.0	0.93	0.08965	1.6	1290.3	47.1	1418.0	30.4	9.0
NE100_83	**1446.5**	**29.5**	$^{207}Pb/^{206}Pb$	2.82861	4.2	0.22544	3.9	0.93	0.09100	1.6	1310.5	46.5	1446.5	29.5	9.4
EV2S_NE180.48	**332.4**	**12.7**	$^{206}Pb/^{238}Pb$	1.97975	3.5	0.19075	3.6	0.85	0.05390	3.5	332.4	12.7	366.7	79.9	9.4

EV2S_NE180.78	**348.8**	**12.2**	$^{206}Pb/^{238}Pb$	1.63328	5.5	0.15889	3.5	0.20	0.05415	7.2	348.8	12.2	377.3	161.8	7.6
EV2S_NE180.67	**352.5**	**12.4**	$^{206}Pb/^{238}Pb$	0.53575	6.0	0.06986	3.5	0.40	0.05443	3.9	352.5	12.4	388.8	87.2	9.3
EV2S_NE180.75	**415.2**	**17.2**	$^{206}Pb/^{238}Pb$	0.50576	9.6	0.06653	4.3	0.40	0.05514	8.9	415.2	17.2	418.0	198.0	0.6
EV2B_NE180.36	**429.0**	**16.1**	$^{206}Pb/^{238}Pb$	0.52308	10.8	0.06881	3.9	0.22	0.05513	10.6	429.0	16.1	417.6	237.0	-2.7
EV2S_NE180.66	**435.3**	**14.9**	$^{206}Pb/^{238}Pb$	1.73563	4.2	0.16914	3.6	0.66	0.05562	5.6	435.3	14.9	437.3	124.1	0.4
EV2B_NE180.38	**555.1**	**17.3**	$^{206}Pb/^{238}Pb$	0.74503	7.7	0.08992	3.3	0.14	0.06009	7.9	555.1	17.3	606.8	171.3	8.5
EV2S_NE180.63	**700.6**	**26.2**	$^{206}Pb/^{238}Pb$	2.12395	3.5	0.19851	3.1	0.65	0.06377	4.7	700.6	26.2	734.2	99.9	4.6
EV2S_NE180.05	**982.8**	**138.6**	$^{207}Pb/^{206}Pb$	1.91157	3.4	0.17924	2.1	0.28	0.07189	6.8	915.9	28.4	982.8	138.6	6.8
EV2B_NE180.22	**1046.1**	**54.3**	$^{207}Pb/^{206}Pb$	1.61489	2.6	0.15791	2.9	0.52	0.07417	2.7	945.2	25.3	1046.1	54.3	9.6
EV2S_NE180.77	**1056.5**	**118.8**	$^{207}Pb/^{206}Pb$	0.46234	4.1	0.05681	2.8	0.40	0.07455	5.9	950.6	30.7	1056.5	118.8	10.0
EV2B_NE180.33	**1007.9**	**129.9**	$^{207}Pb/^{206}Pb$	1.60729	5.8	0.16017	3.5	0.12	0.07278	6.4	957.7	31.2	1007.9	129.9	5.0
EV2S_NE180.26	**1039.4**	**130.8**	$^{207}Pb/^{206}Pb$	1.74780	7.7	0.16130	3.3	-0.04	0.07392	6.5	963.4	28.2	1039.4	130.8	7.3
EV2S_NE180.19	**1050.0**	**63.0**	$^{207}Pb/^{206}Pb$	1.66634	3.5	0.16265	2.3	0.47	0.07431	3.1	971.5	20.4	1050.0	63.0	7.5
EV2S_NE180.21	**986.7**	**54.7**	$^{207}Pb/^{206}Pb$	1.63494	3.6	0.16741	2.7	0.25	0.07203	2.7	972.2	16.3	986.7	54.7	1.5
EV2B_NE180.30	**1051.5**	**44.4**	$^{207}Pb/^{206}Pb$	1.67165	2.6	0.16303	3.4	0.76	0.07437	2.2	973.6	30.6	1051.5	44.4	7.4
EV2S_NE180.68	**1063.9**	**105.0**	$^{207}Pb/^{206}Pb$	0.42178	4.6	0.05620	3.6	0.58	0.07483	5.2	974.4	32.6	1063.9	105.0	8.4
EV2S_NE180.40	**1048.5**	**81.9**	$^{207}Pb/^{206}Pb$	2.06576	4.2	0.18958	3.3	0.65	0.07426	4.1	977.8	32.2	1048.5	81.9	6.7
EV2S_NE180.37	**1010.0**	**46.0**	$^{207}Pb/^{206}Pb$	1.64929	3.6	0.16417	3.4	0.79	0.07286	2.3	979.9	31.0	1010.0	46.0	3.0
EV2B_NE180.07	**1032.5**	**86.3**	$^{207}Pb/^{206}Pb$	1.67402	4.1	0.16480	2.9	0.29	0.07367	4.3	983.4	26.7	1032.5	86.3	4.8
EV2S_NE180.47	**1035.0**	**30.0**	$^{207}Pb/^{206}Pb$	1.69438	4.1	0.16656	3.9	0.93	0.07378	1.5	993.1	36.1	1035.0	30.0	4.1
EV2B_NE180.24	**1067.5**	**67.8**	$^{207}Pb/^{206}Pb$	1.72167	2.8	0.16657	3.8	0.50	0.07496	3.4	993.2	34.5	1067.5	67.8	7.0
EV2S_NE180.24	**1022.9**	**56.2**	$^{207}Pb/^{206}Pb$	0.51197	5.2	0.06466	2.3	-0.02	0.07332	2.8	993.3	19.2	1022.9	56.2	2.9
EV2S_NE180.20	**952.5**	**81.3**	$^{207}Pb/^{206}Pb$	1.88207	3.4	0.18695	2.0	0.31	0.07083	4.0	997.8	25.1	952.5	81.3	-4.8
EV2S_NE180.60	**1033.5**	**82.7**	$^{207}Pb/^{206}Pb$	1.79823	3.2	0.17321	3.3	0.82	0.07371	4.1	998.7	33.8	1033.5	82.7	3.4
EV2S_NE180.43	**1080.7**	**69.8**	$^{207}Pb/^{206}Pb$	1.88954	6.4	0.16914	3.7	0.32	0.07546	3.5	1001.3	31.7	1080.7	69.8	7.3
EV2S_NE180.14	**991.7**	**85.1**	$^{207}Pb/^{206}Pb$	1.81348	2.8	0.16935	1.7	0.47	0.07220	4.2	1003.8	21.5	991.7	85.1	-1.2
EV2B_NE180.31	**1067.5**	**46.2**	$^{207}Pb/^{206}Pb$	1.74425	2.7	0.16876	3.6	0.77	0.07496	2.3	1005.3	33.3	1067.5	46.2	5.8
EV2S_NE180.65	**1053.0**	**65.7**	$^{207}Pb/^{206}Pb$	1.44109	5.3	0.13859	4.1	0.29	0.07442	3.3	1007.4	34.0	1053.0	65.7	4.3
EV2S_NE180.36	**1064.4**	**83.7**	$^{207}Pb/^{206}Pb$	2.56715	9.6	0.15741	3.2	0.28	0.07485	4.2	1007.5	33.0	1064.4	83.7	5.3
EV2B_NE180.15	**1054.1**	**56.8**	$^{207}Pb/^{206}Pb$	1.74256	2.8	0.16972	1.7	0.29	0.07447	2.8	1010.6	15.7	1054.1	56.8	4.1
EV2S_NE180.70	**998.4**	**40.8**	$^{207}Pb/^{206}Pb$	1.82962	4.1	0.17686	3.5	0.62	0.07244	2.0	1013.3	34.8	998.4	40.8	-1.5
EV2S_NE180.55	**1133.5**	**62.2**	$^{207}Pb/^{206}Pb$	2.12915	5.1	0.18866	4.2	0.46	0.07748	3.1	1026.4	37.6	1133.5	62.2	9.5

EV2S_NE180.03	**1117.3**	**63.5**	$^{207}Pb/^{206}Pb$	1.79791	5.0	0.17512	2.9	0.35	0.07685	3.2	1028.3	21.0	1117.3	63.5	8.0
EV2S_NE180.59	**1076.5**	**38.9**	$^{207}Pb/^{206}Pb$	0.42737	5.7	0.05525	4.3	0.57	0.07530	1.9	1029.7	31.6	1076.5	38.9	4.3
EV2B_NE180.08	**1016.1**	**63.2**	$^{207}Pb/^{206}Pb$	1.76330	3.4	0.17500	2.7	0.49	0.07308	3.1	1039.6	25.7	1016.1	63.2	-2.3
EV2S_NE180.02	**1054.0**	**97.7**	$^{207}Pb/^{206}Pb$	1.90437	5.1	0.18954	2.6	0.16	0.07446	4.9	1040.2	27.7	1054.0	97.7	1.3
EV2B_NE180.01	**1027.0**	**66.8**	$^{207}Pb/^{206}Pb$	1.77979	3.2	0.17569	2.5	0.34	0.07347	3.3	1043.4	24.1	1027.0	66.8	-1.6
EV2S_NE180.07	**1109.7**	**63.8**	$^{207}Pb/^{206}Pb$	1.59369	5.0	0.16582	2.8	0.22	0.07656	3.2	1049.2	24.3	1109.7	63.8	5.5
EV2S_NE180.69	**1069.3**	**67.7**	$^{207}Pb/^{206}Pb$	1.68360	5.8	0.16318	3.6	0.47	0.07503	3.4	1049.8	34.0	1069.3	67.7	1.8
EV2S_NE180.12	**1027.5**	**257.3**	$^{207}Pb/^{206}Pb$	1.95209	2.4	0.18069	1.9	0.63	0.07349	12.7	1053.3	45.1	1027.5	257.3	-2.5
EV2S_NE180.57	**1125.9**	**47.4**	$^{207}Pb/^{206}Pb$	1.87819	11.4	0.15563	5.7	0.26	0.07718	2.4	1057.0	37.4	1125.9	47.4	6.1
EV2B_NE180.20	**1157.8**	**42.5**	$^{207}Pb/^{206}Pb$	1.92795	2.0	0.17828	2.8	0.65	0.07843	2.1	1057.6	27.4	1157.8	42.5	8.7
EV2S_NE180.04	**1130.2**	**67.9**	$^{207}Pb/^{206}Pb$	1.83245	3.7	0.17294	2.2	0.51	0.07735	3.4	1062.8	20.5	1130.2	67.9	6.0
EV2B_NE180.26	**1147.8**	**56.2**	$^{207}Pb/^{206}Pb$	1.93848	2.4	0.18016	3.7	0.65	0.07804	2.8	1067.9	36.5	1147.8	56.2	7.0
EV2S_NE180.11	**1155.9**	**37.9**	$^{207}Pb/^{206}Pb$	0.59687	4.8	0.07229	2.4	0.29	0.07836	1.9	1070.7	19.0	1155.9	37.9	7.4
EV2S_NE180.53	**1120.6**	**98.5**	$^{207}Pb/^{206}Pb$	2.51322	4.0	0.21690	3.8	0.77	0.07698	4.9	1074.8	39.3	1120.6	98.5	4.1
EV2S_NE180.17	**1073.7**	**117.4**	$^{207}Pb/^{206}Pb$	0.37919	3.2	0.05195	1.9	0.25	0.07520	5.8	1095.0	26.0	1073.7	117.4	-2.0
EV2B_NE180.37	**1195.1**	**75.9**	$^{207}Pb/^{206}Pb$	2.04855	4.0	0.18590	2.9	0.41	0.07992	3.8	1099.1	29.2	1195.1	75.9	8.0
EV2S_NE180.18	**1230.1**	**125.2**	$^{207}Pb/^{206}Pb$	1.91951	6.3	0.18514	2.6	0.38	0.08136	6.4	1107.7	30.7	1230.1	125.2	9.9
EV2S_NE180.41	**1127.5**	**177.3**	$^{207}Pb/^{206}Pb$	1.67706	4.4	0.16379	3.5	0.49	0.07724	8.9	1109.7	42.2	1127.5	177.3	1.6
EV2B_NE180.21	**1137.7**	**106.9**	$^{207}Pb/^{206}Pb$	2.01417	5.3	0.18815	3.0	0.25	0.07764	5.4	1111.4	31.0	1137.7	106.9	2.3
EV2B_NE180.06	**1172.8**	**86.3**	$^{207}Pb/^{206}Pb$	2.05194	4.5	0.18832	3.2	0.40	0.07903	4.4	1112.3	32.4	1172.8	86.3	5.2
EV2B_NE180.32	**1167.9**	**84.1**	$^{207}Pb/^{206}Pb$	2.04932	4.9	0.18854	4.2	0.57	0.07883	4.2	1113.5	43.1	1167.9	84.1	4.7
EV2S_NE180.39	**1172.8**	**63.4**	$^{207}Pb/^{206}Pb$	2.07815	3.5	0.19001	3.1	0.81	0.07903	3.2	1119.1	34.2	1172.8	63.4	4.6
EV2S_NE180.28	**1184.4**	**46.0**	$^{207}Pb/^{206}Pb$	2.03460	4.1	0.18222	2.3	0.19	0.07949	2.3	1120.1	21.9	1184.4	46.0	5.4
EV2S_NE180.01	**1172.6**	**56.5**	$^{207}Pb/^{206}Pb$	1.68458	4.6	0.16498	2.5	0.52	0.07902	2.9	1120.3	22.2	1172.6	56.5	4.5
EV2S_NE180.73	**1202.2**	**43.1**	$^{207}Pb/^{206}Pb$	3.74181	6.6	0.24791	3.2	0.56	0.08021	2.2	1120.9	37.4	1202.2	43.1	6.8
EV2S_NE180.38	**1180.2**	**41.4**	$^{207}Pb/^{206}Pb$	1.87228	3.5	0.18612	2.9	0.59	0.07932	2.1	1121.4	32.4	1180.2	41.4	5.0
EV2S_NE180.71	**1243.1**	**103.0**	$^{207}Pb/^{206}Pb$	1.70014	3.7	0.17021	3.7	0.85	0.08190	5.3	1128.0	43.2	1243.1	103.0	9.3
EV2B_NE180.18	**1162.8**	**111.5**	$^{207}Pb/^{206}Pb$	2.07486	5.9	0.19138	2.9	0.33	0.07863	5.6	1128.8	30.5	1162.8	111.5	2.9
EV2B_NE180.04	**1216.8**	**107.7**	$^{207}Pb/^{206}Pb$	2.13428	4.8	0.19155	3.3	0.11	0.08081	5.5	1129.8	34.0	1216.8	107.7	7.2
EV2B_NE180.10	**1101.6**	**118.9**	$^{207}Pb/^{206}Pb$	2.01438	5.5	0.19160	2.7	0.08	0.07625	5.9	1130.1	27.8	1101.6	118.9	-2.6
EV2S_NE180.22	**1176.6**	**92.6**	$^{207}Pb/^{206}Pb$	1.61657	2.6	0.16278	1.8	0.30	0.07918	4.7	1135.7	24.2	1176.6	92.6	3.5
EV2S_NE180.46	**1200.4**	**95.9**	$^{207}Pb/^{206}Pb$	3.27965	5.4	0.25948	4.1	0.59	0.08014	4.9	1141.9	46.4	1200.4	95.9	4.9

EV2S_NE180.29	**1252.1**	**95.2**	$^{207}Pb/^{206}Pb$	2.07981	2.9	0.18976	2.1	0.60	0.08228	4.9	1165.5	28.8	1252.1	95.2	6.9
EV2S_NE180.51	**1222.6**	**56.4**	$^{207}Pb/^{206}Pb$	0.44199	7.5	0.05510	4.4	0.39	0.08105	2.9	1179.1	44.6	1222.6	56.4	3.6
EV2S_NE180.79	**1269.7**	**54.9**	$^{207}Pb/^{206}Pb$	0.41513	7.3	0.05560	3.6	0.27	0.08302	2.8	1188.8	30.5	1269.7	54.9	6.4
EV2S_NE180.52	**1293.4**	**51.7**	$^{207}Pb/^{206}Pb$	2.24280	4.7	0.20070	4.1	0.79	0.08403	2.7	1265.5	44.0	1293.4	51.7	2.2
EV2S_NE180.45	**1410.0**	**60.0**	$^{207}Pb/^{206}Pb$	2.99046	4.8	0.24293	3.9	0.76	0.08928	3.1	1401.9	49.5	1410.0	60.0	0.6
EV2B_SE60.47	**304.7**	**5.6**	$^{206}Pb/^{238}Pb$	0.35405	3.8	0.04841	1.9	0.04	0.05305	4.2	304.7	5.6	330.7	95.5	7.9
EV2B_SE60.50	**322.6**	**6.6**	$^{206}Pb/^{238}Pb$	0.37810	4.5	0.05131	2.1	0.12	0.05344	4.7	322.6	6.6	347.6	106.9	7.2
EV2B_SE60.57	**336.2**	**6.2**	$^{206}Pb/^{238}Pb$	0.39084	4.3	0.05354	1.9	0.39	0.05295	3.9	336.2	6.2	326.5	89.3	-3.0
EV2B_SE60.35	**339.4**	**6.9**	$^{206}Pb/^{238}Pb$	0.40201	3.3	0.05406	2.1	0.48	0.05394	2.9	339.4	6.9	368.4	66.3	7.9
EV2B_SE60.45	**424.2**	**9.6**	$^{206}Pb/^{238}Pb$	0.51417	4.7	0.06801	2.3	0.24	0.05483	4.7	424.2	9.6	405.3	105.2	-4.7
EV2B_SE60.36	**425.9**	**13.4**	$^{206}Pb/^{238}Pb$	0.52662	8.2	0.06830	3.3	0.09	0.05592	8.5	425.9	13.4	449.2	189.1	5.2
EV2S_SE60.76	**432.5**	**9.0**	$^{206}Pb/^{238}Pb$	1.70660	5.3	0.16388	2.8	0.21	0.05647	3.6	432.5	9.0	471.0	79.3	8.2
EV2B_SE60.33	**598.2**	**16.1**	$^{206}Pb/^{238}Pb$	0.82551	6.4	0.09724	2.8	0.25	0.06157	6.3	598.2	16.1	659.2	134.6	9.3
EV2B_SE60.60	**852.7**	**27.9**	$^{207}Pb/^{206}Pb$	1.37461	5.9	0.14142	3.5	0.04	0.07050	6.8	852.7	27.9	942.9	138.3	9.6
EV2B.SE60.09	**948.7**	**33.8**	$^{207}Pb/^{206}Pb$	1.59825	7.0	0.15854	3.8	0.21	0.07311	7.2	948.7	33.8	1017.1	145.8	6.7
EV2S_SE60.60	**1014.3**	**145.8**	$^{207}Pb/^{206}Pb$	2.51080	3.6	0.21446	3.4	0.81	0.07301	3.9	949.2	42.5	1014.3	78.0	6.4
EV2S_SE60.04	**1032.2**	**78.0**	$^{207}Pb/^{206}Pb$	2.42156	4.4	0.21901	3.7	0.87	0.07366	2.6	973.8	40.3	1032.2	52.7	5.7
EV2B.SE60.15	**995.7**	**52.7**	$^{207}Pb/^{206}Pb$	1.62713	3.8	0.16312	2.4	0.51	0.07235	3.3	974.1	22.0	995.7	67.6	2.2
EV2S_SE60.01	**1064.3**	**67.6**	$^{207}Pb/^{206}Pb$	1.98550	4.5	0.18436	3.8	0.82	0.07484	2.3	975.3	35.1	1064.3	46.5	8.4
EV2S_SE60.75	**1082.6**	**46.5**	$^{207}Pb/^{206}Pb$	2.26020	3.5	0.19161	2.1	0.29	0.07553	5.4	978.3	25.4	1082.6	109.0	9.6
EV2B_SE60.38	**1080.6**	**109.0**	$^{207}Pb/^{206}Pb$	1.71088	4.1	0.16445	2.2	0.34	0.07545	3.9	981.5	20.0	1080.6	79.1	9.2
EV2S_SE60.82	**1042.9**	**79.1**	$^{207}Pb/^{206}Pb$	2.32103	2.6	0.20189	2.1	0.75	0.07405	4.0	984.4	23.2	1042.9	79.7	5.6
EV2S_SE60.42	**1032.2**	**79.7**	$^{207}Pb/^{206}Pb$	1.86634	3.4	0.16899	3.3	0.84	0.07366	2.4	984.8	32.7	1032.2	49.4	4.6
EV2S_SE60.10	**994.2**	**49.4**	$^{207}Pb/^{206}Pb$	1.78819	4.7	0.17053	4.4	0.90	0.07229	1.7	985.0	41.7	994.2	35.0	0.9
EV2S_SE60.44	**1026.8**	**35.0**	$^{207}Pb/^{206}Pb$	2.35258	4.0	0.18646	3.5	0.60	0.07347	3.9	986.2	34.1	1026.8	78.4	4.0
EV2S_SE60.39	**1007.3**	**78.4**	$^{207}Pb/^{206}Pb$	0.37327	5.4	0.05222	4.0	0.67	0.07276	1.6	990.5	32.8	1007.3	32.7	1.7
EV2B.SE60.20	**1085.8**	**32.7**	$^{207}Pb/^{206}Pb$	1.73470	6.0	0.16631	4.3	0.83	0.07565	3.4	991.8	39.3	1085.8	69.1	8.7
EV2S_SE60.08	**1114.0**	**69.1**	$^{207}Pb/^{206}Pb$	1.78347	5.8	0.16856	4.8	0.742	0.07674	3.9	1004.2	44.9	1114.0	78.0	9.9
EV2S_SE60.57	**1112.7**	**78.0**	$^{207}Pb/^{206}Pb$	0.42179	5.1	0.05439	3.6	0.44	0.07667	2.2	1004.3	31.3	1112.7	43.0	9.7
EV2S_SE60.09	**1096.5**	**43.0**	$^{207}Pb/^{206}Pb$	0.41005	5.7	0.05635	4.4	0.69	0.07605	2.0	1015.0	41.5	1096.5	40.4	7.4
EV2S_SE60.15	**1112.4**	**40.4**	$^{207}Pb/^{206}Pb$	1.96199	4.9	0.18396	4.5	0.88	0.07666	2.4	1021.7	42.6	1112.4	47.5	8.1
EV2S_SE60.49	**1038.0**	**47.5**	$^{207}Pb/^{206}Pb$	1.87138	3.6	0.17482	3.5	0.76	0.07387	2.1	1031.5	32.8	1038.0	41.8	0.6

EV2S_SE60.48	**1137.6**	**41.8**	$^{207}Pb/^{206}Pb$	12.61410	3.8	0.50092	3.6	0.88	0.07764	2.5	1038.6	33.6	1137.6	48.9	8.7
EV2S_SE60.40	**1119.3**	**48.9**	$^{207}Pb/^{206}Pb$	1.66625	3.6	0.16609	3.6	0.90	0.07693	2.2	1040.2	34.5	1119.3	44.6	7.1
EV2S_SE60.30	**1087.4**	**44.6**	$^{207}Pb/^{206}Pb$	1.91654	5.6	0.18360	4.9	0.78	0.07571	3.6	1048.4	42.0	1087.4	71.8	3.6
EV2S_SE60.25	**1058.0**	**71.8**	$^{207}Pb/^{206}Pb$	2.80558	5.2	0.23338	4.3	0.64	0.07461	2.3	1067.7	42.5	1058.0	45.9	-0.9
EV2S_SE60.62	**1125.9**	**45.9**	$^{207}Pb/^{206}Pb$	1.73687	3.2	0.14765	3.2	0.84	0.07718	2.3	1068.8	38.4	1125.9	45.1	5.1
EV2B.SE60.29	**1136.2**	**45.1**	$^{207}Pb/^{206}Pb$	1.95051	6.7	0.18234	4.9	0.74	0.07758	4.5	1079.8	48.5	1136.2	90.2	5.0
EV2S_SE60.29	**1087.4**	**90.2**	$^{207}Pb/^{206}Pb$	3.21435	4.8	0.25572	4.2	0.73	0.07571	3.6	1086.6	48.6	1087.4	71.8	0.1
EV2B_SE60.34	**1202.2**	**71.8**	$^{207}Pb/^{206}Pb$	2.03228	3.9	0.18376	3.2	0.77	0.08021	2.5	1087.5	32.5	1202.2	48.7	9.5
EV2S_SE60.14	**1130.3**	**48.7**	$^{207}Pb/^{206}Pb$	2.44947	5.2	0.20906	4.5	0.85	0.07735	2.4	1088.6	44.9	1130.3	47.0	3.7
EV2B.SE60.11	**1107.8**	**47.0**	$^{207}Pb/^{206}Pb$	1.94318	6.0	0.18426	3.0	0.21	0.07649	6.1	1090.2	29.7	1107.8	122.6	1.6
EV2S_SE60.38	**1208.9**	**122.6**	$^{207}Pb/^{206}Pb$	0.59810	6.8	0.06980	4.6	0.53	0.08048	3.0	1093.0	42.1	1208.9	59.9	9.6
EV2B.SE60.03	**1195.1**	**59.9**	$^{207}Pb/^{206}Pb$	2.09320	4.7	0.18995	2.9	0.19	0.07992	5.0	1121.1	29.7	1195.1	99.2	6.2
EV2B.SE60.23	**1195.1**	**99.2**	$^{207}Pb/^{206}Pb$	2.12475	3.5	0.19281	2.2	0.36	0.07992	3.4	1136.6	23.4	1195.1	67.4	4.9
EV2S_SE60.03	**1199.0**	**67.4**	$^{207}Pb/^{206}Pb$	2.15866	4.7	0.19547	4.1	0.87	0.08009	2.3	1151.0	42.9	1199.0	45.0	4.0
EV2B.SE60.08	**1257.4**	**45.0**	$^{207}Pb/^{206}Pb$	2.23016	7.4	0.19606	3.4	0.26	0.08250	7.3	1154.1	35.8	1257.4	142.9	8.2
EV2B.SE60.19	**1194.4**	**142.9**	$^{207}Pb/^{206}Pb$	2.19012	6.9	0.19881	3.5	0.06	0.07990	7.6	1168.9	37.9	1194.4	149.6	2.1
EV2B.SE60.04	**1307.7**	**149.6**	$^{207}Pb/^{206}Pb$	2.35521	6.9	0.20177	3.5	0.11	0.08466	7.4	1184.8	37.9	1307.7	143.8	9.4
EV2S_SE60.81	**1278.2**	**143.8**	$^{207}Pb/^{206}Pb$	1.44996	4.3	0.14633	3.4	0.69	0.08338	1.7	1185.4	22.2	1278.2	33.2	7.3
EV2S_SE60.73	**1211.3**	**33.2**	$^{207}Pb/^{206}Pb$	0.62521	4.3	0.07311	2.1	0.12	0.08059	4.5	1192.2	23.8	1211.3	88.4	1.6
EV2S_SE60.02	**1256.7**	**88.4**	$^{207}Pb/^{206}Pb$	1.68557	4.6	0.16334	3.9	0.86	0.08247	2.5	1195.8	42.1	1256.7	48.1	4.8
EV2S_SE60.36	**1265.9**	**48.1**	$^{207}Pb/^{206}Pb$	2.29442	4.7	0.19501	4.2	0.86	0.08286	4.1	1198.6	52.2	1265.9	80.1	5.3
EV2B_SE60.53	**1328.4**	**80.1**	$^{207}Pb/^{206}Pb$	2.41273	3.5	0.20450	2.1	0.25	0.08557	3.6	1199.5	23.5	1328.4	69.5	9.7
EV2S_SE60.13	**1315.0**	**69.5**	$^{207}Pb/^{206}Pb$	1.75235	5.5	0.16645	4.7	0.84	0.08498	2.7	1223.8	50.4	1315.0	52.9	6.9
EV2B.SE60.14	**1249.6**	**52.9**	$^{207}Pb/^{206}Pb$	2.40626	3.9	0.21239	2.3	0.32	0.08217	3.9	1241.5	26.2	1249.6	75.7	0.6
EV2S_SE60.59	**1313.5**	**75.7**	$^{207}Pb/^{206}Pb$	0.56965	4.7	0.07144	3.6	0.56	0.08491	2.2	1252.5	38.9	1313.5	42.4	4.6
EV2S_SE60.31	**1354.1**	**42.4**	$^{207}Pb/^{206}Pb$	1.84365	5.2	0.17661	4.3	0.74	0.08671	2.3	1270.3	46.8	1354.1	45.1	6.2
EV2S_SE60.24	**1364.7**	**45.1**	$^{207}Pb/^{206}Pb$	1.70512	5.5	0.16891	4.4	0.66	0.08719	4.1	1352.2	51.8	1364.7	79.5	0.9
EV2S_SE60.66	**1479.1**	**79.5**	$^{207}Pb/^{206}Pb$	0.78467	11.1	0.06995	4.0	0.24	0.09257	2.0	1353.6	40.6	1479.1	38.3	8.5
EV2S_SE60.17	**2570.9**	**16.3**	$^{207}Pb/^{206}Pb$	1.06183	7.9	0.10326	5.0	0.50	0.17136	2.3	2540.8	94.2	2570.9	37.7	1.2
EV2S_SE60.47	**2677.0**	**37.7**	$^{207}Pb/^{206}Pb$	1.64618	4.8	0.15185	4.2	0.64	0.18264	1.8	2617.7	77.6	2677.0	30.5	2.2
SE140_073	**332.7**	**11.1**	$^{206}Pb/^{238}Pb$	0.39196	3.7	0.05297	3.4	0.93	0.05367	1.4	332.7	11.1	357.0	31.7	6.8
SE140_05R	**337.0**	**13.6**	$^{206}Pb/^{238}Pb$	0.39987	4.2	0.05367	4.1	0.97	0.05403	1.0	337.0	13.6	372.0	21.6	9.4

SE140_35	**341.4**	**13.3**	$^{206}Pb/^{238}Pb$	0.40421	4.1	0.05440	4.0	0.98	0.05390	0.9	341.4	13.3	366.5	20.1	6.8
SE140_31	**341.6**	**13.3**	$^{206}Pb/^{238}Pb$	0.40617	4.1	0.05442	4.0	0.98	0.05413	0.8	341.6	13.3	376.0	18.7	9.2
SE140_102	**341.7**	**11.5**	$^{206}Pb/^{238}Pb$	0.40654	3.7	0.05443	3.5	0.93	0.05417	1.4	341.7	11.5	377.5	31.6	9.5
SE140_28	**347.0**	**13.4**	$^{206}Pb/^{238}Pb$	0.41062	4.1	0.05531	4.0	0.98	0.05384	0.8	347.0	13.4	364.5	18.6	4.8
SE140_084C	**351.2**	**12.1**	$^{206}Pb/^{238}Pb$	0.41918	3.9	0.05613	3.6	0.93	0.05416	1.5	351.2	12.1	382.0	33.2	8.1
SE140_084R	**352.0**	**12.3**	$^{206}Pb/^{238}Pb$	0.41898	3.8	0.05599	3.6	0.92	0.05427	1.5	352.0	12.3	377.5	33.3	6.7
SE140_083	**355.6**	**11.9**	$^{206}Pb/^{238}Pb$	0.42290	3.7	0.05672	3.4	0.92	0.05408	1.4	355.6	11.9	374.0	32.3	4.9
SE140_04	**421.0**	**17.0**	$^{206}Pb/^{238}Pb$	0.52379	4.3	0.06749	4.2	0.97	0.05629	1.1	421.0	17.0	463.5	24.4	9.2
SE140_58	**421.2**	**16.1**	$^{206}Pb/^{238}Pb$	0.51946	4.0	0.06752	4.0	0.98	0.05580	0.8	421.2	16.1	444.0	18.7	5.1
SE140_113	**974.5**	**30.5**	$^{207}Pb/^{206}Pb$	1.44364	3.6	0.14623	3.2	0.91	0.07160	1.5	879.8	26.6	974.5	30.5	9.7
SE140_118	**991.0**	**28.0**	$^{207}Pb/^{206}Pb$	1.47854	3.6	0.14855	3.4	0.93	0.07219	1.4	892.8	28.0	991.0	28.0	9.9
SE140_108	**977.5**	**28.1**	$^{207}Pb/^{206}Pb$	1.50542	3.7	0.15225	3.4	0.93	0.07171	1.4	913.5	29.0	977.5	28.1	6.5
SE140_070	**1003.5**	**28.2**	$^{207}Pb/^{206}Pb$	1.57501	3.6	0.15727	3.3	0.92	0.07263	1.4	941.6	28.8	1003.5	28.2	6.2
SE140_44R	**1038.0**	**18.6**	$^{207}Pb/^{206}Pb$	1.60565	3.9	0.15764	3.8	0.97	0.07387	0.9	943.6	33.4	1038.0	18.6	9.1
SE140_51	**1035.5**	**16.6**	$^{207}Pb/^{206}Pb$	1.60882	4.1	0.15812	4.1	0.98	0.07379	0.8	946.3	35.7	1035.5	16.6	8.6
SE140_101	**1049.5**	**29.7**	$^{207}Pb/^{206}Pb$	1.62823	3.8	0.15894	3.5	0.92	0.07430	1.5	950.9	30.9	1049.5	29.7	9.4
SE140_098	**995.5**	**28.2**	$^{207}Pb/^{206}Pb$	1.58949	3.8	0.15935	3.5	0.93	0.07235	1.4	953.1	31.3	995.5	28.2	4.3
SE140_105	**1013.5**	**28.0**	$^{207}Pb/^{206}Pb$	1.60947	3.7	0.15991	3.4	0.93	0.07300	1.4	956.3	30.4	1013.5	28.0	5.6
SE140_09	**1037.0**	**19.3**	$^{207}Pb/^{206}Pb$	1.62835	4.1	0.15994	4.0	0.97	0.07384	1.0	956.4	35.2	1037.0	19.3	7.8
SE140_02R	**1028.0**	**17.7**	$^{207}Pb/^{206}Pb$	1.62465	4.2	0.16028	4.1	0.98	0.07352	0.9	958.3	36.3	1028.0	17.7	6.8
SE140_27	**1034.0**	**19.0**	$^{207}Pb/^{206}Pb$	1.63306	4.0	0.16064	3.9	0.97	0.07373	0.9	960.3	35.1	1034.0	19.0	7.1
SE140_106	**1038.0**	**28.9**	$^{207}Pb/^{206}Pb$	1.64022	3.7	0.16103	3.4	0.92	0.07388	1.4	962.5	30.7	1038.0	28.9	7.3
SE140_42	**1058.5**	**17.0**	$^{207}Pb/^{206}Pb$	1.66381	4.0	0.16169	3.9	0.98	0.07463	0.8	966.1	34.7	1058.5	17.0	8.7
SE140_02C	**1014.0**	**16.3**	$^{207}Pb/^{206}Pb$	1.63531	4.3	0.16243	4.2	0.98	0.07302	0.8	970.2	37.9	1014.0	16.3	4.3
SE140_29	**1070.5**	**17.0**	$^{207}Pb/^{206}Pb$	1.69364	4.2	0.16358	4.1	0.98	0.07509	0.8	976.6	36.9	1070.5	17.0	8.8
SE140_062	**1017.5**	**27.9**	$^{207}Pb/^{206}Pb$	1.65073	3.6	0.16369	3.3	0.92	0.07314	1.4	977.2	30.0	1017.5	27.9	4.0
SE140_111C	**1040.5**	**28.0**	$^{207}Pb/^{206}Pb$	1.72043	4.0	0.16827	3.8	0.94	0.07415	1.4	978.1	31.5	1040.5	28.0	6.0
SE140_34	**1002.0**	**16.7**	$^{207}Pb/^{206}Pb$	1.64455	4.2	0.16433	4.1	0.98	0.07258	0.8	980.7	37.4	1002.0	16.7	2.1
SE140_55	**1055.0**	**17.3**	$^{207}Pb/^{206}Pb$	1.68988	4.0	0.16449	3.9	0.98	0.07451	0.9	981.6	35.6	1055.0	17.3	7.0
SE140_14	**1038.5**	**16.8**	$^{207}Pb/^{206}Pb$	1.67667	4.2	0.16456	4.1	0.98	0.07390	0.8	982.0	37.1	1038.5	16.8	5.4
SE140_44C	**1065.5**	**22.3**	$^{207}Pb/^{206}Pb$	1.70010	4.4	0.16465	4.3	0.97	0.07489	1.1	982.5	39.0	1065.5	22.3	7.8
SE140_06	**1055.5**	**17.0**	$^{207}Pb/^{206}Pb$	1.69358	4.2	0.16479	4.1	0.98	0.07454	0.8	983.3	37.5	1055.5	17.0	6.8

SE140_090	**1092.0**	**28.9**	$^{207}Pb/^{206}Pb$	1.73323	3.6	0.16566	3.3	0.92	0.07588	1.4	988.1	30.3	1092.0	28.9	9.5
SE140_50	**1057.5**	**19.9**	$^{207}Pb/^{206}Pb$	1.70513	4.1	0.16577	4.0	0.97	0.07460	1.0	988.7	36.6	1057.5	19.9	6.5
SE140_16	**1045.5**	**16.1**	$^{207}Pb/^{206}Pb$	1.69481	4.2	0.16577	4.1	0.98	0.07415	0.8	988.7	37.5	1045.5	16.1	5.4
SE140_20C	**1081.5**	**16.3**	$^{207}Pb/^{206}Pb$	1.72833	4.1	0.16603	4.0	0.98	0.07550	0.8	990.2	36.9	1081.5	16.3	8.4
SE140_20R	**1080.5**	**20.9**	$^{207}Pb/^{206}Pb$	1.72938	3.9	0.16624	3.8	0.96	0.07545	1.0	991.3	34.8	1080.5	20.9	8.3
SE140_57	**1047.5**	**16.8**	$^{207}Pb/^{206}Pb$	1.71446	4.0	0.16752	3.9	0.98	0.07423	0.8	998.4	35.9	1047.5	16.8	4.7
SE140_109	**1021.5**	**27.6**	$^{207}Pb/^{206}Pb$	1.69524	3.7	0.16776	3.4	0.93	0.07329	1.4	999.7	31.9	1021.5	27.6	2.1
SE140_111R	**1045.5**	**28.5**	$^{207}Pb/^{206}Pb$	1.67112	3.7	0.16385	3.5	0.93	0.07397	1.4	1002.6	35.1	1045.5	28.5	4.1
SE140_30R	**1092.5**	**15.8**	$^{207}Pb/^{206}Pb$	1.76285	4.1	0.16842	4.0	0.98	0.07591	0.8	1003.4	37.1	1092.5	15.8	8.2
SE140_072	**1062.0**	**27.7**	$^{207}Pb/^{206}Pb$	1.73768	3.7	0.16858	3.4	0.93	0.07476	1.4	1004.3	31.6	1062.0	27.7	5.4
SE140_53	**1083.5**	**15.8**	$^{207}Pb/^{206}Pb$	1.76541	4.2	0.16944	4.1	0.98	0.07557	0.8	1009.0	38.2	1083.5	15.8	6.9
SE140_088	**1012.0**	**27.7**	$^{207}Pb/^{206}Pb$	1.70519	3.7	0.16956	3.4	0.93	0.07294	1.4	1009.6	32.1	1012.0	27.7	0.2
SE140_107	**1064.5**	**27.8**	$^{207}Pb/^{206}Pb$	1.75088	3.7	0.16961	3.4	0.93	0.07487	1.4	1009.9	31.8	1064.5	27.8	5.1
SE140_26	**1054.5**	**16.6**	$^{207}Pb/^{206}Pb$	1.74717	4.3	0.17011	4.2	0.98	0.07449	0.8	1012.7	39.0	1054.5	16.6	4.0
SE140_59	**1074.0**	**16.7**	$^{207}Pb/^{206}Pb$	1.77291	4.0	0.17094	4.0	0.98	0.07522	0.8	1017.3	37.1	1074.0	16.7	5.3
SE140_49	**1035.0**	**16.9**	$^{207}Pb/^{206}Pb$	1.75172	4.1	0.17223	4.0	0.98	0.07377	0.8	1024.4	38.3	1035.0	16.9	1.0
SE140_077	**1117.0**	**27.8**	$^{207}Pb/^{206}Pb$	1.84348	3.7	0.17399	3.5	0.93	0.07684	1.4	1034.0	32.9	1117.0	27.8	7.4
SE140_61	**1118.0**	**17.6**	$^{207}Pb/^{206}Pb$	1.86930	4.0	0.17632	3.9	0.98	0.07689	0.9	1046.8	37.9	1118.0	17.6	6.4
SE140_115	**1160.5**	**28.0**	$^{207}Pb/^{206}Pb$	1.91746	3.8	0.17704	3.5	0.93	0.07855	1.4	1050.8	34.3	1160.5	28.0	9.5
SE140_064	**1122.5**	**27.5**	$^{207}Pb/^{206}Pb$	1.90730	3.6	0.17949	3.3	0.92	0.07707	1.4	1064.2	32.2	1122.5	27.5	5.2
SE140_21	**1180.0**	**16.1**	$^{207}Pb/^{206}Pb$	1.98320	4.1	0.18132	4.0	0.98	0.07933	0.8	1074.1	39.8	1180.0	16.1	9.0
SE140_30C	**1151.5**	**16.6**	$^{207}Pb/^{206}Pb$	1.96855	4.0	0.18258	3.9	0.98	0.07820	0.8	1081.0	39.2	1151.5	16.6	6.1
SE140_077R	**1148.0**	**27.5**	$^{207}Pb/^{206}Pb$	1.96756	3.6	0.18281	3.4	0.92	0.07806	1.4	1082.3	33.5	1148.0	27.5	5.7
SE140_104	**1180.0**	**28.6**	$^{207}Pb/^{206}Pb$	2.00366	3.6	0.18322	3.3	0.92	0.07931	1.4	1084.5	33.4	1180.0	28.6	8.1
SE140_074	**1169.5**	**27.5**	$^{207}Pb/^{206}Pb$	1.99942	3.6	0.18378	3.3	0.92	0.07891	1.4	1087.5	33.5	1169.5	27.5	7.0
SE140_33	**1185.5**	**16.5**	$^{207}Pb/^{206}Pb$	2.03714	4.1	0.18576	4.0	0.98	0.07954	0.8	1098.3	40.2	1185.5	16.5	7.4
SE140_07	**1219.5**	**16.6**	$^{207}Pb/^{206}Pb$	2.09816	4.2	0.18803	4.2	0.98	0.08093	0.8	1110.7	42.4	1219.5	16.6	8.9
SE140_01	**1168.5**	**16.6**	$^{207}Pb/^{206}Pb$	2.04520	4.2	0.18810	4.1	0.98	0.07886	0.8	1111.1	41.7	1168.5	16.6	4.9
SE140_110	**1153.0**	**27.0**	$^{207}Pb/^{206}Pb$	2.03710	3.7	0.18883	3.5	0.93	0.07824	1.4	1115.0	35.7	1153.0	27.0	3.3
SE140_10	**1225.0**	**19.5**	$^{207}Pb/^{206}Pb$	2.12675	4.1	0.19008	4.0	0.97	0.08115	1.0	1121.8	41.0	1225.0	19.5	8.4
SE140_092C	**1230.5**	**27.6**	$^{207}Pb/^{206}Pb$	2.04691	3.5	0.18375	3.3	0.92	0.08079	1.4	1122.9	33.3	1230.5	27.6	8.7
SE140_46	**1178.0**	**15.7**	$^{207}Pb/^{206}Pb$	2.08165	4.2	0.19054	4.1	0.98	0.07924	0.8	1124.3	42.7	1178.0	15.7	4.6

SE140_03	**1234.5**	**15.6**	$^{207}Pb/^{206}Pb$	2.14667	4.9	0.19089	4.8	0.99	0.08156	0.8	1126.2	49.7	1234.5	15.6	8.8
SE140_15	**1181.5**	**16.3**	$^{207}Pb/^{206}Pb$	2.09400	4.1	0.19130	4.0	0.98	0.07939	0.8	1128.4	41.5	1181.5	16.3	4.5
SE140_085	**1145.0**	**27.6**	$^{207}Pb/^{206}Pb$	2.05779	3.7	0.19149	3.4	0.93	0.07794	1.4	1129.4	35.3	1145.0	27.6	1.4
SE140_13	**1186.5**	**16.3**	$^{207}Pb/^{206}Pb$	2.10840	4.0	0.19213	4.0	0.98	0.07959	0.8	1132.9	41.0	1186.5	16.3	4.5
SE140_103	**1185.0**	**27.2**	$^{207}Pb/^{206}Pb$	2.11101	3.7	0.19253	3.5	0.93	0.07952	1.4	1135.0	36.1	1185.0	27.2	4.2
SE140_56	**1175.5**	**16.6**	$^{207}Pb/^{206}Pb$	2.10521	4.0	0.19291	3.9	0.98	0.07915	0.8	1137.1	40.7	1175.5	16.6	3.3
SE140_067	**1268.0**	**27.8**	$^{207}Pb/^{206}Pb$	2.21776	3.6	0.19388	3.3	0.92	0.08296	1.4	1142.3	34.7	1268.0	27.8	9.9
SE140_100	**1236.5**	**27.1**	$^{207}Pb/^{206}Pb$	2.19225	3.7	0.19479	3.5	0.93	0.08163	1.4	1147.2	36.4	1236.5	27.1	7.2
SE140_082	**1193.5**	**27.2**	$^{207}Pb/^{206}Pb$	2.20727	3.8	0.20046	3.6	0.93	0.07986	1.4	1177.8	38.6	1193.5	27.2	1.3
SE140_086	**1195.5**	**27.4**	$^{207}Pb/^{206}Pb$	2.23408	4.1	0.20264	3.9	0.94	0.07996	1.4	1189.5	42.3	1195.5	27.4	0.5
SE140_087	**1240.0**	**27.7**	$^{207}Pb/^{206}Pb$	2.29393	3.8	0.20343	3.5	0.93	0.08178	1.4	1193.7	38.1	1240.0	27.7	3.7
SE140_093	**1300.5**	**27.3**	$^{207}Pb/^{206}Pb$	2.38368	3.5	0.20495	3.2	0.92	0.08435	1.4	1201.8	35.3	1300.5	27.3	7.6
SE140_114	**1326.0**	**27.0**	$^{207}Pb/^{206}Pb$	2.45643	3.8	0.20846	3.6	0.93	0.08547	1.4	1220.5	39.4	1326.0	27.0	8.0
SE140_41	**1352.5**	**16.8**	$^{207}Pb/^{206}Pb$	2.50960	4.1	0.21006	4.0	0.98	0.08665	0.9	1229.1	44.3	1352.5	16.8	9.1
SE140_095	**1390.0**	**29.3**	$^{207}Pb/^{206}Pb$	2.70469	3.6	0.22204	3.2	0.90	0.08835	1.5	1292.6	37.8	1390.0	29.3	7.0
SE140_17	**1478.0**	**16.2**	$^{207}Pb/^{206}Pb$	3.08416	4.1	0.24176	4.0	0.98	0.09252	0.9	1395.8	50.0	1478.0	16.2	5.6
SE140_47	**1489.0**	**18.4**	$^{207}Pb/^{206}Pb$	3.15894	4.1	0.24616	3.9	0.97	0.09307	1.0	1418.6	50.1	1489.0	18.4	4.7
EV2S_SE200.06	**349.0**	**12.6**	$^{206}Pb/^{238}Pb$	1.60397	16.0	0.13529	11.5	0.93	0.05347	4.1	349.0	12.6	348.8	93.4	-0.1
EV2S_SE200.15	**415.3**	**16.8**	$^{206}Pb/^{238}Pb$	0.46272	6.4	0.06393	4.2	0.44	0.05507	4.9	415.3	16.8	414.9	110.6	-0.1
EV2S_SE200.19	**434.7**	**19.2**	$^{206}Pb/^{238}Pb$	3.57720	4.9	0.24049	4.3	0.85	0.05567	5.2	434.7	19.2	439.3	116.7	1.0
EV2S_SE200.48	**439.9**	**16.4**	$^{206}Pb/^{238}Pb$	2.13605	4.6	0.18949	4.3	0.94	0.05692	3.2	439.9	16.4	488.3	70.1	9.9
EV2S_SE200.02	**683.6**	**26.7**	$^{206}Pb/^{238}Pb$	1.77515	4.8	0.17394	3.5	0.55	0.06275	7.0	683.6	26.7	699.9	148.4	2.3
EV2S_SE200.44	**888.2**	**23.4**	$^{207}Pb/^{206}Pb$	0.39012	4.2	0.05115	2.9	0.47	0.07165	2.4	888.2	23.4	975.9	48.3	9.0
EV2S_SE200.27	**899.0**	**36.6**	$^{207}Pb/^{206}Pb$	2.09842	7.4	0.19187	4.6	0.48	0.07200	4.4	899.0	36.6	986.0	89.0	8.8
EV2B_SE200.24	**910.6**	**38.2**	$^{207}Pb/^{206}Pb$	1.51815	5.5	0.15171	4.5	0.84	0.07257	2.9	910.6	38.2	1002.1	59.7	9.1
EV2B_SE200.21	**918.6**	**16.4**	$^{207}Pb/^{206}Pb$	1.53871	2.8	0.15314	1.9	0.26	0.07287	2.9	918.6	16.4	1010.4	59.4	9.1
EV2S_SE200.11	**937.4**	**32.7**	$^{207}Pb/^{206}Pb$	1.70568	3.8	0.16776	3.7	0.86	0.07305	3.3	937.4	32.7	1015.4	65.9	7.7
EV2B_SE200.23	**938.6**	**15.8**	$^{207}Pb/^{206}Pb$	1.56405	2.5	0.15673	1.8	0.40	0.07238	2.4	938.6	15.8	996.5	49.1	5.8
EV2S_SE200.33	**959.4**	**25.5**	$^{207}Pb/^{206}Pb$	1.65711	8.7	0.15860	4.4	0.34	0.07459	3.2	959.4	25.5	1057.6	63.8	9.3
EV2S_SE200.08	**965.4**	**34.6**	$^{207}Pb/^{206}Pb$	0.41020	5.2	0.05564	3.7	0.61	0.07117	6.2	965.4	34.6	962.2	125.7	-0.3
EV2S_SE200.28	**972.4**	**34.8**	$^{207}Pb/^{206}Pb$	1.48569	5.9	0.14965	4.4	0.68	0.07408	2.4	972.4	34.8	1043.7	47.5	6.8
EV2S_SE200.09	**979.3**	**32.7**	$^{207}Pb/^{206}Pb$	1.58515	6.7	0.16155	3.9	0.43	0.07443	3.9	979.3	32.7	1053.2	79.4	7.0

EV2S_SE200.25	**982.3**	**38.0**	$^{207}Pb/^{206}Pb$	0.73813	7.7	0.07425	4.8	0.44	0.07200	2.8	982.3	38.0	985.9	56.8	0.4
EV2S_SE200.17	**982.5**	**39.9**	$^{207}Pb/^{206}Pb$	2.23645	5.0	0.19345	4.4	0.85	0.07317	3.7	982.5	39.9	1018.7	73.9	3.5
EV2B_SE200.01	**990.3**	**14.3**	$^{207}Pb/^{206}Pb$	1.68186	2.9	0.16604	1.6	0.46	0.07346	2.6	990.3	14.3	1026.8	51.9	3.6
EV2S_SE200.10	**999.8**	**34.6**	$^{207}Pb/^{206}Pb$	1.68363	4.8	0.16406	3.6	0.58	0.07374	2.0	999.8	34.6	1034.4	40.5	3.3
EV2B_SE200.15	**1032.4**	**20.5**	$^{207}Pb/^{206}Pb$	1.77602	2.9	0.17369	2.2	0.40	0.07416	2.8	1032.4	20.5	1045.8	57.1	1.3
EV2S_SE200.01	**1033.8**	**33.1**	$^{207}Pb/^{206}Pb$	0.38243	4.1	0.05276	3.2	0.57	0.07402	4.1	1033.8	33.1	1042.0	82.2	0.8
EV2S_SE200.46	**1041.1**	**25.2**	$^{207}Pb/^{206}Pb$	1.75331	4.5	0.17528	2.6	0.33	0.07255	4.4	1041.1	25.2	1001.0	±90	-4.0
EV2B_SE200.26	**1047.5**	**26.2**	$^{207}Pb/^{206}Pb$	1.88378	6.1	0.17644	2.7	0.39	0.07743	5.6	1047.5	26.2	1132.4	111.5	7.5
EV2B_SE200.02	**1067.5**	**40.2**	$^{207}Pb/^{206}Pb$	1.96705	8.7	0.18010	4.1	-0.08	0.07921	9.9	1067.5	40.2	1177.5	195.6	9.3
EV2S_SE200.30	**1074.2**	**34.8**	$^{207}Pb/^{206}Pb$	2.48634	3.4	0.21834	3.6	0.83	0.07676	2.8	1074.2	34.8	1114.9	56.6	3.7
EV2S_SE200.38	**1074.3**	**28.8**	$^{207}Pb/^{206}Pb$	2.13836	3.3	0.18817	2.8	0.48	0.07549	2.4	1074.3	28.8	1081.7	47.8	0.7
EV2B_SE200.19	**1074.4**	**20.3**	$^{207}Pb/^{206}Pb$	1.98094	2.8	0.18136	2.1	0.34	0.07922	2.8	1074.4	20.3	1177.6	55.9	8.8
EV2B_SE200.20	**1079.3**	**22.1**	$^{207}Pb/^{206}Pb$	1.98830	3.8	0.18227	2.2	0.34	0.07912	3.7	1079.3	22.1	1175.1	73.0	8.1
EV2S_SE200.52	**1090.8**	**38.0**	$^{207}Pb/^{206}Pb$	1.66987	7.6	0.15447	4.8	0.34	0.07811	2.6	1090.8	38.0	1149.6	51.5	5.1
EV2B_SE200.17	**1092.6**	**17.3**	$^{207}Pb/^{206}Pb$	1.99962	2.2	0.18469	1.7	0.43	0.07852	2.1	1092.6	17.3	1160.1	42.1	5.8
EV2S_SE200.39	**1093.0**	**35.8**	$^{207}Pb/^{206}Pb$	1.96621	4.8	0.18477	3.6	0.46	0.07718	4.4	1093.0	35.8	1126.0	±89	2.9
EV2S_SE200.47	**1118.6**	**43.7**	$^{207}Pb/^{206}Pb$	2.07738	5.9	0.19642	4.1	0.61	0.08176	1.5	1118.6	43.7	1239.7	30.4	9.8
EV2S_SE200.13	**1118.6**	**40.7**	$^{207}Pb/^{206}Pb$	1.72072	5.1	0.16206	4.3	0.74	0.08116	1.9	1118.6	40.7	1225.3	36.7	8.7
EV2S_SE200.20	**1124.8**	**44.6**	$^{207}Pb/^{206}Pb$	0.53547	6.5	0.06976	4.6	0.60	0.07941	3.9	1124.8	44.6	1182.3	76.4	4.9
EV2S_SE200.26	**1131.5**	**47.8**	$^{207}Pb/^{206}Pb$	1.63398	5.1	0.16459	4.2	0.84	0.07932	6.6	1131.5	47.8	1180.2	129.7	4.1
EV2B_SE200.13	**1133.2**	**24.5**	$^{207}Pb/^{206}Pb$	2.16483	3.1	0.19219	2.4	0.45	0.08169	2.9	1133.2	24.5	1238.2	57.3	8.5
EV2B_SE200.12	**1136.8**	**33.3**	$^{207}Pb/^{206}Pb$	2.06153	3.9	0.19285	3.2	0.83	0.07753	2.2	1136.8	33.3	1134.9	43.6	-0.2
EV2S_SE200.31	**1185.1**	**37.4**	$^{207}Pb/^{206}Pb$	0.54541	5.1	0.05656	3.2	0.45	0.08221	3.2	1185.1	37.4	1250.4	63.3	5.2
EV2S_SE200.40	**1190.3**	**32.1**	$^{207}Pb/^{206}Pb$	2.31573	3.6	0.20279	2.9	0.60	0.08282	3.0	1190.3	32.1	1265.0	58.0	5.9
EV2B_SE200.29	**1201.9**	**24.0**	$^{207}Pb/^{206}Pb$	2.26113	3.5	0.20496	2.2	0.79	0.08001	2.2	1201.9	24.0	1197.3	44.1	-0.4
EV2S_SE200.06	**1245.0**	**29.9**	$^{207}Pb/^{206}Pb$	2.54836	5.2	0.21305	2.6	0.39	0.08675	4.8	1245.0	29.9	1355.0	93.4	8.1
EV2S_SE200.04	**1254.4**	**40.7**	$^{207}Pb/^{206}Pb$	2.79198	3.5	0.23048	3.4	0.82	0.08272	4.0	1254.4	40.7	1262.7	78.3	0.7
EV2S_SE200.29	**1273.1**	**41.6**	$^{207}Pb/^{206}Pb$	1.66302	4.6	0.16281	3.9	0.86	0.08259	2.1	1273.1	41.6	1259.6	40.2	-1.1
EV2S_SE200.03	**1337.0**	**41.2**	$^{207}Pb/^{206}Pb$	0.96796	7.2	0.11187	4.1	0.35	0.08786	2.0	1337.0	41.2	1379.4	39.3	3.1

APPENDIX C: KOLMOGOROV-SMIRNOV TEST RESULTS

K-S P-values using error in the CDF	Sample 1	Sample 2	Sample 3	Sample 4	Sample 5	Sample 6	Sample 7	Sample 8	Sample 9	Sample 10	Sample 11	Sample 12
Sample 1		0.000	0.000	0.000	0.000	0.000	0.000	0.006	0.001	0.027	**0.083**	0.001
Sample 2	0.000		0.000	0.000	0.000	0.000	**0.652**	0.000	**0.165**	0.000	0.009	0.002

Table C1—Northern and Southern Samples and comparison data K-S Statistical Tests.

Sample 3	0.000	0.000		0.000	0.000	0.000	0.000	0.000	0.000	0.000	0.000
Sample 4	0.000	0.000	0.000		0.000	0.003	0.000	0.000	0.000	0.000	0.000
Sample 5	0.000	0.000	0.000	0.000		0.026	0.000	0.000	0.000	0.000	0.000
Sample 6	0.000	0.000	0.000	0.003	0.026		0.000	0.000	0.000	0.011	0.000	0.000
Sample 7	0.000	0.652	0.000	0.000	0.000	0.000		0.000	0.620	0.000	0.026	0.010
Sample 8	0.000	0.001	0.000	0.000	0.000	0.000	0.000		0.000	0.000	0.000	0.000

K-S P-values using error in the CDF

	NE-S	NE0	NE100	NE180	SE60	SE140	SE200	TR-01	TR-02	TR-03	TR-04
NE-S		**0.996**	**0.069**	**0.231**	**0.800**	**0.145**	0.026	**0.989**	**0.992**	**1.000**	**1.000**
NE0	**0.996**		**0.609**	**0.941**	**0.998**	**0.865**	**0.316**	**0.998**	**0.732**	**1.000**	**0.956**
NE100	**0.069**	**0.609**		**0.593**	**0.321**	**0.476**	**0.612**	**0.099**	0.001	0.019	0.002
NE180	**0.231**	**0.941**	**0.593**		**0.766**	**0.995**	**0.607**	**0.359**	0.008	**0.129**	**0.072**
SE60	**0.800**	**0.998**	**0.321**	**0.766**		**0.586**	**0.182**	**0.997**	**0.364**	**0.784**	**0.565**
SE140	**0.145**	**0.865**	**0.476**	**0.995**	**0.586**		**0.235**	**0.232**	0.002	**0.058**	0.009
SE200	0.026	**0.316**	**0.612**	**0.607**	**0.182**	**0.235**		0.041	0.001	0.006	0.001
TR-01	**0.989**	**0.998**	**0.099**	**0.359**	**0.997**	**0.232**	0.041		**0.929**	**1.000**	**0.917**
TR-02	**0.992**	**0.732**	0.001	0.008	**0.364**	0.002	0.001	**0.929**		**0.685**	**0.623**
TR-03	**1.000**	**1.000**	0.019	**0.129**	**0.784**	**0.058**	0.006	**1.000**	**0.685**		**0.999**
TR-04	**1.000**	**0.956**	0.002	**0.072**	**0.565**	0.009	0.001	**0.917**	**0.623**	**0.999**	

Table C2—Northern and Southern Samples K-S Statistical Tests.

APPENDIX D: XRD RESULTS

TR-01

#	Phase ID	Chemical Formula	PDF-#	RIR	Wt%	BR%	FOM (n)	Scale(I)	Shift(x)	Cell Type	a (Å)	b (Å)
1	Quartz, syn	SiO_2	00-046-1045	4.12	49.8	24.9	3.8 (17)	0.762	0.000°	Hexagonal	4.9145	4.9145
2	Kaolinite-1A	$Al_2Si_2O_5(OH)_4$	00-058-2001	0.89	21.9	25.5	'25.3 (15)	0.038	-0.060°	Triclinic (P1)	5.1497	8.9351
3	Muscovite-2M1, heated	$KAl_2(Si,Al)_4O_{10}(OH)_2$	00-058-2037	0.37	13.9	23.9	25.3 (04)	0.098	0.040°	Monoclinic	5.2007	9.0052
4	Illite-2M2 (NR)	$(K,H_{30})Al_2(Si_3Al)O_{10}(OH)_2•xH_2O$	00-058-2015	(1.0)	10.8	30.5	9.6 (04)	0.054	0.040°	Monoclinic	8.9975	5.2949
5	Montmorillonite	$(Ca,Na)_{0.3}Al_2(Si,Al)_4O_{10}(OH)_2•xH_2$	00-060-0318	(1.0)	3.6	18.4	---	1.000	0.000°	Monoclinic	5.2913	9.1904
6	Montmorillonite	$Na_{0.3}(Al,Mg)_2Si_4O_{10}(OH)_2•xH_2O$	00-058-2011		0.0		---	1.000	0.000°	Orthorhombi	5.0932	9.2167
7	Birnessite	$Na_{0.55}Mn_2O_4•1.5H_2O$	00-043-1456	6.70	0.0		'28.3 (06)	0.041	0.000°	Monoclinic	5.1750	2.8490

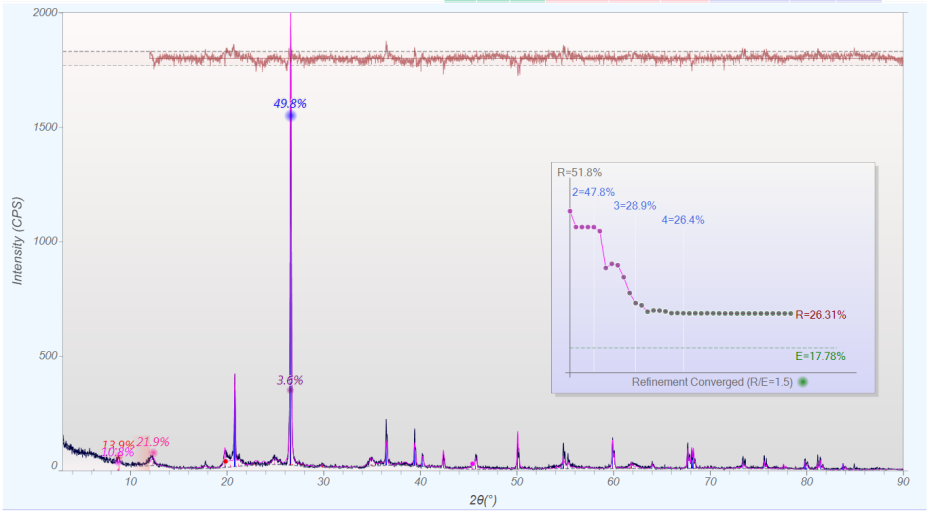

[H:\Desktop\U3_Data_Files\Olemiss\Jennifer Gifford\TR-01.raw] 3.0°/90.0°/0.02°/1.2(s), I(p)=2332.0/3.0, Cu(40kV,44mA) Tuesday, July 03, 2018, 4:49 PM ● MS State Univ.

TR-04

#	Phase ID	Chemical Formula	PDF-#	RIR	Wt%	BR%	FOM (n)	Scale(I)	Shift(x)	Cell Type	a (Å)	b (Å)
1	Quartz, syn	SiO_2	00-046-1045	4.12	56.9	22.0	3.8 (17)	0.762	0.000°	Hexagonal	4.9131	4.9131
2	Kaolinite-1A	$Al_2Si_2O_5(OH)_4$	00-058-2001	0.89	17.2	24.9	'25.3 (15)	0.038	-0.060°	Triclinic (P1)	5.1497	8.9351
3	Illite-2M2 (NR)	$(K,H_{30})Al_2(Si_3Al)O_{10}(OH)_2•xH_2O$	00-058-2015	(1.0)	10.0	20.2	9.6 (04)	0.054	0.040°	Monoclinic	8.9975	5.2949
4	Muscovite-2M1, heated	$KAl_2(Si,Al)_4O_{10}(OH)_2$	00-058-2037	0.37	9.7	22.7	25.3 (04)	0.098	0.040°	Monoclinic	5.1974	9.0094
5	Montmorillonite	$(Ca,Na)_{0.3}Al_2(Si,Al)_4O_{10}(OH)_2•xH_2$	00-060-0318	(1.0)	6.2	20.8	---	1.000	0.000°	Monoclinic	5.2913	9.1904
6	Montmorillonite	$Na_{0.3}(Al,Mg)_2Si_4O_{10}(OH)_2•xH_2O$	00-058-2011		0.0		---	1.000	0.000°	Orthorhombi	5.0932	9.2167
7	Birnessite	$Na_{0.55}Mn_2O_4•1.5H_2O$	00-043-1456	6.70	0.0		'28.3 (06)	0.041	0.000°	Monoclinic	5.1750	2.8490

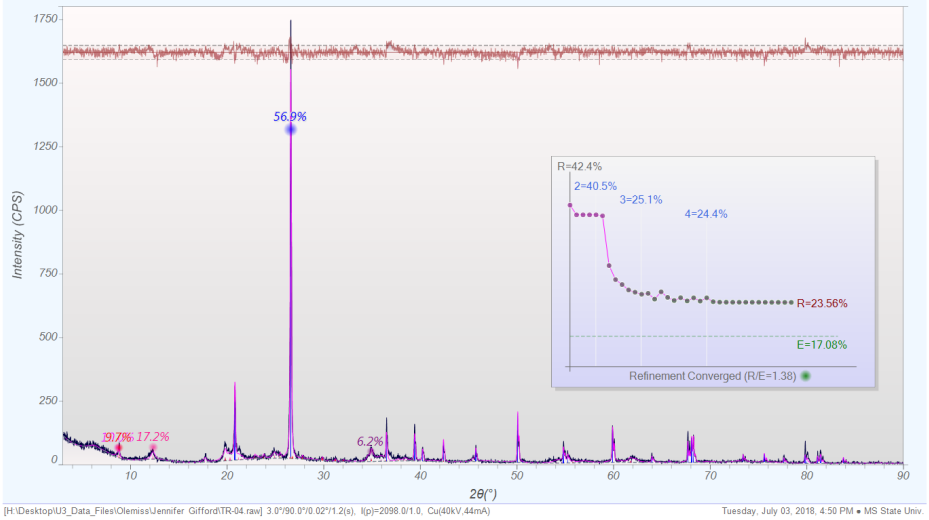

[H:\Desktop\U3_Data_Files\Olemiss\Jennifer Gifford\TR-04.raw] 3.0°/90.0°/0.02°/1.2(s), I(p)=2098.0/1.0, Cu(40kV,44mA) Tuesday, July 03, 2018, 4:50 PM ● MS State Univ.

Pontotoc-01

#	Phase ID	Chemical Formula	PDF-#	RIR	Wt%	BR%	FOM (n)	Scale(I)	Shift(x)	Cell Type	a (Å)	b (Å)
1	Quartz, syn	SiO_2	00-046-1045	4.12	39.9	19.3	3.8 (17)	0.762	0.000°	Hexagonal	4.9146	4.9146
2	Montmorillonite	$Na_{0.3}(Al,Mg)_2Si_4O_{10}(OH)_2 \cdot xH_2O$	00-058-2011	(1.0)	15.5	18.3	---	1.000	0.000°	Orthorhombi	5.0932	9.2167
3	Muscovite-2M1, heated	$KAl_2(Si,Al)_4O_{10}(OH)_2$	00-058-2037	0.37	14.1	23.1	25.3 (04)	0.098	0.040°	Monoclinic	5.2053	9.0264
4	Illite-2M2 (NR)	$(K,H_{30})Al_2(Si_3Al)O_{10}(OH)_2 \cdot xH_2O$	00-058-2015	(1.0)	12.3	20.8	9.6 (04)	0.054	0.040°	Monoclinic	8.9975	5.2949
5	Kaolinite-1A	$Al_2Si_2O_5(OH)_4$	00-058-2001	0.89	9.0	25.4	'25.3 (15)	0.038	-0.060°	Triclinic (P1)	5.1497	8.9351
6	Montmorillonite	$(Ca,Na)_{0.3}Al_2(Si,Al)_4O_{10}(OH)_2 \cdot xH_2$	00-060-0318	(1.0)	4.9	20.6	---	1.000	0.000°	Monoclinic	5.2913	9.1904
7	Birnessite	$Na_{0.55}Mn_2O_4 \cdot 1.5H_2O$	00-043-1456	6.70	4.1	21.6	'28.3 (06)	0.041	0.000°	Monoclinic	5.1750	2.8490

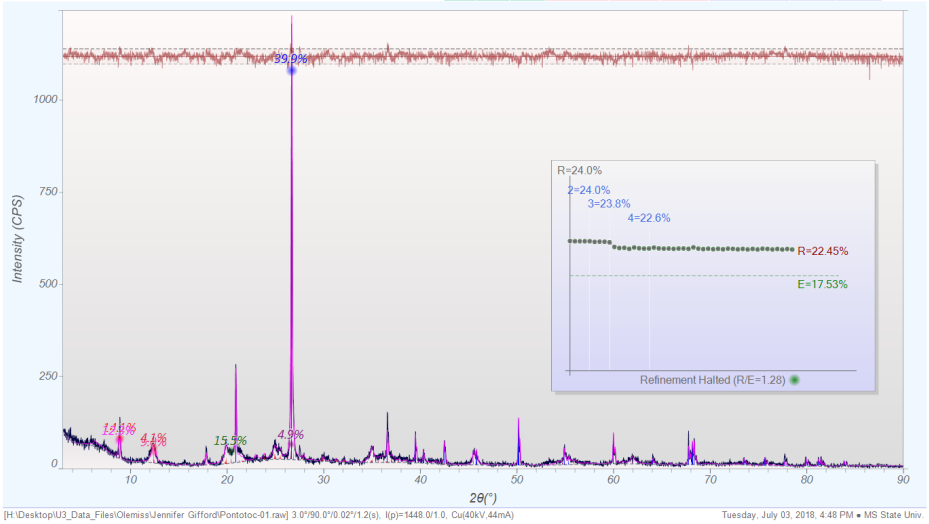

[H:\Desktop\U3_Data_Files\Olemiss\Jennifer Gifford\Pontotoc-01.raw] 3.0°/90.0°/0.02°/1.2(s), I(p)=1448.0/1.0, Cu(40kV,44mA) Tuesday, July 03, 2018, 4:48 PM ● MS State Univ.

Pontotoc-02

#	Phase ID	Chemical Formula	PDF-#	RIR	Wt%	BR%	FOM (n)	Scale(I)	Shift(x)	Cell Type	a (Å)	b (Å)
1	Quartz, syn	SiO_2	00-046-1045	4.12	46.0	22.8	3.8 (17)	0.762	0.000°	Hexagonal	4.9143	4.9143
2	Muscovite-2M1, heated	$KAl_2(Si,Al)_4O_{10}(OH)_2$	00-058-2037	0.37	16.5	19.9	25.3 (04)	0.098	0.040°	Monoclinic	5.2254	9.0120
3	Kaolinite-1A	$Al_2Si_2O_5(OH)_4$	00-058-2001	0.89	16.4	22.9	'25.3 (15)	0.038	-0.060°	Triclinic (P1)	5.1497	8.9351
4	Illite-2M2 (NR)	$(K,H_{30})Al_2(Si_3Al)O_{10}(OH)_2 \cdot xH_2O$	00-058-2015	(1.0)	10.4	19.0	9.6 (04)	0.054	0.040°	Monoclinic	8.9975	5.2949
5	Montmorillonite	$(Ca,Na)_{0.3}Al_2(Si,Al)_4O_{10}(OH)_2 \cdot xH_2$	00-060-0318	(1.0)	7.8	19.0	---	1.000	0.000°	Monoclinic	5.2913	9.1904
6	Birnessite	$Na_{0.55}Mn_2O_4 \cdot 1.5H_2O$	00-043-1456	6.70	2.9	19.0	'28.3 (06)	0.041	0.000°	Monoclinic	5.1750	2.8490
7	Montmorillonite	$Na_{0.3}(Al,Mg)_2Si_4O_{10}(OH)_2 \cdot xH_2O$	00-058-2011		0.0		---	1.000	0.000°	Orthorhombi	5.0932	9.2167

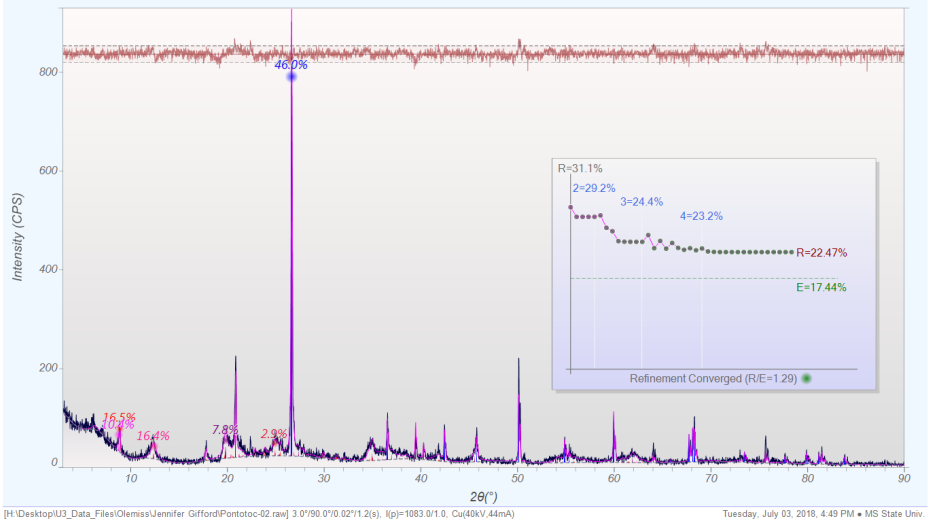

[H:\Desktop\U3_Data_Files\Olemiss\Jennifer Gifford\Pontotoc-02.raw] 3.0°/90.0°/0.02°/1.2(s), I(p)=1083.0/1.0, Cu(40kV,44mA) Tuesday, July 03, 2018, 4:49 PM ● MS State Univ.

VITA

Elizabeth J. Vitale was born and raised in Saint Louis, Missouri. Elizabeth graduated from Oakville Senior Highschool in 2013 and earned a Bachelor of Science in Geological Engineering from the University of Mississippi in 2017. She enjoyed her time and studies at the University of Mississippi so much that she decided to stay and accept a Teaching Assistant Position in the Department of Geology and Geological Engineering. Elizabeth decided to work and study under Dr. Jennifer Gifford to earn a Master of Science in Engineering Science with an Emphasis in Geology.

In the Department of Geology and Geological Engineering she worked as a Teaching Assistant from her junior year through her final year of graduate school. She was a Teaching Assistant for many courses including: Field Camp, Geomorphology, Structural and Tectonic Geology, Mineralogy and Petrology, and many more. She is an active member in Sigma Gamma Epsilon, Phi Kappa Phi, Gamma Beta Phi, and American Association of Petroleum Geologists.

Elizabeth is graduating in May of 2019 with her Master of Science and was a recipient of the Dawn Blackledge Scholarship (2018-2019), Co-Outstanding Teaching Assistant for the Department of Geology and Geological Engineering (2018-2019), and University of Mississippi School of Engineering Outstanding Teaching Assistant (2018-2019). After graduation Elizabeth will start her career as a Field/Office Engineer for Kiewit Constructions Underground District.